Photodynamics of

Phototropin and Cryptochrome

Blue-Light Photoreceptors

vorgelegt von

Sang-Hun Song

aus Seoul, Korea

Regensburg 2006

_____

Table of Contents
_____

_____

_____

Teile dieser Arbeit wurden bereits veröffentlicht:

S.-H. Song, B. Dick, Z. Peyman, A. Penzkofer, T. Schireis, and P. Hegemann.
Absorption and Emission Spectroscopic Characterisation of Combined Wildtype
LOV1-LOV2 Domain of Phot from *Chlamydomonas reinhardtii*
Journal of Photochemistry and Photobiology B: Biology (2005) **81**: 55-65.

S.-H. Song, B. Dick, A. Penzkofer, R. Pokorny, A. Batschauer, and L.-O. Essen.
Absorption and Fluorescence Spectroscopic Characterisation of Cryptochrome 3
from *Arabidopsis thaliana*
Journal of Photochemistry and Photobiology B: Biology (2006) **85**: 1-16.

1. Introduction

Photoreceptors

The plant responding on blue light was reported as early as 1881 by Darwin [1]. Since then different photoreceptors have been studied. Light signals regulate plant growth and development through the action of specialized photoreceptors, working alone or in combination. The photoreceptors convert their signals into photobiological response and they have their own distinct photo-dynamic cycles. The photoreceptor families are the phytochromes, the rhodopsins, the photoactive yellow proteins (PYP), the BLUF-domains (sensor for blue light using flavins), the phototropins, and the cryptochromes.

Their biological functions including signal transduction and their photo-cycles under illumination have been studied. The most important concepts are as follows: Phytochromes and rhodopsins undergo *trans-cis* photo-isomerization. Phytochromes (chromophore tetrapyrroles) are sensitive to red/far-red light. Rhodopsins (chromophore retinal) are sensitive initially to red light but after primary process it changes to intermediate states having sensitivity for shorter wavelengths. PYP undergoes *trans-cis* isomerization as responses to blue light. BLUF-domains, phototropins, and cryptochromes have blue light absorbing flavin chromophores as photoreceptors. The photocycle of phototropin involves the reversible formation of a flavin- cysteinyl adduct. The cryptochromes generally have two blue-light absorbing chromophores (FAD-MTHF, see below) and different flavin redox states in the photocycle dynamics.

The spectral sensitivity of the photoreceptors is determined by the absorption region of the active chromophores. Specially four classes of blue light photoreceptors have been identified, they are PYP, BLUF-proteins, phototropins, and cryptochromes. BLUF-proteins, phototropins, and cryptochromes are flavoproteins. Their biological functions and signal pathways upon light absorption are different.

The phototropins use flavin mononucleotide (FMN) as chromophore. The cryptochrome and the BLUF-proteins use flavin adenine dinucleotide (FAD) as chromophore. All are activated by UVA-light and blue-light. These receptors cause a number of light-dependent responses, including hypocotyl/cotyledon growth and phototropism, pigmentation, stomatal opening, de-etiolation response, and circadian clock.

The phototropin responses are relocation of chloroplasts, and stomata opening in plants. The phototropins have two chromophoric domains designated as Light-Oxygen-Voltage sensitive domains named LOV1 and LOV2 domain in the N-terminal region, and a serine/threonine (Ser/Thr) protein kinase motif in the C-terminal region. LOV1 and LOV2 domains bind the chromophore flavin mononucleotide (FMN). After light activation the LOV domains undergo a photocycle, which involves the formation of a covalent adduct between a cysteine residue and the FMN chromophore.

The phototropins are essential for the initiation of plant growth, whereas the cryptochromes are associated with the maintenance of the growth. Recently it was found that cryptochromes also involve phototropic response [2]. The cryptochromes are found in lower and higher eukaryotes, plants (*Arabidopsis thaliana*), algae (*Chlamydomonas*), one prokaryote (*Synechocystis*), and insects (*Drosophila*). They are involved in processes such as synchronization of the circadian clock, seed germination, and regulation of pigment synthesis. They share sequence and structural homology with photolyases.

Aims

A primary purpose of investigating the biophysics of photoreceptors is to determine their photo-cycles and to understand their light-induced biological function.

The photo-dynamics of LOV1 domains and LOV2 domains have been studied by many scientists. In this dissertation I study the absorption and emission spectroscopic behaviour of a LOV1/2 double domain from *Chlamydomonas reinhardtii* and compare with the behaviour of LOV single domains from *Chlamydomonas reinhardtii*. The photo-cyclic behaviour of adduct formation and recovery is determined by absorption and emission spectroscopy. Time-resolved fluorescence measurements have been carried out with blue light exposure using a femtosecond laser. The quantum efficiency of adduct formation was determined by intensity dependent absorption measurements.

Recently the cryptochrome cry3 from *Arabidopsis thaliana* became available. The biological function of cry3 in *Arabidopsis thaliana* is not yet known. In cry3 the chromophores are FAD and 5,10-methenyltetrahydrofolate (MTHF). The two chromophores within cryptochrome protein interact with one another. In this dissertation an absorption and emission spectroscopic characterization of cry3 is undertaken. The complex photocycle dynamics of cry3 due to light exposure will be clarified.

2. Review : Blue-Light Photoreceptors

2.1 Phototropin with LOV Domain

Phototropins upon excitation with blue-light and UV light regulate the plant growth toward the light source (phototropism), light mediated chloroplast movement, rapid inhibition of stem growth, and stomata opening [3]. Phototropins have been identified in several plant species including *Arabidopsis thaliana*, *Avena sativa* (oat), *Oryza sativa* (rice), and *Zea mays* (corn) [4].

The phototropins are called Phot. In most phototropin containing species there are two phototropins, Phot1 and Phot2 present. Phot1 and Phot2 genes in *Arabidopsis* encode the Phot1 and Phot2 proteins of 996 and 915 amino acids which have approximately 60% sequences identity [5].

The cellular localization of chloroplasts is dependent on light intensity [6]. At low light intensity, chloroplasts capture light energy for photosynthesis [7]. At high light intensity, chloroplasts are localized in opposite direction to light for avoidance of damaging effects [8]. Accordingly, low light intensity regulates an accumulation of chloroplasts and high light intensity regulates an avoidance movement of chloroplasts. Phot1 mediates the accumulation movement of chloroplast at low or high light intensity [9]. Phot2 regulates an accumulation of
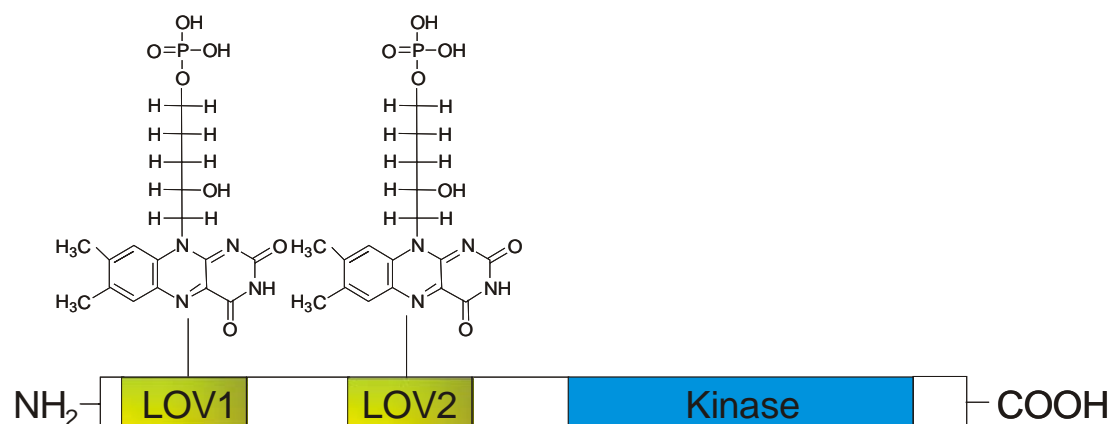
Fig.2.1 Primary structure of the amino acid sequence in phototropin of *Chlamydomonas reinhardtii*. Each LOV domain contains one FMN.

chloroplast at low light intensity [9] and regulates the avoidance movement of chloroplasts at high light intensity [10].

Seedlings grow toward the light and this phenomenon named the phototropism. Phot1 regulates the phototropism at low or high light intensity, however, phot2 is responsible for the phototropism at high light intensity. Phot1 and phot2, both are responsible for stomatal opening independent on light intensity [11].

The primary structure of a phot is shown in Fig. 2.1. In each phototropin, phot, there are two LOV domains (light-oxygen-voltage sensitive domain). The phot1 and phot2 belong to the class of PER/ARNT/SIM (PAS) domains [12]. They are a subset of proteins within the PAS domain superfamily. They are regulated by two LOV domains in the N-terminal region [5]. A serin/threonine protein kinase domain is located at the C-terminal region and is responsible for blue light-induced autophosphorylation [13].

Each LOV domain binds oxidized flavin mononucleotide (FMN) as chromophore [14]. The FMN is non-covalently bound to the LOV domain (located in a binding pocket). Illumination of a LOV domain causes the formation of an intermediate, the photo-adduct state via singlet-excited state relaxation to the triplet state [15]. The triplet state has its absorption spectral maximum at 715 nm, and is therefore called LOV-715. The photoadduct intermediate
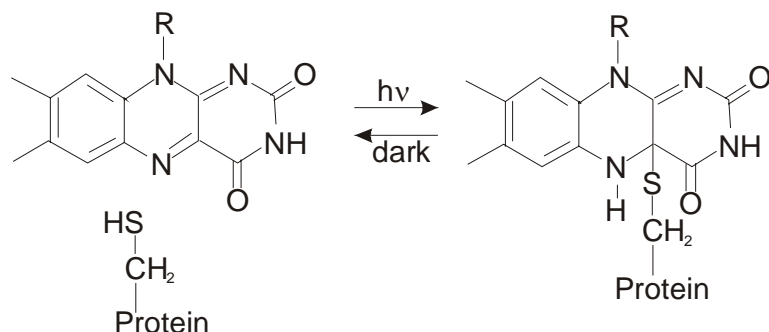
Fig.2.2   The formation of a cysteinyl-flavin-C(4a) covalent adduct in LOV domain after the absorption of blue light by the FMN cofactor.

has its absorption maximum at 390nm, and is therefore called LOV-390. This intermediate reverts to the ground state in the dark. The spectrum of intermediate agrees with that of the covalent C(4a) flavin-cysteinyl adduct [16], so it is generally accepted that the formed photo-adduct in the LOV domains is the C(4a) flavin-cysteinyl adduct. The scheme of photo induced formation and recovery is shown in Fig. 2.2. The absorption spectra of the initial ground state and the photoproduct share three isosbestic points, at 330, 375, and 410 nm.

The adduct formation activates the serine-threonine kinase region of the enzyme [17]. For further study of the kinase activity of phototropin, the autophosphorylation has been studied in *At*phot2 [18]. The results show that the two LOV domains function in different ways in the *in vitro* phosphorylation as shown in Fig. 2.3. Major roles of LOV2 domain in the photoregulation are shown with the substrate phosphorylation. The kinase domain (KD) expresses kinase activity constitutively and LOV2-KD shows light activation of kinase. LOV1-LOV2-KD does not exhibit the activation because of attenuation by LOV1 under low light conditions, however, the attenuation is overcome under high light conditions.
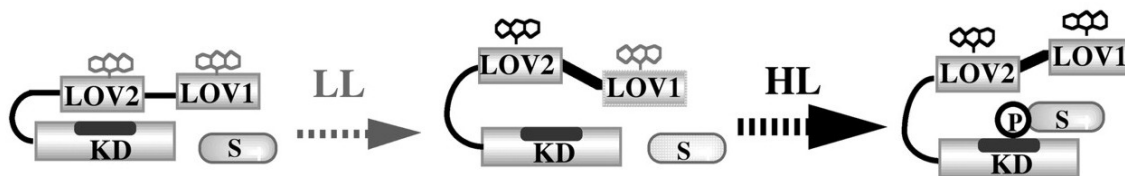
Fig. 2.3   Schematic illustration of the LOV domains in light regulation of substrate phosphorylation by kinase domain (KD) in *At*phot2 [18]. P, phosphate; S, substrate; LL, low light conditions; HL, high light conditions. LOV1 and LOV2 domains showed distinct roles in photoregulation of kinase activity in *At*phot2.

In the FT-IR spectroscopy the S—H and O—H stretching bands in LOV2 domain from *Adiantum* phy3 were studied [19]. Two water molecules were found to be located in the flavin-binding pocket by van der Waals and electrostatic interactions as shown in Fig. 2.4 [17].

A hydrogen atom is not found to be bound to N5 position of the isoalloxazine ring. Upon light illumination, there occur structural changes in internal water molecules (water25 and water 45) like the bacteriorhodopsin. The changes induce loosening of hydrogen bond network via perturbation [19]. As a result, the S—H group of Cys966 moves to the C(4a) position of isolloxazine ring and forms the C(4a) flavin-cysteinyl adduct.
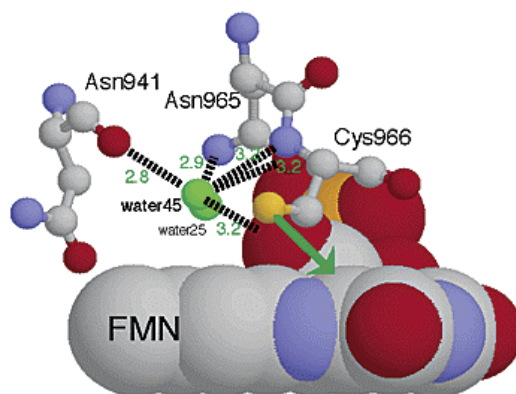

Fig. 2.4   Water molecules near FMN in LOV2 domain from *Adiantum* phy3 [19]. Upon illumination, the S—H group of Cys966 forms an adduct with FMN at C(4a) position as described arrow.

The structure of the LOV2 domain of *Adiantum* phy3 is shown in Fig. 2.5. Three helical segments flanking a five-stranded antiparallel β-sheet are seen. This is characteristic for PAS domains [20]. LOV domain is connected to the helix-turn-helix αA/αB, five-stranded β scaffold, and helical connector αC. The central α´A helix includes Cys966 [17]. The amino acids in α´A helix and β – strands (βC, βD and βE) make the majority of flavin contacts [17].

The structural alignment of LOV domains extends more up toward αA/αB helices as compared to PYP, another member of PAS superfamily. The LOV domains include a salt
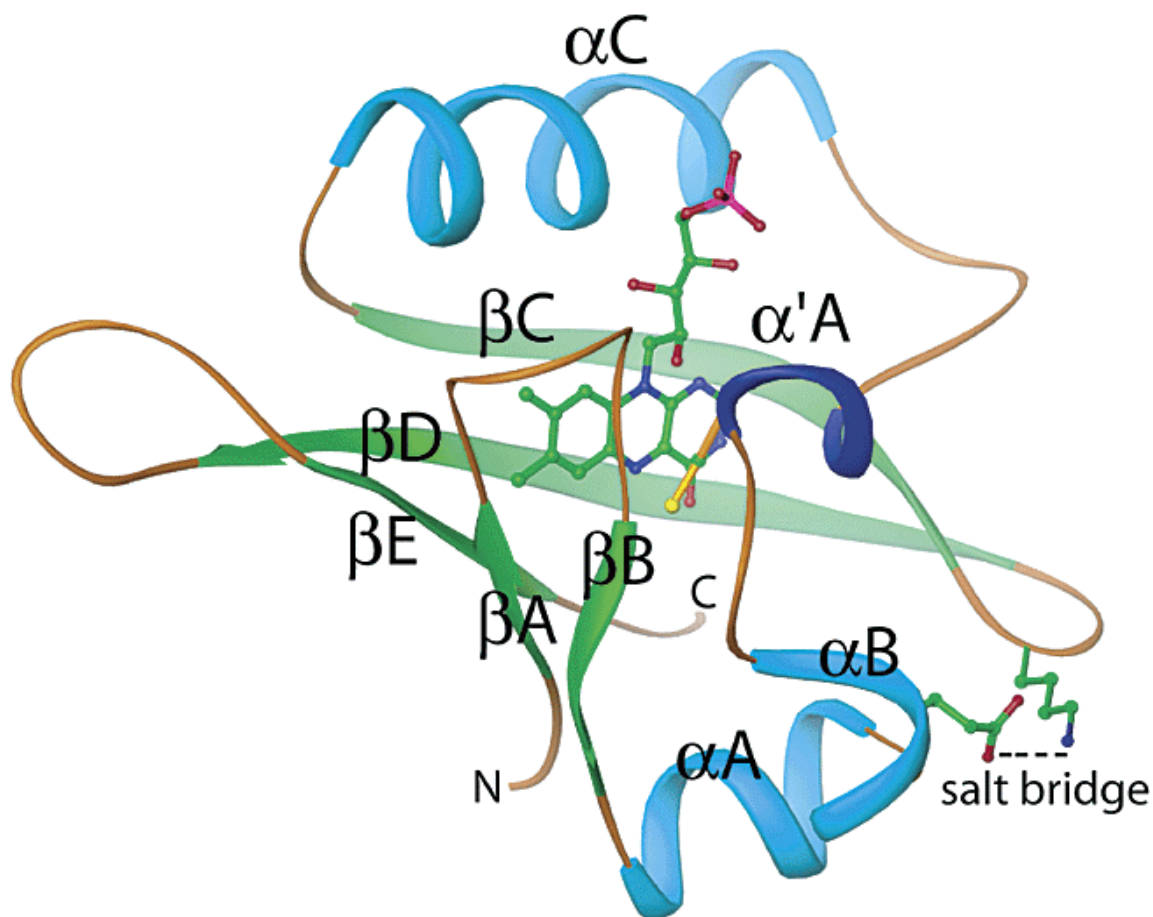

Fig. 2.5   Ribbon diagram of LOV2 domain structure from *Adiantum* phy3 [21]. Cys966 is located at the N-terminus of α´A helix.

bridge between αB – αA helices and βC – βD loop for a light-responsive signaling module [21].

A photochemical understanding of LOV domains has been obtained with site-directed mutagenesis of a single cysteine. The mutant LOV1-C57S (cystein57 replaced by serine) and LOV2-C250S (cystein250 replaced by serine) of phot from *Chlamydomonas reinhardtii* do not form the photoproduct LOV-390. Upon excitation and intersystem crossing of the molecules to the triplet state they recover directly to the initial ground state. These results are illustrated in Fig. 2.6. The decay time of LOV1 triplet state to the ground state is 27 μs [22]. The decay of triplet state in wild type is fitted as bi-exponential function. This result indicates two triplet states, LOV1-715a and LOV1-715b. LOV1-715a state could be transformed into LOV1-715b state within time constant of 4 μs. From the triplet state to the adduct state the decay times of LOV1-715 are 800 ns with 80 % and 4 μs with 20 %.

(a) (b)
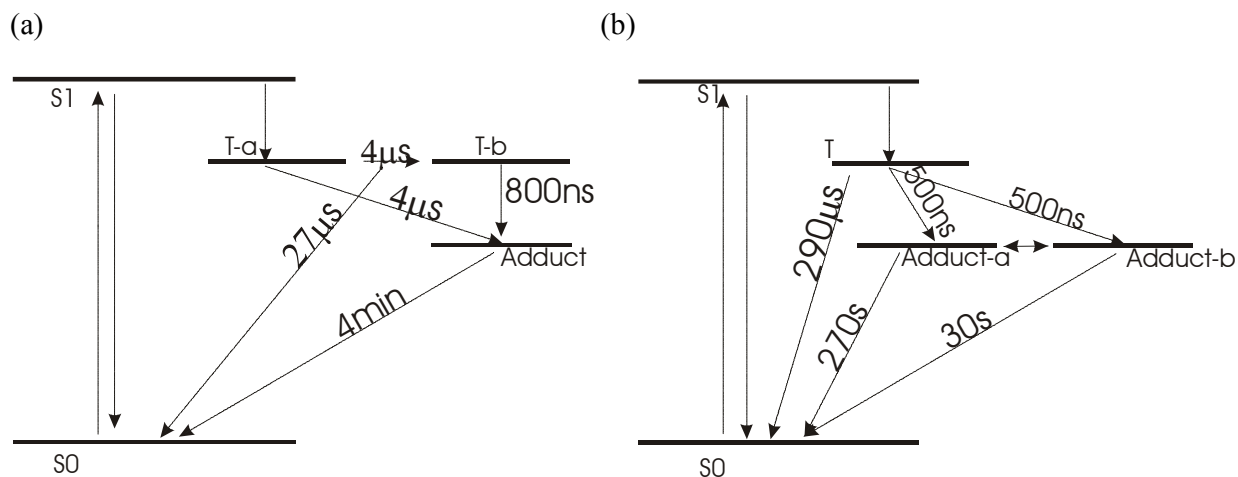
Fig. 2.6   (a) Photo-cyclic scheme of LOV1 wild type domain [22].
(b) Photo-cyclic scheme of LOV2 wild type domain [21,23].
Both LOV domains are from phot of *Chlamydomonas reinhardtii*. S0 is singlet ground state and S1 is singlet excited state. T is triplet state and two types of T are suggested in LOV1 domain. In LOV2 domain there are two photo-adduct states.

In the LOV2 domain it is known that only one triplet state exits and the decay time of the LOV2 triplet state to the singlet ground state is 290 μs and to the adduct state is 500 ns [21]. In the photo-cyclic behaviour of the LOV2 domain, two photo-adduct states are suggested by global fit [23]. The decay times of adduct states to the ground state are 270 s with 75 % and 30 s with 25 % ratio.

Further studies suggest an additional donor-acceptor state (DA state) involvement in the photo-adduct formation as shown in Fig. 2.7 [24]. FMN is electron acceptor (A), an amino acid in LOV domain acts as electron donor (D), and they form [FMN⁻…D⁺] charge-transfer complexes by photo-induced reductive electron transfer [25]. The molecules in the DA state also can form the flavin-cysteinyl adduct and return to the singlet ground state.
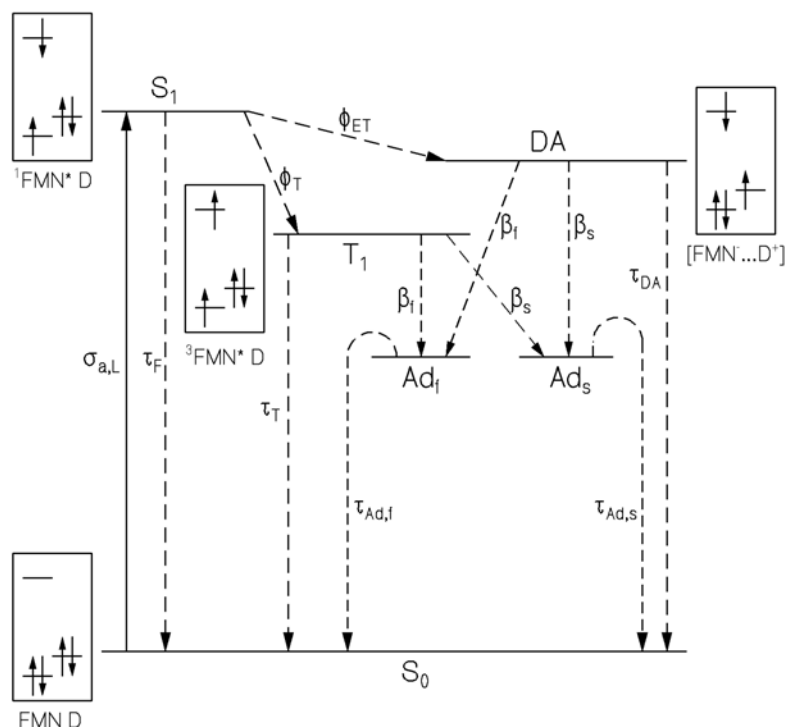
Fig. 2.7   Photo-cycle model of non-covalently bound FMN in LOV2-MBP of phot from *Chlamydomonas reinhardtii* assuming excited-state relaxation branching to fast and slow photo-adduct components (β_f and β_s). The formation of two fractions of flavin-cysteinyl adducts are shown with Ad_f and Ad_s. At the various excitation states HOMO-LUMO schemes of acceptor, A, FMN and an amino-acid donor, D, are included [24].

LOV domains of phot1 and phot2, have different quantum efficiencies and reaction kinetics (*Arabidopsis*, rice, and *C. reinhardtii*) [26,27]. This suggests that LOV1 and LOV2 may have different light-sensing roles in regulating phototropin activity. Quantum efficiencies for the phot1 LOV1 domains are much lower than those of phot2 LOV1 domains. For phot1 the quantum efficiency of adduct formation in the LOV2 domain is around 10 times larger than in the LOV1 domain, but for phot2 both quantum efficiencies are not so strongly different.

For the LOV1/LOV2 double domain from *Arbidopsis thaliana* the removal of the cystein out of the LOV1 part has little influence on the phototropic response as compared to the wild type [13]. But the LOV1/LOV2 double domain with LOV1 wild type and LOV2 cystein mutant has weak light sensing effect and is not sufficient for phototropism. This indicates that the LOV2 domain is the dominant light-sensing domain in phot.

The mechanism of the formation of the flavin-cysteinyl adduct is not yet established. Three mechanisms are suggested which are ionic reaction [15], nucleophilic attack [17], and radical-pair mechanism [28].

Initially, a deprotonated cysteine was proposed [15]. Because the cysteinyl group is deprotonated in the ground state, to stabilize the thiolate, the presence of a counter charge, an XH^+ group is suggested [15,28]. However crystal structural studies show no suitable XH^+ group [6]. An XH^+ group is not yet identified as redox-active amino acid residue in the protein backbone. Because of this, the cysteine of LOV domains is thought to be protonated in S—H form [19].

The N(5) position of FMN in the triplet state may be protonated from the cystein group in an ionic reaction between the C(4a) position and cystein to form the flavin-cysteinyl adduct [15,29]. In the ionic reaction the protonated triplet state of FMN ($^3FMNH^+$) is required as an intermediate as shown in Fig. 2.8. But $^3FMNH^+$ is found only at pH < 4.4 and ^3FMN forms a neutral flavin radical for pH 4.4 ~ 8.4 following electron transfer by protonation [30].
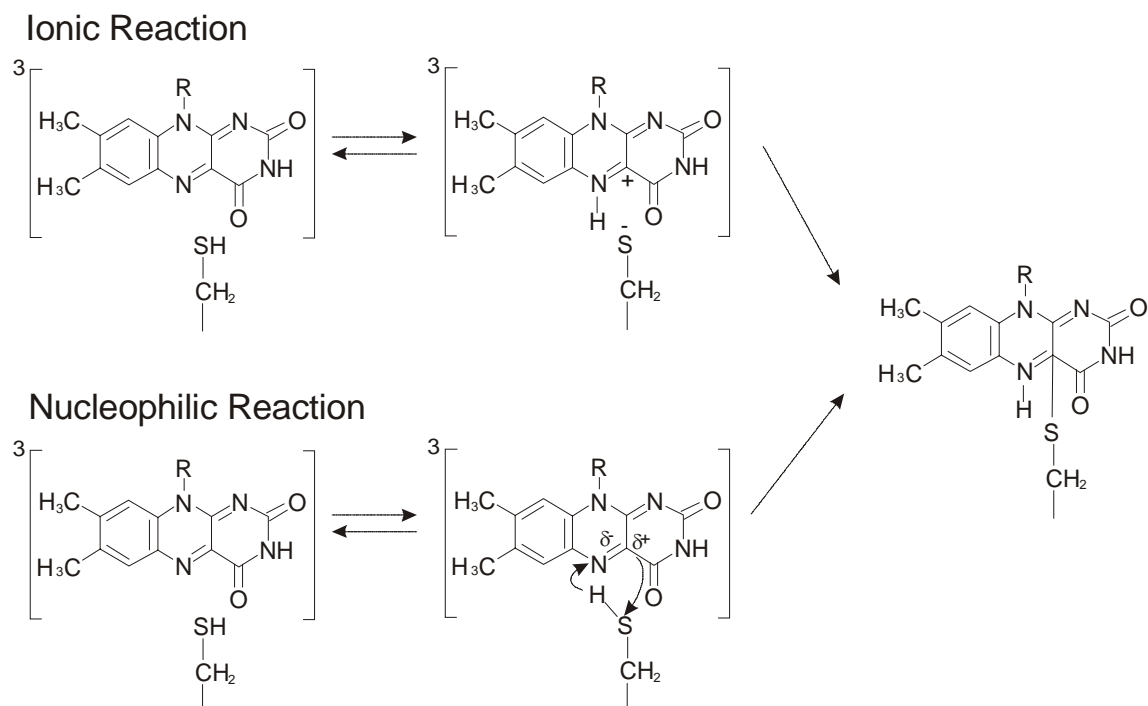
Fig. 2.8   Photoreaction scheme for the formation of C(4a) flavin-cysteinyl adduct of LOV domain. Up panel shows ionic reaction [15] and down panel shows nucleophilic reaction [17].

The nucleophilic model suggests that the C(4a) position of the isoalloxazine ring is nucleophilic attacked by the cysteine thiolate anion [17]. The redistribution of electronic charges around the C(4a) position alters the electronic state of isoalloxazine ring and the N(5) position is protonated as the thiol group attacks at C(4a) position as shown down panel of Fig 2.8.

Direct transition from triplet state (^{3}FMN) to the photoadduct was not observed by EPR spectra so ionic and radical intermediates are suggested [28]. The photoreaction of LOV domain was studied at low temperature for capturing proton transfer. A protonation of the triplet state can occur. The ^{3}FMN protonation facilitates the thioadduct formation. As a result the C(4a) position of FMN becomes to be more electrophilic, thus the nucleophilic attack of the cysteine's thiol group on C(4a) occurs like in B species of Fig. 2.9 [15].
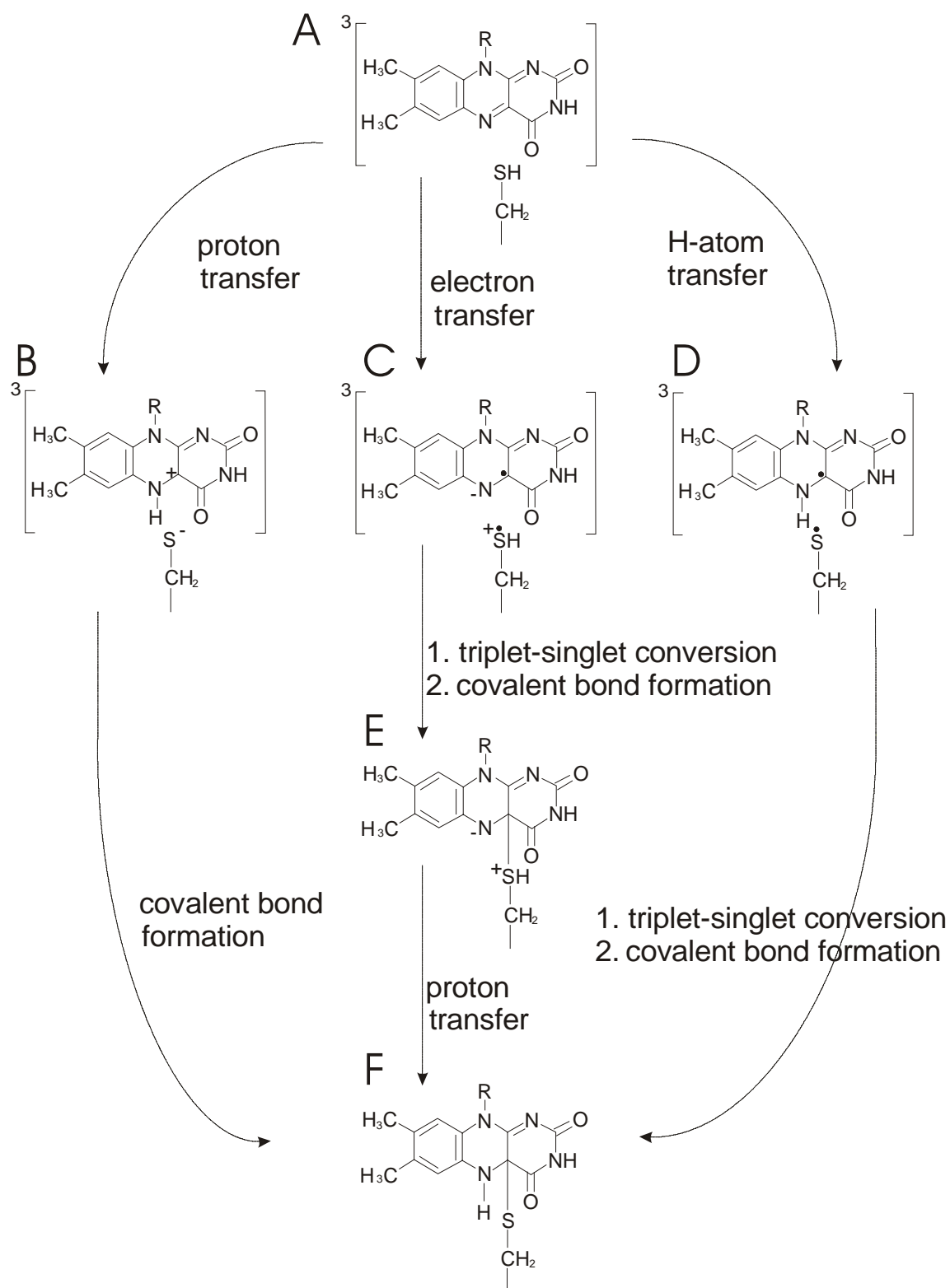
Fig. 2.9   The photoadduct formation of LOV domain from triplet state [28]. This scheme
from A to F, via C and E, bases on FMN radical and ionic reaction. The proton
transfer (B) is inhibited below temperature 80 K.

[3]FMN is more reactive with cystein than the protonated triplet state ([3]FMNH[+]) [31]. FMN in frozen aqueous solution has shown no proton transfer [32]. In LOV domain the formation of [3]FMNH[+] from [3]FMN was not observed at 77 K by tr-EPR spectroscopy [28]. This indicates that there is no protonation of the FMN triplet at 77 K.

When the triplet state removes the neutral hydrogen atom from the sulfur group of the cysteine residue, a radical-pair is proposed to be present since triplet state lacks potential energy to form an adduct [33]. In the radical-pair mechanism, the adduct formation does not require prior protonation of [3]FMN because cysteine was found to be more reactive with [3]FMN than with [3]FMNH[+] as shown C panel in Fig. 2.9 [28,29]. But in species E a proton transfer is necessary for the formation of photoadduct F.

Electron transfer from cysteine to the triplet state makes a radical-pair species C in Fig. 2.9, and it follows triplet-to-singlet state conversion by formation of zwitterionic species E. The negative charge at N(5) is protonated by the sulfur group (step E to F).

At low temperature in the glassy state [34] molecules are disordered but rigidly bound. In this state quantum mechanical tunnelling occurs [35,36]. [3]FMN can directly abstract a hydrogen atom from cysteine, giving a neutral radical pair by quantum mechanical tunnelling in the glassy state as shown by species D [28]. Initially the radical pair has the same spin state (*i.e.* [3][FMNH[•] ⋯ RS[•]]), due to the conservation of angular momentum [29]. At low temperature the protein is not able to relax, thus a conformational strain is imposed on the photoadduct. However, at low temperature, the absorption spectrum of the photoadduct is red-shifted 10 nm in LOV1 domain and 13 nm in LOV2 domain in comparison to the room temperature [28]. This result indicates that hydrogen-atom transfer is more unlikely than electron transfer in the mechanism of the formation of the photoadduct (otherwise the same red-shift would be expected at room temperature).

Electron transfer occurs with proton transfer and it generates a neutral radical pair in the triplet state and C(4a)-sulfur bond [37,38]. The photoreduction agents such as EDTA and β-

Mercaptoethanol are electron donors to ^{3}FMN [39] and both have a similar effect on LOV domains [40]. The FMN cofactor in LOV2-C57A domain with EDTA is fully converted from the oxidized FMN (FMN_{ox}) to the one-electron reduced semiquinone form ($FMNH^{\bullet}$) [29]. Initially ^{3}FMN takes an electron from cystein. Then a spin-correlated ionic radical pair consisting of an anionic flavin radical, $FMN^{\bullet-}$, and a sulfur-centered radical, $RS^{\bullet+}$ is formed. A proton transfer forms the neutral flavin radical ($FMNH^{\bullet}$), and the sulfur-centered radical, (RS). A proton transfer to give $FMNH^{\bullet}$ causes a photoreduction of one electron. These mechanisms produce flavin semiquinone [41]. Trp(W), His(H), or Tyr(Y) are likely candidates for electron transfer to ^{3}FMN [29].

2.2 Cryptochrome and Photolyase

Cryptochromes are widely involved in the management of life [42]. Cryptochromes share sequence similarity to the DNA repair photolyase [43]. Photolyase can repair DNA after UV-damage, but, cryptochrome does not have the DNA repair ability [44]. Cryptochromes and DNA photolyases have a similar amino acid sequences and show a similar light-induced response. UV illumination of a cell induces the formation of a cyclobutane pyrimidine dimer (CPD) or pyrimidine (6-4) pyrimidone dimer. Photolyases have the ability to revert CPD or pyrimidine (6-4) pyrimidone dimer by light-induced electron transfer from $FADH^-$ to the dimer. Cryptochromes do not have this ability.
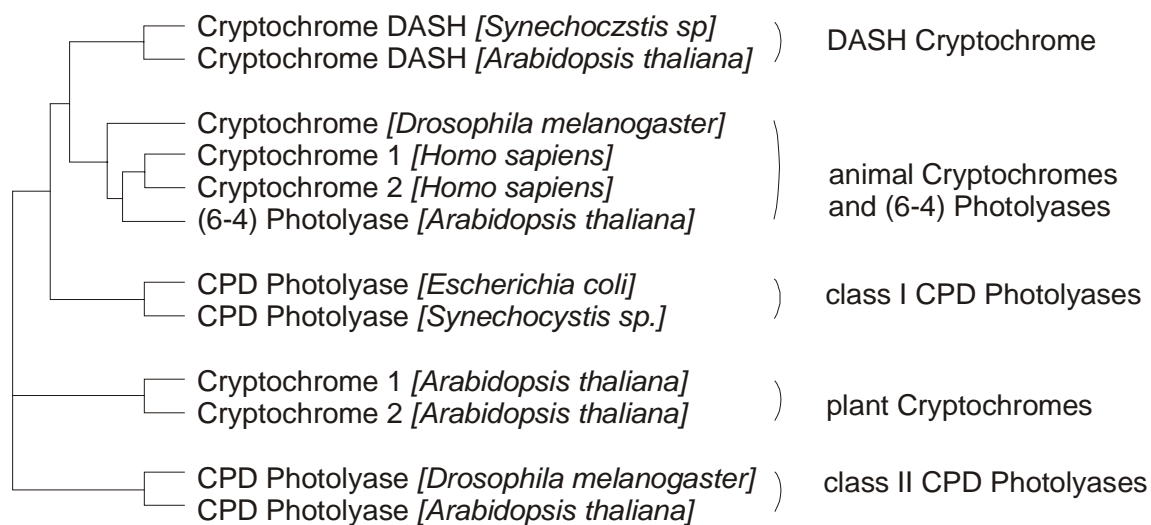
Fig. 2.10   Phylogenetic tree of the Cryptochrome/Photolyase protein family [45].

16

Cryptochrome mediates blue-light signaling and photolyase repairs damaged DNA. Both cryptochrome and photolyase have similar flavin binding sites [46].

The Cryptochrome/Photolyase protein family was identified by the computational maximum likelihood method. The obtained phylogenetic tree is shown in Fig. 2.10 [45]. This scheme of the Cryptochrome/Photolyase protein family divides into four subfamilies, animal cryptochromes and photolyases, plant cryptochromes, class I CPD photolyases, and class II CPD photolyases. A fifth subfamily is CRY-DASH (*D*rosophila—*A*rabidopsis—sis— *S*ynechocytstis—**H**uman). Transactivations of the reporter plasmid have shown that CRY-DASH is a transcriptional repressor [49]. A weak CPD photolyase activity is observed in CRY-DASH [49]. CRY-DASH is found mostly in bacteria but also in the plant *Arabidopsis thaliana*. It is named CRY3 [50].

2.2.1 Photolyase

The photolyase family is composed of CPD photolyases and (6-4) photolyases. They are involved in the photoreactivation of CPD and (6-4) photoproducts. CPD photolyase is classified into two subclasses, class I and class II, based on amino acid sequence similarity [51,52]. These two classes are only distantly related enzymes which have separated at early formation.

The CPD photolyase repairs DNA damaged by UV light [44]. When a blue light photon is absorbed to CPD photolyase, an electron of flavin-adenine dinucleotide (FAD) is excited. This excited electron is transferred to CPD bound to the enzyme, and then the damaged DNA is repaired by cleaving CPD. This mechanism is named photorepair.

Photolyases contain 450-550 amino acids and two non-covalently bound chromophore cofactors. One is FAD and the second is methenyltetrahydrofolate (MTHF) or 8-hydroxy-7,8-didemethyl-5-deazariboflavin (8-HDF). The distance between the two chromophores is about 8.9 Å [53]. The second chromophore is not necessary for the FAD induced photorepair. However, it has a higher absorption than FADH$^-$ which is the active form of FAD in the DNA-repair and excites FADH$^-$ by energy transfer (antenna effect).

The photolyase consists of the N-terminal α/β domain and the C-terminal α helical domain as shown in Fig. 2.11. The folate and deaza-flavin cofactors bind to the C-terminal 150 acids [54]. The catalytic cofactor FAD is bound at the C-terminal regions as was found out by crystal structure studies of *E. coli* [55], *A. nidulans* [56], *T. thermophilus* [57] photolyases. The second chromophore is a light-harvesting cofactor and bound at the N-terminal half [57]. The backbone structures of photolyases include the α/β domain and the α helical domain. The Cα-traces backbone is in superimposition. The structures were measured with a resolution of than 2 Å [58,59].
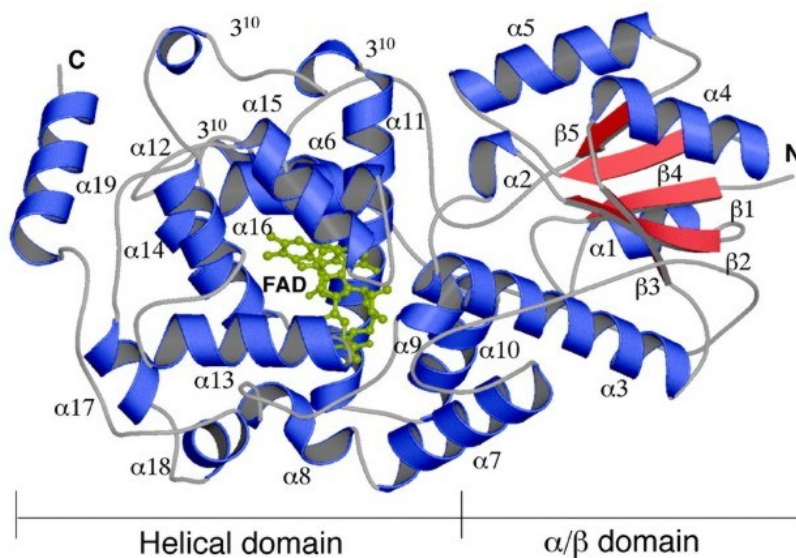

Fig. 2.11   Crystal structure of *Thermus thermophilus* photolyase. The N and C termininal are labeled N and C, respectively. Figure was copied from Ref. [57]. It consists of the α/β domain in the N-terminal region and the α helical domain in the C-terminal region. FAD is bound at the C-terminal regions.

Each photolyase enzyme contains one FAD molecule [60]. Flavin can be reduced or oxidized by electron reactions. There are three redox states: oxidized form (FAD_{ox}), one-electron-reduced form ($FADH^\bullet$), and two-electron-reduced form ($FAD_{red}H^-$) [43]. Photolyase contains $FAD_{red}H^-$ [61]. The absorption spectrum of photolyase *E. coli* shows FAD in the neutral radical form ($FADH^\bullet$) during the purification [61]. In studies on *Saccharomyces cerevisiae* photolyase it was shown that FAD can be converted to $FADH^\bullet$ or to FAD_{ox} [62]. Under physiological conditions FAD is synthesized in the FAD_{ox} form and it incorporates into apoenzymes [43]. This FAD_{ox} is converted into $FADH^\bullet$ or $FAD_{red}H^-$ during catalytic cycle of FAD.

Photolyase contains FAD and either MTHF or deazaflavin which have a pterin group as photoantenna. The 5,10-methenyl bridge of the folate in MTHF is responsible for the absorption spectral band near to 360 nm. The methenyl group is hydrophobic, and pterin ring induces positive charge on the methenyl group. This positive charge interacts with the apoenzyme, and then the absorption is red-shifted [63].

The MTHF in photolyase of *E. Coli* is binding with His44 (H), Asn108 (N), Glu109 (E), Cys292 (C), and Leu375 (L) as shown in Fig. 2.12 [64]. Glu109 makes two H-bonds with N^1 and N^3. The pteridine part of MTHF is packed between His44 and Leu375. The oxygen of
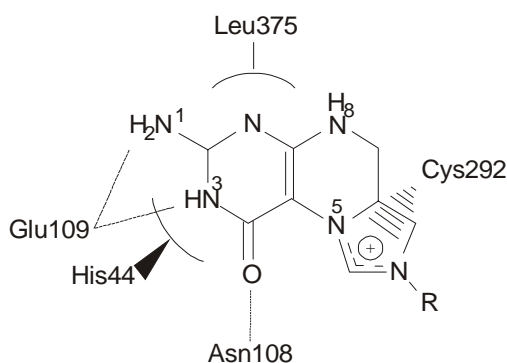

Fig. 2.12   MTHF in *E. coli* DNA photolyase binding site, from Ref. [64]. Glutamic acid is combined with two H- Bonds, N^1 and N^3 [55].

Cys292 is located near to N^5 position where there is a delocalized positive charge. These specific bindings between protein and cofactor influence the behaviour of MTHF [55,64].

The photolyase class with the deazaflavin 8-HDF is named F_0 [65]. F_0 was first discovered in methanogenic bacteria [66]. Since the absorption maximum peak of F_0 is at 420 nm, F_0 is also called F420. The absorption spectrum of 8-HDF in the F_0 photolyase is red-shifted like MTHF. The absorption peak is at 440 nm because of strong interaction with the apoenzyme.

The F_0 photolyase also contains FAD [43]. The deazaflavin molecule has a capacity to reduce flavoproteins [67]. This indicates that the $FAD_{red}H^-$ is the universal photocatalyst in all photolyases [68]. The deazaflavin is a strong one-electron reductant and responsible for Pyr < > Pyr photosplitting [67].

The photolyase binds to thymine (T< >T) with high efficiency and other pyrimidine (Pyr< >Pyr) dimers on DNA, and splits the dimers when exposed to UV-visible light [63]. The key element in the repair mechanism is electron transfer from an excited $FAD_{red}H^-$ to the
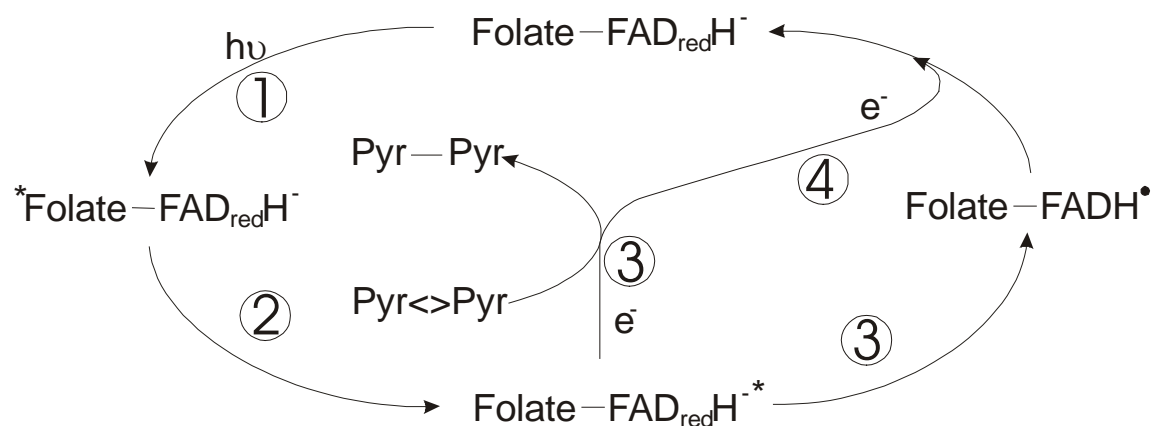

Fig. 2.13   Photo-cyclic mechanism of photolyase [43]. ①Photolyase absorbs a photon, ②The folate transfers energy to $FAD_{red}H^-$. ③A single electron is transferred from FAD to the cyclobutane ring of pyrimidine dimer to generate two pyrimidines. Concomitantly, $FADH^\bullet$ is generated by electron transfer from the two pyrimidines. ④The electron is transferred from the remaining pyrimidine radical back to FAD.

pyrimidine dimer on DNA.

The reaction mechanism of photolyase is shown in Fig. 2.13. First, a blue light photon is absorbed by MTHF or by $FAD_{red}H^-$. Second, the excited MTHF transfers its energy to $FAD_{red}H^-$ over a distance of 16.8 Å [69]. As a result of this electron transfer reaction, the two bonds between the pyrimidine bases break up as shown in the third step. The excited $FAD_{red}H^-$ transfers an electron to Pyr $<>$ Pyr over a distance 5~10 Å [70] at a rate of 7×10^9 to 2×10^{10} s^{-1} [71]. Upon dimer splitting the $FAD_{red}H^-$ is converted to the one-electron-reduced form ($FADH^{\bullet}$). Finally the electron from pyrimidine is transferred back to the $FADH^{\bullet}$ and the $FAD_{red}H^-$ is regenerated. The photolyase enzyme and the repaired DNA are seperated [44]. The photo-repair is performed.

2.2.2 Cryptochrome

Plant cryptochromes have an amino N-terminal PHR (*Photolyase Homology Region*) and this shares sequence homology with photolyases [72,73]. The C-terminal domain has been found to be critical to the function of *Arabidopsis* cry1 and cry2 [74]. Cryptochrome contains two non-covalently bounding chromophores [75]. One chromophore is flavin-adenine dinucleotide (FAD) as the key cofactor to carry out initial biological function upon photoexcitation. The other is a pterin in the form of methenyltetrahydrofolate (MTHF).
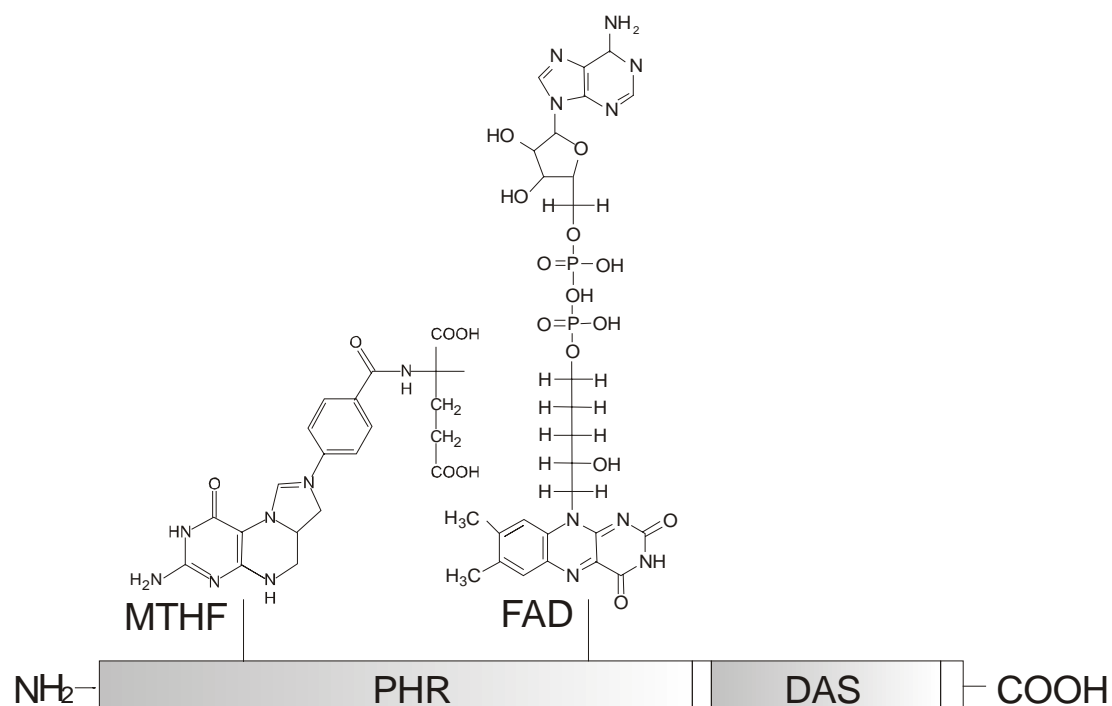

Fig. 2.14   Cryptochrome contains two non-covalently bound chromophores. One chromophore is flavin-adenine dinucleotide (FAD) and the other is methenyltetrahydrofolate (MTHF) [76].

_At_-cry1
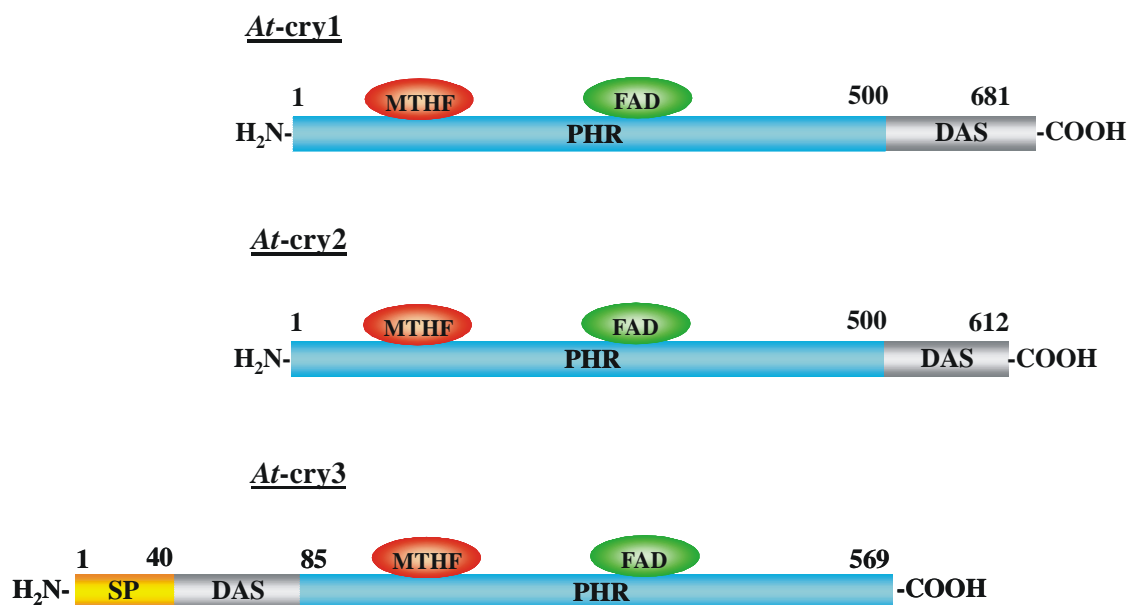
_At_-cry2

_At_-cry3

Fig. 2.15   Schematic primary structures of full-length _At_-cry1, _At_-cry2 and _At_-cry3 [77].
PHR : photolyase homology region (contains binding sites for MTHF and FAD cofactors).
SP : signal peptide (contains signal sequences for import into chloroplasts and mitochondria; this signal peptide is cleaved off after import).
DAS : N-terminal extension unique for _At_-cry3 containing DAS-like motif.

Cryptochromes share with photolyases a sequence of about 500 amino acid residues with high degree of similarity between all members of cryptochrome/photolyase family. This sequence is called Photolyase Homology Region or PHR domain. Most of plant and animal cryptochromes have a C-terminal extension (also called Cryptochrome C-Terminus or CCT domain) which contains so-called DAS motif ("D" stays for conserved aspartic acid residue, "A" stays for tandem of acidic residues (glutamic or aspartic acid) and "S" stays for tandem of 4-6 serine residues) which is of a functional importance. This C-terminal extension is missing in most of prokaryotic cryptochromes as well as in the members of cryptochromeDASH subfamily.

At-cry3 is a member of cryDASH subfamily so it has no C-teminal extension but, surprisingly, it has an unique N-terminal extension before PHR domain. This N-terminal extension consists of a signal peptide (first 40 amino acid residues) which contains signal sequences for import into chloroplasts and mitochondria (this signal peptide is cleaved off after import) and of a further sequence of about 45 amino acid residues that comprises putative DAS motif (or DAS motif-like sequence).

In the C-terminal region amino acids exhibit high homology of the folate and deaza-flavin photolyase classes, therefore, FAD seems to be located in C-terminal region [43]. Almost all residues are known to be important for chromophore binding in cryptochrome. Cryptochromes share much higher sequence similarity in N-terminal PHR domain than in C-terminal region [78].

The C-terminal domain of cryptochromes contains motifs as the DQXVP-acidic-STAES (DAS domain), but in cry3 the N-terminal domain contains DAS domain (Fig.2.15). In this region three recognizable motifs exist and they are DQXVP, E/D and STAES. The role of the STAES is known to be a protein phosphorylation site but the function of the DAS domain is not yet clear [73].

Cryptochromes are expressed in many plants like *Arabidopsis thlaiana*, *Chlamydomonas reinhardtii*, rice and *physcomitrella patens*. Most plants studied so far contain multiple cryptochromes [76]. For example, CRY in tomato and barley have three cryptochrome genes, CRY1a, CRY1b, and CRY2 [78]. Recently CRY3 has been found in *Arabidopsis thlaiana* [41]. Its biological function is not yet known [50]. Specially many studies of *Arabidopsis* cry1 and cry2 suggest their function of the de-etiolation which regulate inhibition of hypocotyls elongation, stimulation of cotyledon opening, change of gene expression, and induction of chloroplast development.

Phototropin also regulates on blue light inhibition of plant growth, however, phototropin corresponds in initial inhibition and cryptochromes is associated with the maintenance of the growth inhibition [79].

Cry1 mutants reduce the inhibition of hypocotyls1 elongation by illumination of blue-light [80]. An overexpressed CRY1 of *Arabidopsis* has shorter hypocotyls elongation than wild type when grown in blue light and this indicates that CRY1 is also an important factor in plant growth [75]. An overexpressed CRY2 mutant also has a weak response on long-hypocotyl seedings in blue light. Continuous exposure makes long hypocotyls, if the intensity

24
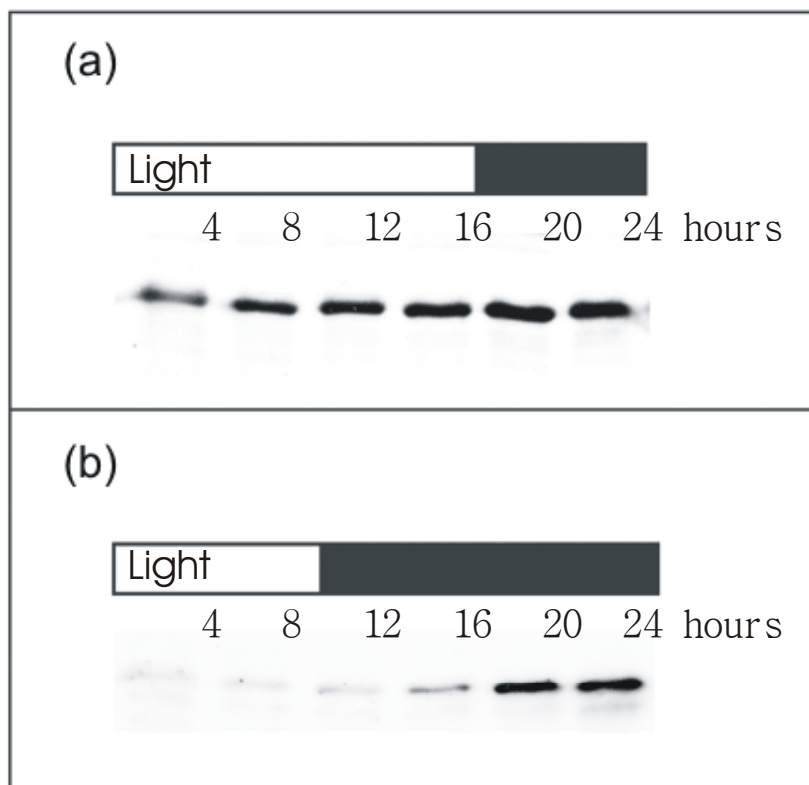
Fig. 2.16   Immunoblot of *Arabidopsis thaliana* CRY2 under blue light illumination for 7 day old seedlings [85]. Open bars represent light periods and solid bars represent dark periods.
(a) Protein levels of seedlings under 16-hr-blue light illumination/8-hr-dark conditions (b) Protein levels of seedlings under 8-hr-blue light illumination/16-hr-dark conditions. The cycle of the CRY2 protein level is not apparent in plants grown in (a). In (b) CRY2 protein level is apparent (lower during the day but higher in the night).

of blue light is high, then the CRY2 protein is degraded and the response on blue light disappears [81]. An *Arabidopsis* cry1 mutant is defective in thocyanin accumulation [82]. An *Arabidopsis* cry2 mutant reduces opening of cotyledon development in blue light [83].

The result of immunoblot at different times of illumination of *Arabidopsis* shows that the CRY1 protein is not affected by light [76]. But CRY2 protein level shows a photoperiod-dependent diurnal cycle as shown in Fig. 2.16 [85]. This photoperiod is consistent with photoperiodic flowering, which is controlled by a network of signal transduction such as day length and the photoperiod [81,84].

The cry1 regulates the floral initiation [86]. An *Arabidopsis* cry1 mutant causes later flowering compared to the wild type. A cry2 mutant also causes later flowering and longer photoperiods than the wild type. The cry2 photoresponse depends on light illumination wavelength because of interaction between cryptochromes and phytochromes (Phy) [87]. This interaction effects the flowering time under natural light condition. PhyA mediates flowering by illumination with far-red light. A PhyA mutant fails to flower upon far-red light illumination. The illumination of a cry2 mutant with far-red light stimulates the phyA activity and this compensates the loss of the CRY2 gene, as a result the cry2 mutant can promote flowering [80,88].

Animals have an innate *circadian clock*. *Circa* means about, *dies* means day. Any response to photoperiod requires a method of keeping time and that is *clock*. These are rhythms of biological activities that repeat over a period of approximately 24 hours even under constant environmental conditions. Under constant light conditions the cycles may drift out of phase with the environment.

Cryptochrome in animals regulates on the circadian clock by the entrainment. This is well established in *Drosophila*. Transgenic flies with overexpressed cryptochrome showed increased circadian photosensitivity [89]. A mouse cry mutant retained its ability to mediate light input. Mice without mCRY1 and mCRY2 miss normal response on daylight and dark condition [90].

In *Drosophila* cryptochrome exerts its function on the circadian clock by physical interaction with PER(period), TIM(timeless), CLK(clock), and CYC(cycle) [91]. PER and TIM are negative regulators and CLK and CYC are positive regulators. CLK and CYC are basic helix-loop-helix-PAS proteins. They activate the transcription of clock-regulated genes, *PER* and *TIM*. The transcription of the clock genes *PER* and *TIM* is negatively regulated on their own gene products. PER and TIM form heterodimers in the cytosol. They enter the nucleus to retain their own transcription. The interaction between cryptochrome and TIM

controls a light-dependent function. This interaction results in sequestration of TIM [92]. Animals without PER and TIM reduce their sensitivity to blue light and abrogate the circadian behaviour. A mouse cry double mutant retained its ability to mediate light input, but if the mouse also has a retinal degenerative mutant then it has an irregular cycle [93].

The photoresponse of cryptochrome seems to be similar to the redox reaction with electron transfer in photolyase [94]. The N-terminal domain is classified α/β class, while α helices are abundant in the C-terminal domain. FAD is bound in the center of the α helical domain. The folate is the light-harvesting chromophore. It is bound to a cleft between a α/β domain and a α helical domain [55]. The light-harvesting chromophore captures the energy of light. This captured energy is transferred to FAD. The crystal structure of *Arabidopsis thaliana* CRY1-PHR contains only FAD, while *E. Coli* photolyase contains both FAD and folate. The important function of the C-terminal domains is the regulation of phototransduction.

Since CRY1 is currently the best available model for cryptochrome signal transduction, CRY1 is much studied in photoactivation. Upon blue light illumination CRY1 in *Arabidopsis thaliana* undergoes neutral flavin radical reaction with Trp (W) and Tyr (Y) [95]. During the photo-cycle a proton transfer occurs from Asp (D) or Gln (Q) to flavin [38]. Even though CRY1 in *Escherichia coli* possesses MTHF as second chromophore [96], the N-terminal PHR domains is devoid of MTHF in crystal structure studies with a resolution of 2.6 Å [58]. In transient spectral studies dark-adapted cry1 was found to have FAD_{ox} non-covalently bound, and upon light illumination FAD_{ox} is converted to $FADH^\bullet$ [97]. At light switch-off a back-reaction is observed. A present involvement of MTHF is not seen.

The fluorescence lifetime of excited MTHF in VcCry1 cryptochrome from *Vibrio cholerae* is 845 ps [47] and the lifetime of excited *E. coli* photolyase is 354 ps [48]. The fluorescence lifetime for cryptochrome is more than 2 times longer than that in photolyase. VcCry1 cryptochrome is in a more hydrophobic and rigid environment than *E. coli*

photolyase. The energy-transfer from MTHF to $FAD_{red}H^-$ in VcCry1 cryptochrome is 60 ps [47] and that in photolyase is 292 ps [48], so the energy-transfer process in cryptochrome is more than 4 times faster than that in photolyase. This indicates the VcCry1 cryptochrome has a shorter distance or a more favourable orientation of the two chromophores.

2.3 BLUF-Domain

BLUF is a short writing for sensor for *B*lue *L*ight *u*sing *F*lavins. BLUF-domains are the members of the blue-light receptor family. BLUF-domains are involved in cellular signaling processes in the photosynthesis [98]. There are several types of BLUF-domains, which are AppA [99] and BlrB [100] in *Rhodobacter sphaeroides*, PAC (photo-activated adenylylcyclase) [101] in the alga *Euglena gracilis*, Slr1694 (designated as PixD) [102] in cyanobacterium *Synechocystis*. Sp. PCC6803 [102], YcgF [103] in *Escherichia coli*, and Tll0078 [104] in cyanobacterium *Thermosynechococcus elongatus* BP-1. A common feature of BLUF-domains is a red-shift in S_0-S_1 absorption upon UV-blue light illumination. This is caused by a local change of the flavin binding site.

BLUF-domains bind FAD noncovalently in the N-terminal region, however the C-terminal regions are distinct domains that have different function in each BLUF-domain [105]. For example, in *Escherichia coli* an EAL domain exists in the C-terminal region, and YcgF has an EAL domain which causes the cyclic phosphodiesterase behaviour [106]. The EAL domain in YcgF has cyclic-di-GMP phosphodiesterase activity.

The full name of AppA is *A*midino*p*henyl*p*yruvic *A*cid. The AppA protein has a cystein-rich C-terminal domain [98]. AppA is a regulator of light and redox signals [99]. AppA activates *puc* expression and regulates the expression of the photosynthesis gene as antirepressor by light and high oxygen tension [107]. AppA acts by the interaction with the repressor PpsR [107]. When the oxygen content in the environment decreases, AppA binds to
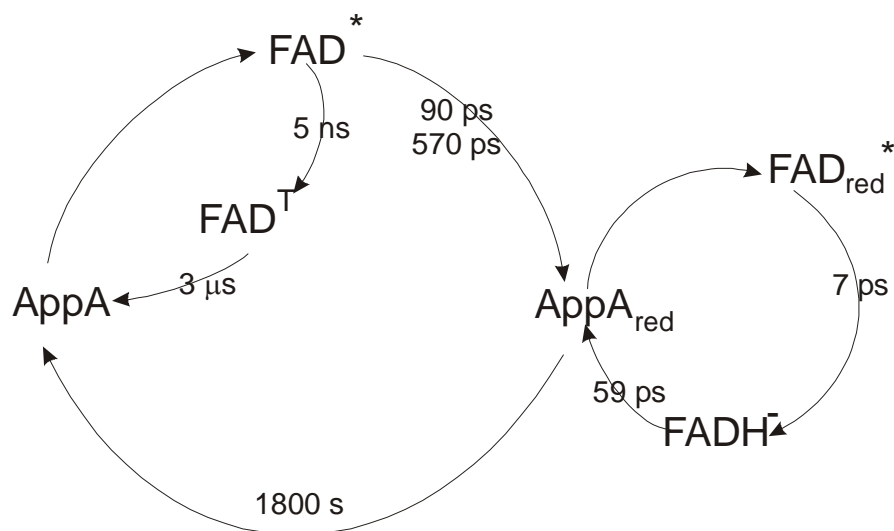
Fig. 2.17   The photocycle of AppA from *Rhodobacter sphaeroides* by the species-associated difference spectra [109,110]. AppA$_{RED}$ indicates the red-shifted product state. Right part shows the photocycle of AppA signaling state [110].

PpsR for restraining the transcription of the photosynthesis genes. This interaction is disrupted by blue light illumination and the repressor activity of PpsR is restored.

Dark adaptable AppA has two absorption peaks at 370 nm 447 nm [108]. After blue light-exposure the spectrum shows a red-shift. It reverts to the ground state in dark (Fig. 2.17) [109,110].

BlrB is an abbreviated word of putative *b*lue-*l*ight *r*eceptor *B*. FAD is the physiological cofactor of BLUF domain [100]. The dark-adapted BlrB consists of two-protein conformations with sub-nanosecond fluorescence lifetimes. The light-adapted BlrB is the putative signaling state. Excitation of the signaling state causes the formation of the FAD semiquinone form. This semireduced form further reduces. In the dark the reduced BlrB gets re-oxidized.

2.4 PYP (Photoactive Yellow Protein)

PYP (*P*hotoactive *Y*ellow *P*rotein) is a photoreceptor that has been found in several purple bacteria [111]. PYP has attracted further attention as the structural prototype for the Per-Arnt-Sim (PAS) [112] and LOV domains of a large class of receptor proteins. PYP is a member of xanthopsin, which is one family of blue-light photoreceptors. The first studied example was a bright-yellow protein found in a purple phototrophic bacterium, *Ectothiorhodospira halophila* (E-PYP). PYP is a 125-residue photoreceptor protein.

PYP has *p*-coumaric acid as chromophore binding to the cysteine residue at the position 69 via a thiol-ester linkage as shown in Fig. 2.18 [113,114]. In the ground state the chromophore *p*-coumaric acid (4-hydroxy-cinnamic acid) resides in the trans configuration and is deprotonated [115].
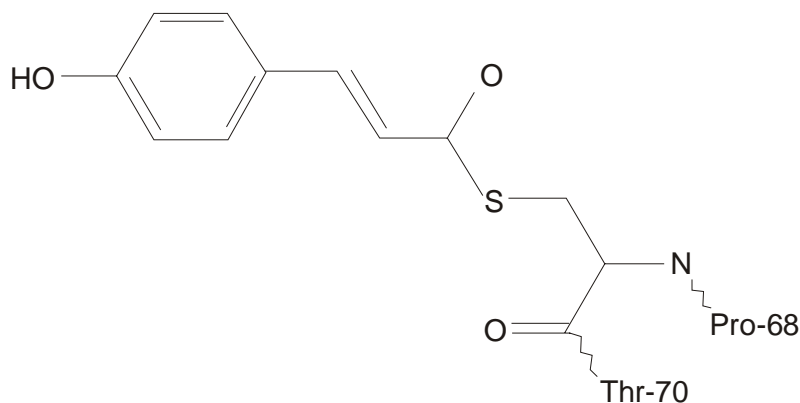

Fig. 2.18   The imidazole esters of 4-hydroxy-cinnamic acid react with the single cysteine (Cys 69) of PYP (*Escherichia coli*).

31

The PYP is a small cytosolic photoreceptor. PYP is responsible for the negative phototactic response, which is a blue-light-induced avoidance response [116]. PYP serves as the structural prototype for the widely-distributed PAS domain class of signal transduction, which is a key element in biological signal transfer [117].

Upon photon absorption PYP undergoes a photocycle in which several distinct intermediates are formed. The covalently bound 4-hydroxy cinnamate chromophore of PYP enters a cyclic chain of reaction is as shown in Fig. 2.19 [118]. The photocycle includes the isomerization and the protonation of the chromophore, in addition to a partial protein unfolding.

The absorption maximum of the initial pG state is at 446 nm [119]. The blue light absorption induces an isomerization of the double bond in the chromophore [120]. The chromophore in pG is deprotonated and buried in a hydrophobic pocket of the protein where
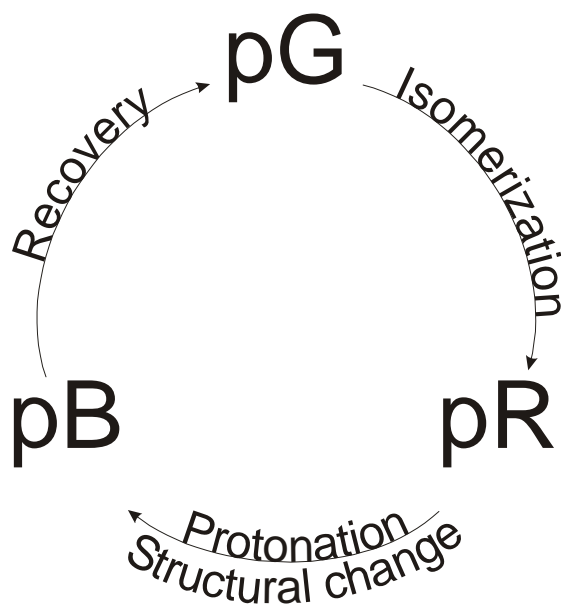
Fig. 2.19   The photocycle of PYP (Photoactive Yellow Protein) has two intermediates. pG is the ground state. The absorption spectrum is red-shifted upon light illumination. pR is formed on a pico- to nano-second time scale. pR is blue-shifted to 355 nm, forming the intermediate pB. pB is reverted to the initial pG state in the dark.

its negative charge is stabilized via a hydrogen bonding network.

Within a few nanoseconds an intermediate is formed with a red-shifted absorption spectrum (λ_{max} = 465 nm) [121]. This intermediate is named pR. pR decays into a blue-shifted intermediate (λ_{max} = 355 nm) with time constants of 200 µs and 1.2 ms [120,122]. This intermediate is named pB. This latter transition is accompanied by protonation of the phenolic oxygen of the chromophore and by subsequent conformational changes of the protein (partial unfolding) [123,124]. It is suggested that pB is the signaling state of PYP [125].

pB recovers to the ground state pG by a bi-exponential process with time constants of 200 ms and ~1 s [123]. The photocycle is very sensitive to both temperature and pH [126].

The PYP-phytochrome fusion protein, Ppr from *Rs. Centenum*, has a PYP amino-terminal domain and a central domain with similarity to phytochrome [127]. Ppr regulates the chalcone synthase gene expression in response to blue light [127,128]. Ppr provides phosphorylation to a signal transduction cascade under illuminated conditions. The biological function of the PYP was first identified with Ppr.

3. Experimental Procedures

3.1 Samples

The dye (6R,S)-5,10-Methenyl-5,6,7,8-tetrahydrofolic acid chloride (MTHF-Cl), folic acid and (6,R,S)-5-Formyl-5,6,7,8-tetrahydrofolic (5-formyl-THF) were purchased from commercial company (Schircks Laboratories, CH-8646 Jona, Switzerland). The aqueous solution for dissolving these materials stands on Millipore water. The pH value of aqueous solution was adjusted with HCl in acid regime and with NaOH in basic regime. Final pH value of aqueous solution is confirmed with digital pH meter (Orion Research).

The dye FAD was purchased by Sigma (flavin adenine dinucleotide disodium salt hydrate, order number F 6625) and was used without further purification.

The LOV1/2 domains were prepared by the group of professor Hegemann [24]. The preparation of cry3 was done by the group of professor Batschauer [94].

3.1.1 LOV1/2 domain Preparation

A DNA-sequence encoding 15 histidines was inserted into the EcoRI-site of the *E. coli* expression vector pMALC2x (New England Biolabs, Frankfurt, Germany) giving the vector His-pMALC2x. The LOV1/2-encoding gene fragment (base paris 170 to 1130) from the full-length cDNA clone (Acc. No: AV 394090) of the *Chlamydomonas reinhardtii* phot was inserted in frame to the His-tag sequence of His-pMALC2x. A TEV-protease restriction site was included into the EcoRI site. The protein, carrying a maltose binding-protein fusion at the *N*-terminus, a TEV site and 15 His (LOV1/2-MBP), was expressed in *E. coli* strain BL21 as shown in Fig 3.1. The protein with a calculated molecular weight of 81021.46 g mol^{-1} was purified via Amylose Resin (New England Biolabs, Frankfurt, Germany) according to the supplier's instructions.

10 mM phosphate buffer was made by mixing of 10mM Na_2HPO_4, and 10mM NaH_2PO_4. 10mM NaH_2PO_4 aqueous solution is added to 10mM Na_2HPO_4 aqueous solution as 1 : 8.19 ratio. Thereby a pH value of the solution of about pH 8.0 is obtained. Subsequently, NaCl is added to get a concentration of 10mM NaCl. The LOV1/2-MBP-fusion protein was diluted in this 10 mM phosphate buffer, pH = 8, 10 mM NaCl, 100 mM phenylmethanesulfonyl fluoride (PMSF). For the production of LOV1/2-His, the MBP-encoding DNA-segment was excised

from the plasmid and the protein, carrying 15 His at the N-terminus end was expressed in *E. coli* strain BL21. The protein with a molecular weight of 36738.54 g mol^{-1} was purified via

Ni-NTA resins according to the instructions of the supplier (Quiagen, Hilden, Germany). The LOV1/2-His protein was diluted in 10 mM phosphate buffer, pH = 8, 10 mM NaCl, 100 mM phenylmethanesulfonyl fluoride (PMSF). LOV1/2-MBP is kept at −20°C in dark. Before measuring the sample brought to 0°C environment for 2 hours and then moved to the measurement cell to avoid sample denaturation.
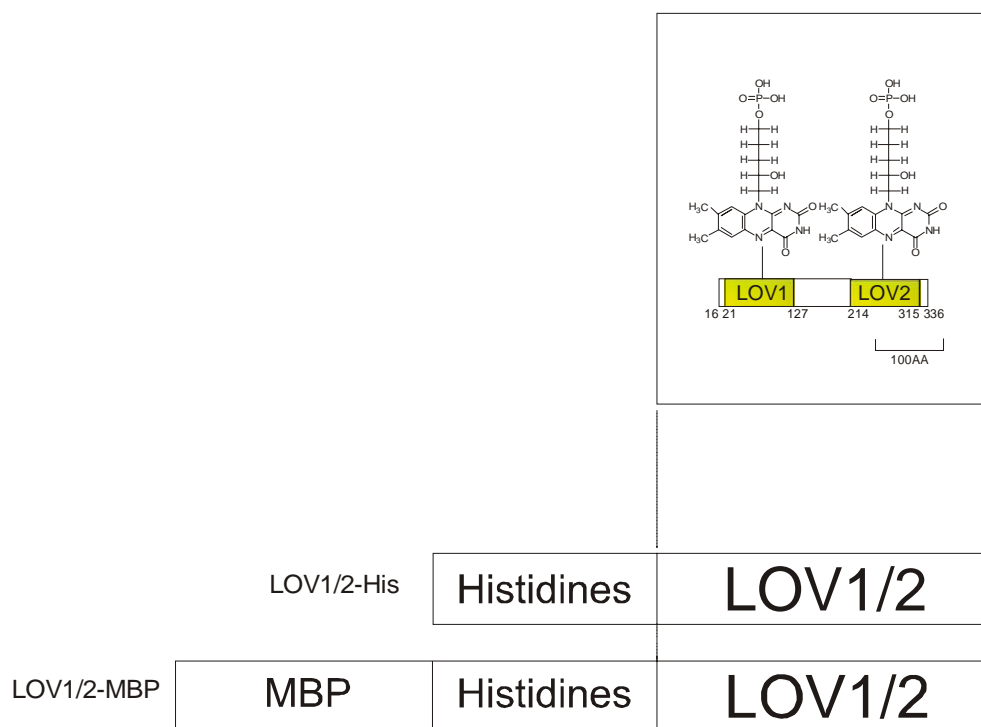

Fig. 3.1 Primary structures of LOV1/2-MBP and LOV1/2-His.
LOV1/2-MBP : LOV1/2 protein is captured by 15 histidines and MBP at the N-terminal region and dissolved in pH 8 phosphate buffer.
LOV1/2-His : LOV1/2 protein is captured by 15 histidines at the N-terminal region and dissolved in pH 8 phosphate buffer.

3.1.2 Cryptochrome 3 Preparation

Cloning, expression in *E. coli* and chromatographic purification of cry3 has been described in Ref. [94]. In brief, cry3 was overexpressed in *E. coli* M15[pREP4] cells that were grown after IPTG (iospropylthiogalactosid) induction in 1.5 l of LB medium containing 100 μg ml^{-1} ampicillin and 25 μg ml^{-1} kanamycin at 30°C for 12 h by shaking at 250 rpm. The overexpressed cry3 protein was then purified by the following chromatography steps on the ÄKTApurifier (Amersham Biosciences, Buckinghamshire, UK): By Ni^{2+}-affinity chromatography on a HisTrap HP column, by Heparin chromatography on HiTrap Heparin HP column, and finally by size-exclusion chromatography on Superdex 200 GL column in buffer containing 50 mM Na-phosphate pH 7.5, 200 mM NaCl, 10 mM β-mercaptoethanol and 10 % glycerol. The final concentration of NaCl in the sample was adjusted to 50 mM, the other components remained unchanged (this final composition of the buffer is abbreviated as pH 7.5 buffer). Purified cry3 was concentrated to about 3-10 mg ml^{-1} as estimated by the Bradford method and analyzed by SDS-PAGE under reducing conditions. The identity of cry3 was confirmed by MALDI-TOF MS analysis. The cofactor composition and the ratio to cry3 apoprotein was determined after apoprotein precipitation with 7.2 % (final, 440 mM) TCA (tricarboxylic acid) on ice for 1h with shaking at 100 rpm followed by separation of the released cofactors by reversed phase chromatography on Nucleosil 100-10 C18 column connected to the ÄKTApurifier (Amersham Biosciences, Buckinghamshire, UK) and pre-equilibrated with a 9:1 mixture of phosphate-citrate buffer pH 2.5 (10 mM Na$_2$HPO$_4$ and 45 mM citric acid) and methanol. Upon releasing from the apoprotein, all different redox states of flavin should be converted to the oxidized form due to oxidation by air oxygen.

Precipitated apoprotein was pelleted at 20000 g and 4 ˚C for 10 min, re-suspended in 1 M NaOH at 70˚C for 10 min, its absorption spectrum was taken to ensure that it contains no remaining cofactors and its molar amount was estimated based on its absorbance, A_{280}, at 280 nm using the theoretical value of molar extinction coefficient at 280 nm for cry3 with no cystine (110950 M^{-1} cm^{-1}) calculated by ProtParam software on ExPASy Proteomics server (www.expasy.org). Supernatant containing released cofactors was 9-times diluted into the phosphate-citrate buffer pH 2.5 (final composition after dilution was as above) containing 49 mM NaOH (for neutralization of TCA), filtered through 0.2 μm filter (Sarstedt, Nümbrecht, Germany), mixed 9:1 with methanol and injected to the column. Cofactors were separated and eluted from the column using a continuous linear gradient of methanol (60-80 %) mixed with the aforementioned buffer and monitored by absorption at 360 nm (both MTHF and oxidized flavin species) and 450 nm (only oxidized flavin species). For comparison, known amounts of each standard (MTHF-Cl, FAD, FMN and riboflavin) were processed analogously and aliquots corresponding to 5 nmols were separated as above. Based on the elution peak area ratios between cofactors released from cry3 and corresponding standards, a 1:1 MTHF to FAD ratio was found within the experimental accuracy while no other cofactor was present. The identities of released and separated cofactors were further confirmed by their absorption spectra which corresponded to those of standards (not shown). The ratio of cofactors to crptochrome 3 protein was estimated to be 0.8:1. ([FAD] = [MTHF] = $0.8 \times C_0$, where C_0 is the total cryptochrome 3 concentration). The sample was divided into several aliquots, flash-frozen in liquid nitrogen and stored at -80˚C or -20˚C. The yield of purified protein was 2-3 mg per liter of induced *E. coli* culture.

Fig. 3.2   Primary structure of At-Cry3, used for this study, without signal peptide.

3.2 Spectroscopic Techniques

Absorption spectra were measured with a commercial spectrophotometer (Beckmann ACTA M IV). The absorption coefficient α and the absorption cross-section $\sigma(\lambda)_\alpha$ are defined by,

$$\alpha(\lambda) = \frac{1}{l}\ln\frac{1}{T} = \varepsilon(\lambda)C \,,$$

$$\sigma(\lambda) = \frac{\alpha}{N_0} = \frac{\alpha}{C \cdot N_A} \,,$$
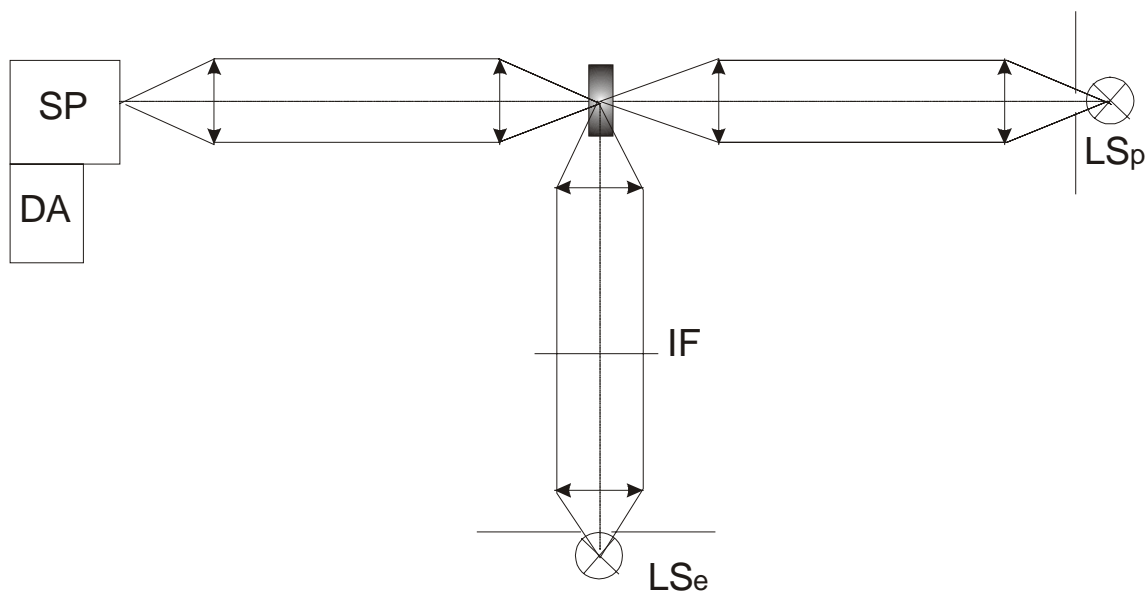
Fig. 3.3   Schematic representation of the experimental setup for transmission and absorption spectrum measurements. LS_p is a tungsten lamp for probe light and LS_e is a mercury lamp for exposure light. IF is the interference filter for selecting a certain wavelength. SP-DA is a spectrometer – silicon-diode-array detector.

where ℓ is sample length, N_0 is number density of molecules, and N_A is Avogadro number. $\varepsilon(\lambda)$ is the molar decadic extinction coefficient [Lmol^{-1}cm^{-1}]. C is the concentration in [mol/l].

For transient absorption measurements, a tungsten lamp and a mercury lamp are used as probing and excitation light. The experimental setup is shown in Fig. 3.3. In local region of the light path the sample is located. The size of used cell was 1.5 mm × 1.5 mm × 5 mm and the amount of sample for LOV domain and cry3 investigations was normally about 15 μl. A spectrometer – silicon-diode-array detection system was used for spectra recording (TN-1710 multichannel analyser with diode array rapid scan spectrometer system from Tracor Northern). A 200 W mercury lamp was used for sample excitation. The excitation wavelength was selected with an interference filter.

The intensity dependence of the absorption spectra was measured by light attenuating with neutral density filters. The temporal development of absorption spectra was studied by first measuring the spectrum with closed excitation path (dark spectrum). Then the sample was permanent exposed and spectra was recorded at certain times. After a certain time of light exposure the excitation light was switched off and the absorption spectra was recorded with the probe light at certain time positions to follow the sample recovery to the initial dark state.

The experimental setup for fluorescence measurement is shown in Fig. 3.4. A front-face fluorescence collection arrangement is used similar to the Ref. [129].

The samples were excited with vertically polarized light. The fluorescence signal was detected under conditions of parallel, perpendicular or magic-angle (54.7°) polarized light relative to the polarization direction of the excitation light. The degree of fluorescence polarization is defined by
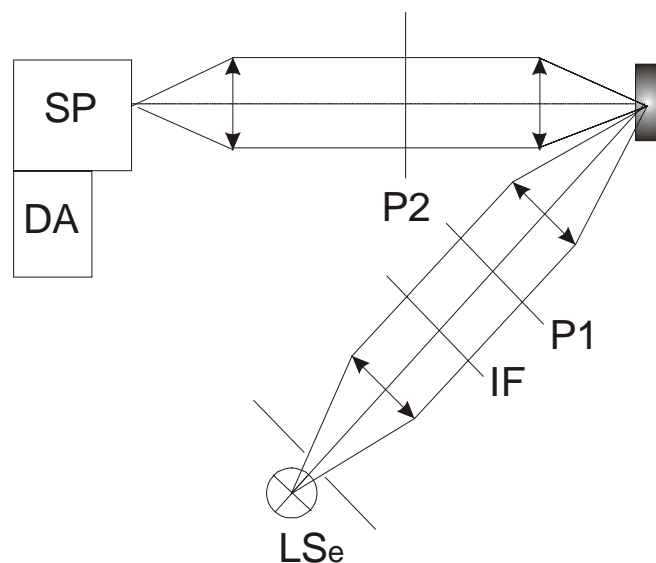
Fig. 3.4 Schematic representation of the experimental setup for fluorescence measurements. LS_e is light source (a mercury lamp). IF is the interference filter for selecting a certain wavelength. P1 and P2 are polarizers. SP-DA is a spectrometer – silicon-diode-array detector.

$$P = \frac{I_{//} - I_{\perp}}{I_{//} + I_{\perp}},$$

where $I_{//}$ is the intensity of the parallel polarized light and $I_{\perp}$ is the perpendicular polarized light intensity.

The fluorescence quantum distribution, $E_F(\lambda)$ was calculated under conditions of magic angle polarization from the fluorescence spectra by using reference dyes of known fluorescence quantum yield. The fluorescence quantum yield, ϕ_F was calculated by integration over the fluorescence quantum distribution,

$$\phi_F = \int E_F(\lambda) d\lambda.$$

For light exposure at λ_{exc} =365nm, quinine-sulphate dihydrate in 1 N H_2SO_4 was used as reference dye. For 428 nm exposure coumarin 314T in ethanol was used as fluorescence standard. The fluorescence quantum yield of quinine-sulphate dihydrate is $\phi_{F,R} \approx 0.546$ [130] and that of coumarin is $\phi_{F,R} \approx 0.87$ [131].
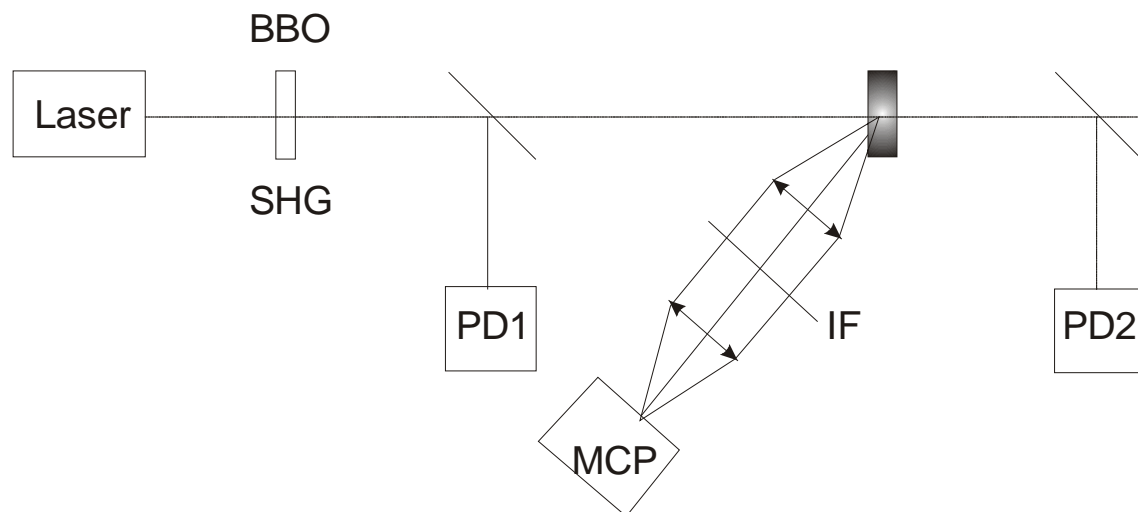
Fig. 3.5   The experimental setup of femtosecond laser system. IF is interference filter, SHG is second harmonic generator and MCP is micro-channle-plate photomultiplier.

For cryptochrome3, most fluorescence studies were carried with an intensified silicon-diode-array detector (OMA system from EG&G Princeton Applied Research) to avoid changes of the sample condition by the necessary light for fluorescence probing.

Fluorescence lifetime measurements have been carried out with second harmonic light pulses of a mode-locked Ti:sapphire laser [132]. A schematic arrangement is shown in Fig. 3.5. The used laser system was the Hurricane system from Spectra-Physics. The laser operates at 800 nm. For the experiments the second harmonic at 400 nm was used (generated in BBO crystal [133]). The input energy was detected with a silicon photodiode PD1. The fluorescence was detected with a micro-channel-plate photomultiplier (MCP) from Hamamatsu (type R1564-U01) and the photomultiplier signal is recorded with a fast digital oscilloscope (600 MHz analogue bandwidth, digitizing rate 10^{10} samples per second). The fluorescence light was filtered with an interference filter. The polarization was selected with a thin film polarizer sheet. The transmitted energy through the cell was detected with a silicon

photodiode PD2. The laser pulse duration (FWHM), was set to $\Delta t_L \approx 120$ fs for the LOV domain measurements and it was set to $\Delta t_L \approx 3.5$ ps for the cry3 measurements.

The first absorption band of MTHF peaks at around 360 nm region, therefore the fluorescence lifetime measurements on MTHF were carried out with second harmonic pulse of a mode-locked ruby laser [134]. The excitation wavelength is 347.1 nm, and the pulse duration time was 35 ps.

4. Results and Discussion I :

LOV1/2 Domain

4.1 Dark-Adapted Behaviour
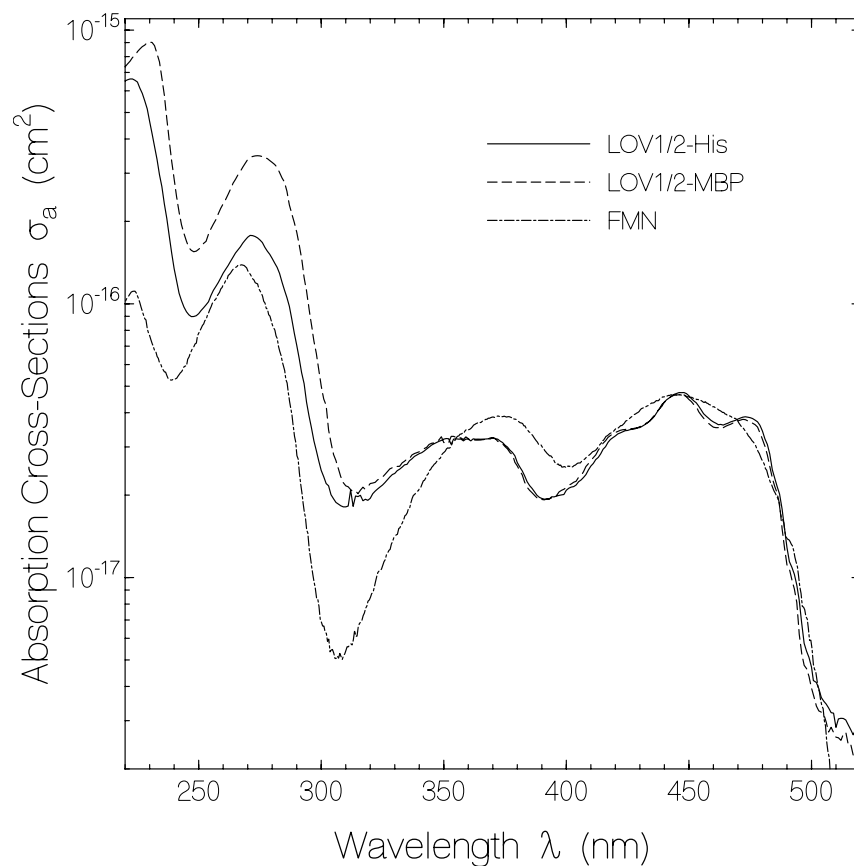
Fig. 4.1   The absorption cross-section spectra of LOV1/2 His and LOV1/2 MBP of phot from *Chlamydomonas reinhardtii* in pH 8 aqueous solution. The absorption cross-section spectrum of FMN in neutral aqueous solution is included.

44

The absorption cross-section spectra, $\sigma_a(\lambda)$, of LOV1/2-His and LOV1/2-MBP are shown in Fig. 4.1. The solid curve is for LOV1/2-His and the dashed curve is for LOV1/2-MBP. The two absorption cross-sections are similar in the visual region.

The absorption cross-section spectrum of FMN in neutral aqueous solution is included for comparison. Since the number density of the LOV domains is unknown the absorption cross-section, $\sigma_a(\lambda)$ of LOV1/2 domain is determined by normalization to the absorption spectrum of FMN (same absorption cross-section integral for $\lambda > 310$ nm). The absorption of amino acids of the proteins sets in below 310 nm.

The dark-adapted fluorescence quantum distributions, $E_F(\lambda)$, of LOV1/2-His and LOV1/2-MBP are shown in Fig. 4.2 (a). For these measurements the LOV domain samples were kept in the dark state during measurement by circulating the samples with a magnetic stirrer in a 4.0 mm $\times$ 10 mm $\times$ 35 mm quartz glass cell. The fluorescence quantum distribution of LOV1/2-His is represented by the solid line and the dashed line curve belongs to LOV1/2-MBP. The fluorescence quantum distribution, $E_F(\lambda)$ of LOV1/2-MBP is a little bit larger than $E_F(\lambda)$ of LOV1/2-His. The fluorescence quantum yield, ϕ_F is obtained from the relation, $\phi_F = \int E_F(\lambda)d\lambda$. The fluorescence quantum yield ϕ_F of FMN is 0.26 [135]. The fluorescence quantum yield of LOV1/2-His is 0.15 and that of LOV1/2-MBP is 0.17. These values are collected together with the LOV single-domain values in Table 1. The LOV single-domains values are taken from [136] (LOV1-His), [137] (LOV1-MBP), [138] (LOV2-His), and [24] (LOV2-MBP).

The fluorescence quantum yield of the LOV1 domain has a value of 0.17 for both the His-tag and the MBP-tag. For LOV2-His the fluorescence quantum yield is 0.12, while for LOV2-MBP, it is 0.07. Comparing the LOV1/2 double domain with the LOV1 and LOV2 single-domains, the fluorescence quantum yield of LOV1 is similar to that of the LOV1/2 domain.

45

The degrees of fluorescence polarization, $P_F(\lambda)$, of LOV1/2-His and LOV1/2-MBP are shown in Fig. 4.2(b). From the degree of fluorescence polarization, P_F, the reorientation time, τ_{or}, of the S_1-S_0 transition dipole moment can be calculated by the relation [140].

$$\tau_{or} = \frac{1/P_{F,0} - 1/3}{1 - P_F/P_{F,0}} P_F \tau_F .$$

(4.1)

The fluorescence quantum yield, ϕ_F, the averaged fluorescence quantum distribution, $P_F(\lambda)$, and the reorientation times, τ_{or} of the LOV1/2 double domains are also collected together with the LOV single-domain values in Table 1.
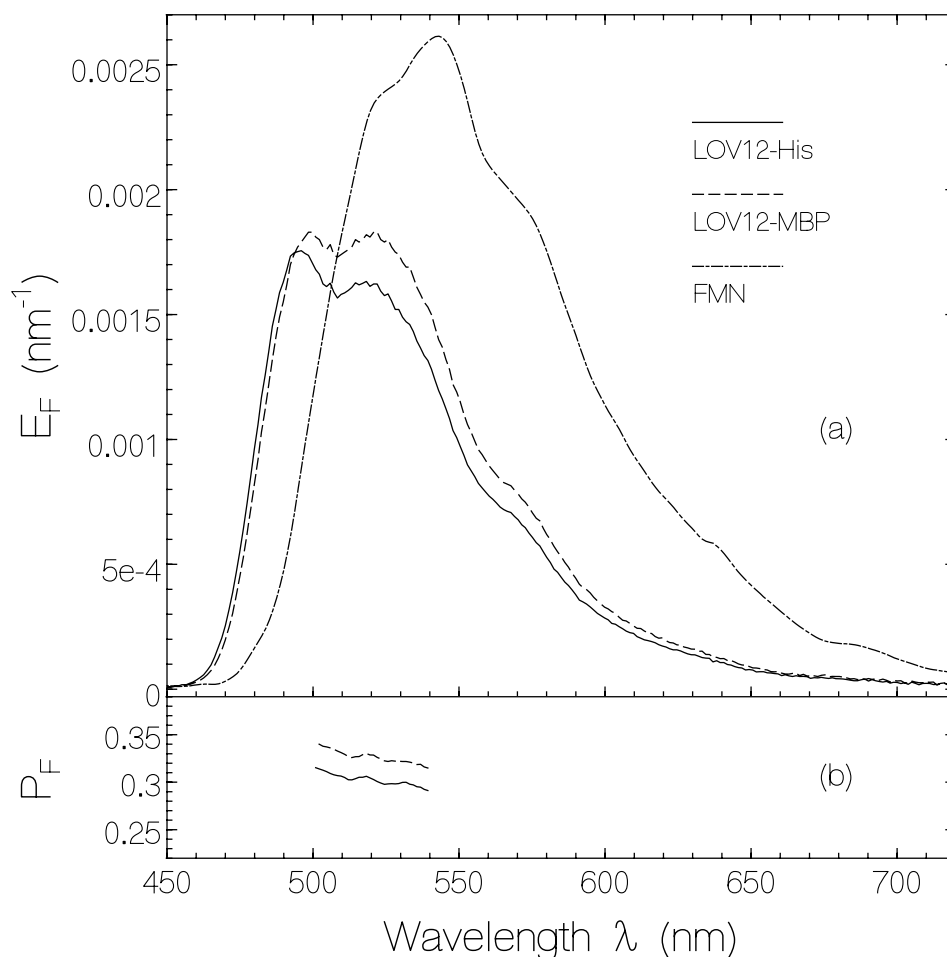
Fig. 4.2   (a) Dark-adapted Fluorescence quantum distributions, $E_F(\lambda)$, of LOV1/2-His, LOV1/2-MBP in pH 8 buffer solution, and of FMN in neutral aqueous solution.
(b) The degree of fluorescence polarization, $P_F(\lambda)$, of LOV1/2-His (solid curve), and LOV1/2-MBP (dashed curve).

Parameter	LOV1/2 -His	LOV1 -His	LOV2 -His	LOV1/2 -MBP	LOV1 -MBP	LOV2 -MBP	FMN pH 7
M (g mol^{-1})	36 738.54	15609		81 021.46			455.36
ϕ_F	0.152±0.01	0.17	0.12	0.166±0.01	0.17	0.08	0.26
τ_F (ns)	2.59±0.1	2.9	2.3	3.11±0.1	2.7	1.25	5.0
P_F	0.30	0.41	0.375	0.33		0.45	0.0146
τ_{or} (ns)	3.24	11	5.75	5.03		9.4	0.125
x_1	≈0.99	0.983	0.962	≈0.99	0.983	0.93	
x_2	≈0.01	0.017	0.038	≈0.01	0.017	0.07	
β_{nc}	≈0.02	0.082	0.07	≈0.04	0.05	0.07	
β_f	0.61	0	0.476	0.74	≈ 0.37	≈ 0.67	
β_s	0.39	1	0.524	0.26	˜0.63	≈ 0.33	
$\tau_{Ad,f}$ (s)	30		19	100	˜61	41	
$\tau_{Ad,s}$ (min)	8.7	5.8	5.5	8.1	˜7	10	
ϕ_{Ad}		0.5	0.9		0.6	0.9	
$\phi_{Ad,0}(\lambda_{exc}=470nm)$	0.1			0.4			
$\phi_{Ad,1}(\lambda_{exc}=470nm)$	0.05			0.2			
$\phi_{Ad,0}(\lambda_{exc}=428nm)$	0.2			0.4			
$\phi_{Ad,1}(\lambda_{exc}=428nm)$	0.1			0.2			
$\phi_{Ad,0}(\lambda_{exc}=365nm)$	0.11			0.4			
$\phi_{Ad,1}(\lambda_{exc}=365nm)$	0.08			0.05			

Table1. Photochemical parameters of LOV domains from *Chlamydomonas reinhardtii* in aqueous solution. Data for LOV1 and LOV2 are from [24,137,138].

The full names of the abbreviated parameters: M: molar mass; ϕ_F: the fluorescence quantum yield; τ_F: the fluorescence lifetime; P_F: the degree of fluorescence polarization; τ_{or}: S_1-S_0 transition dipole moment reorientation time; x_1: mole-fraction of non-covalently bound FMN; x_2: mole-fraction of free FMN; β_{nc}: fraction of non-covalently bound FMN not convertible to adduct state; β_f: fraction of non-covalently bound FMN which forms fast recovering adduct; β_s: fraction of non-covalently bound FMN which forms slow recovering adduct. $\tau_{Ad,f}$ and $\tau_{Ad,s}$: fast and slow adduct recovery times, respectively; ϕ_{Ad}: quantum efficiency of adduct formation (for mono-domains); $\phi_{Ad,0}$ and $\phi_{Ad,1}$: quantum efficiencies of adduct formation for the first FMN and for the remaining second adduct, respectively.

Despite the fact the ϕ_F of LOV1 is near to that of LOV1/2, the degree of fluorescence polarization, $P_F(\lambda)$ of the LOV1/2 domains is lower than that of the LOV1. The estimated reorientation times, τ_{or} of the LOV1/2 domain is shorter than that of the LOV single-domains despite of larger size of the LOV1/2 domain compared to single-domains. The shorter reorientation time of the LOV1/2 domain indicates the FMN molecules in the LOV1 and LOV2 domain of LOV1/2 domain are not exactly parallel oriented, and that Förster type energy transfer between the two FMN molecules occurs.

Photo-induced reductive electron transfer between FMN and amino-acids (Tyr (Y), Trp (W), His (H), Cys (C), and Phe (F)) in the LOV domains is thought to be responsible for the reduction of fluorescence quantum efficiency and the shortening fluorescence lifetime of non-covalently bound FMN in the LOV1, LOV2 and LOV1/2 domains [24]. Subtle distance changes between amino acid residues as electron donors and the FMN as electron acceptor determine the efficiency of photo-induced electron transfer [141].

An estimate of the efficiency of Förster-type energy transfer is given in the following: Assuming that the shape of the LOV1/2-double domain is spherical, the volume of the LOV1/2-His domain is given by

$$V = M /(N_A \rho) = (\pi / 6)d^3 ,\tag{4.2}$$

where mass density $\rho = 1$ g cm^{-3}, molar mass $M \approx 36700$ g mol^{-1}, and N_A is the Avogadro number. d is the molecule diameter.

Diameters, $d \approx 4.9$ nm for LOV1/2-His and $d \approx 6.4$ nm for LOV1/2-MBP are obtained. The rate of fluorescence emission is $k_F = \tau_F^{-1}$ (in energy transfer between equal molecules the fluorescence lifetime remains unchanged). The distance between the two FMN molecules in the LOV1/2 domains (one molecule excited, other in ground-state) is R_d, with $R_d \leq d$. The ratio of Förster-type energy transfer, k_{ET}, to fluorescence rate k_F is as follows [140,142~144]

$$\frac{k_{ET}}{k_F} = \left(\frac{R_0}{R_d}\right)^6 . \tag{4.3}$$

R_0 is the critical distance of energy transfer (Förster distance, at R_0 k_{ET} is equal to k_F) and it is obtained by the relation [142-144]

$$R_0^6 = \frac{9\overline{\kappa^2}}{128\pi^5 n^4} \int E_F(\lambda)\sigma_a(\lambda)\lambda^4 d\lambda , \tag{4.4}$$

where n is the average refractive index in the overlap region of absorption and emission. The orientation factor κ is determined by the orientation of the transition dipole moments of the interacting FMN molecules A and B according to [142]

$$\kappa = \cos(\varphi_{AB}) - 3\cos(\varphi_A)\cos(\varphi_B) , \tag{4.5}$$

where φ_A and φ_B are the angles of the transition dipole moments to the connection line between A and B, and φ_{AB} is the mutual angle between the transition dipole moments. Since the mutual angle in LOV1/2 domain is unknown, a statistical isotropic orientation of the transition dipole moments is assumed. In this case it is used as $\overline{\kappa^2} = 2/3$ [142].

Because of Eq. 4.4 the critical Förster distances are obtained to be R_0 (LOV1/2-MBP)= 6.4 nm and R_0 (LOV1/2-His)= 4.9 nm using these values and $R_0 \approx d/2 \approx 3$ nm gives (Eq. 4.3).

$$\frac{k_{ET}}{k_F} \approx 0.035$$

This ratio shows that some energy transfer occurs which may have the degree of fluorescence polarization and the reorientation time of the transition dipoles.

The temporal fluorescence signal traces of dark adapted samples, obtained after femtosecond laser pulse are shown in Fig 4.3. The fluorescence signals are normalized to a peak height of one. The response function of the detection system is shown as dotted lines. The fluorescence signal decay time is fitted by a single exponential function. The fluorescence
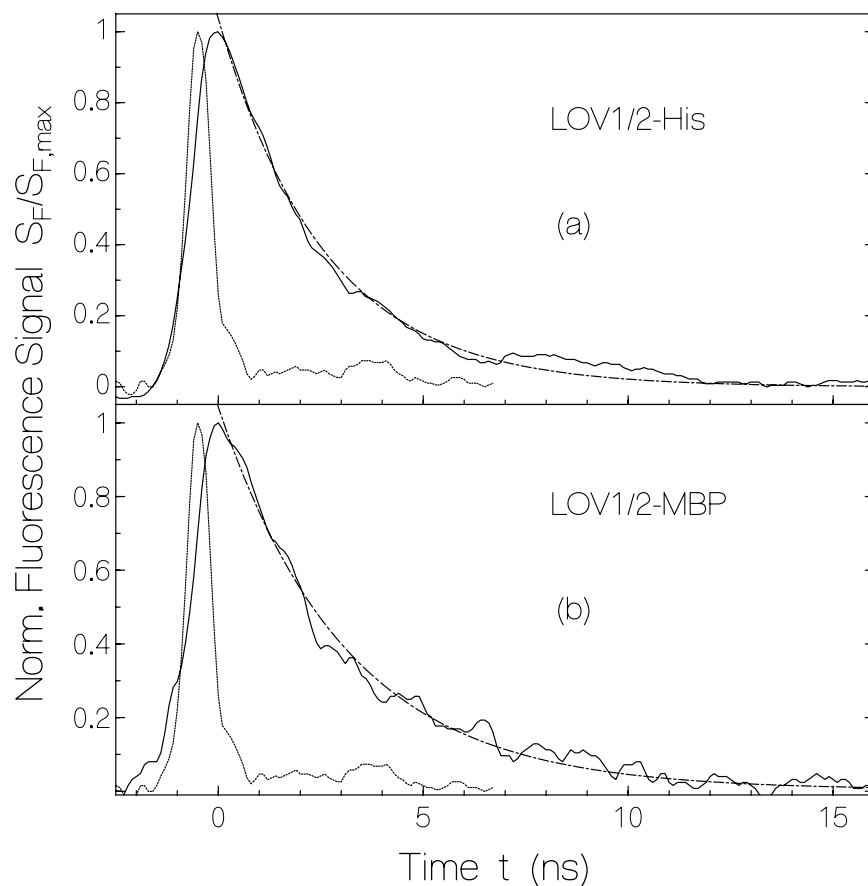
Fig. 4.3   Temporal fluorescence traces. Fluorescence excitation with laser pulses of Δt_L = 120 fs duration at wavelength of λ_L = 400 nm. Solid curves are normalized fluorescence signals. Dotted curves show system response function. Dash-dotted curves are single-exponential fits. Samples were dark adapted.
(a) Wild-type LOV1/2-His in pH 8 buffer solution. Time constant of fit curve, τ_F = 2.59 ns.
(b) Wild-type LOV1/2-MBP in pH 8 buffer solution. τ_F = 3.11 ns.

lifetime, τ_F for LOV1/2-His is 2.6±0.1 ns and the fluorescence lifetime for LOV1/2-MBP is

3.1±0.1 ns.

4.2 Light-Induced Behaviour

The intensity dependent absorption spectra are displayed for LOV1/2-His in panel (i) and for LOV1/2-MBP in panel (ii) of Fig. 4.4. The LOV1/2 domain was excited at various excitation wavelengths. Excitation wavelength in (a) is 470 nm, in (b) is 428 nm, in (c) is 365 nm, and in (d) is broad-band 365 ~ 440 nm regime. LOV domain samples are excited for a fixed exposure time of 4 min. Initially the absorption spectrum for the dark state of LOV domain is measured. Step by step the excitation light intensity was increased and between successive measurements the dark period was 5 min for back-reaction to dark state. For excitation intensities larger than 0.01 W cm^{-2}, the dark period was increased to 10 min.

The FMN S_0-S_1 absorption band around 446 nm and the FMN S_0-S_2 absorption band around 360 nm decreased with increasing excitation intensity. Between 380 nm and 410 nm the absorption rises. The initial ground state and the photoproduct share two isosbestic points, at 378 nm and 410 nm for LOV1/2-His, and at 381 and 411 nm for LOV1/2-MBP. The absorption peak at 390 nm belongs to the formed LOV-390. At the same excitation intensity, the absorption spectral change of LOV1/2-MBP is larger than that of LOV1/2-His.
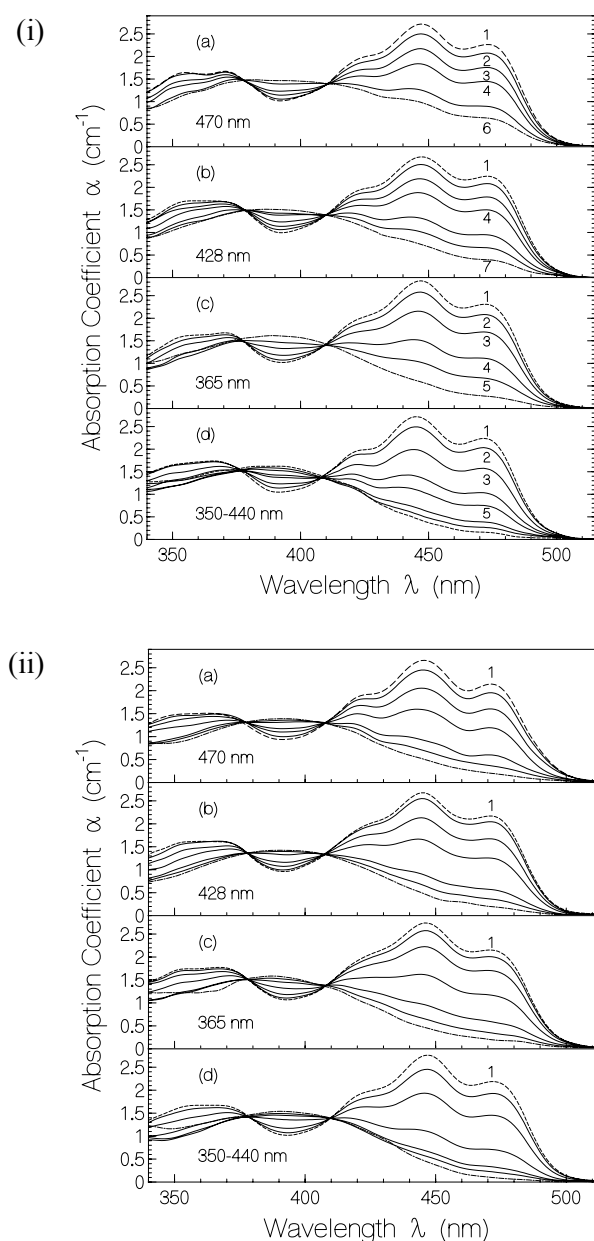
Fig. 4.4   Dependence of absorption-coefficient spectra, $\alpha(\lambda)$, on excitation light intensity for LOV1/2-His (i) and LOV1/2-MBP (ii). Curves are measured by successive increase of excitation intensity, λ_{exc}. Every interval time between measurements δt_{sep} was 5 min, only at maximum intensity δt_{sep} was 10 min.

For (i) the curves belong to
(a) $\lambda_{exc} = 470$ nm. (1) $I_{exc} = 0$, (2) 7.8×10^{-5} W cm^{-2}, (3) 2.9×10^{-4} W cm^{-2}, (4) 7.0×10^{-4} W cm^{-2}, (5) 3.3×10^{-3} W cm^{-2}, (6) 7.8×10^{-3} W cm^{-2}, and (7) 2.4×10^{-2} W cm^{-2}.
(b) $\lambda_{exc} = 428$ nm. $t_{exp} = 4$ min. (1) $I_{exc} = 0$, (2) 6.2×10^{-5} W cm^{-2}, (3) 2.7×10^{-4} W cm^{-2}, (4) 6.0×10^{-4} W cm^{-2}, (5) 3.5×10^{-4} W cm^{-2}, (6) 7.9×10^{-3} W cm^{-2}, and (7) 2.8×10^{-2} W cm^{-2}.
(c) $\lambda_{exc} = 365$ nm. $t_{exp} = 4$ min. (1) $I_{exc} = 0$, (2) 1.1×10^{-4} W cm^{-2}, (3) 3.8×10^{-4} W cm^{-2}, (4) 2.0×10^{-3} W cm^{-2}, (5) 8.3×10^{-3} W cm^{-2}, and (6) 6.0×10^{-2} W cm^{-2}.

(d) λ_{exc} = 350 nm ~ 440 nm. t_{exp} = 4 min. (1) I_{exc} = 0, (2) 1.1×10^{-4} W cm^{-2}, (3) 5.4×10^{-4} W cm^{-2}, (4) 2.6×10^{-3} W cm^{-2}, (5) 5.9×10^{-3} W cm^{-2}, (6) 4.2×10^{-2} W cm^{-2}, (7) 6.8×10^{-2} W cm^{-2}, and (8) 9.2×10^{-1} W cm^{-2}.

For (ii) the curves belong to
(a) λ_{exc} = 470 nm. Exposure times, t_{exp} = 4 min. (1) I_{exc} = 0, (2) 4.3×10^{-5} W cm^{-2}, (3) 1.6×10^{-4} W cm^{-2}, (4) 3.8×10^{-4} W cm^{-2}, (5) 1.8×10^{-3} W cm^{-2}, (6) 4.3×10^{-3} W cm^{-2}, and (7) 1.3×10^{-2} W cm^{-2}.
(b) λ_{exc} = 428 nm. t_{exp} = 4 min. (1) I_{exc} = 0, (2) 3.1×10^{-5} W cm^{-2}, (3) 1.9×10^{-4} W cm^{-2}, (4) 3.0×10^{-4} W cm^{-2}, (5) 1.8×10^{-3} W cm^{-2}, (6) 3.9×10^{-3} W cm^{-2}, and (7) 1.4×10^{-2} W cm^{-2}.
(c) λ_{exc} = 365 nm. t_{exp} = 4 min. (1) I_{exc} = 0, (2) 1.1×10^{-4} W cm^{-2}, (3) 3.8×10^{-4} W cm^{-2}, (4) 2.0×10^{-3} W cm^{-2}, (5) 8.3×10^{-3} W cm^{-2}, and (6) 6.0×10^{-2} W cm^{-2}.
(d) λ_{exc} = 350 nm ~ 440 nm. t_{exp} = 4 min. (1) I_{exc} = 0, (2) 9.0×10^{-5} W cm^{-2}, (3) 2.7×10^{-4} W cm^{-2}, (4) 1.3×10^{-3} W cm^{-2}, (5) 6.2×10^{-3} W cm^{-2}, (6) 1.4×10^{-2} W cm^{-2}, (7) 7.8×10^{-1} W cm^{-2}.
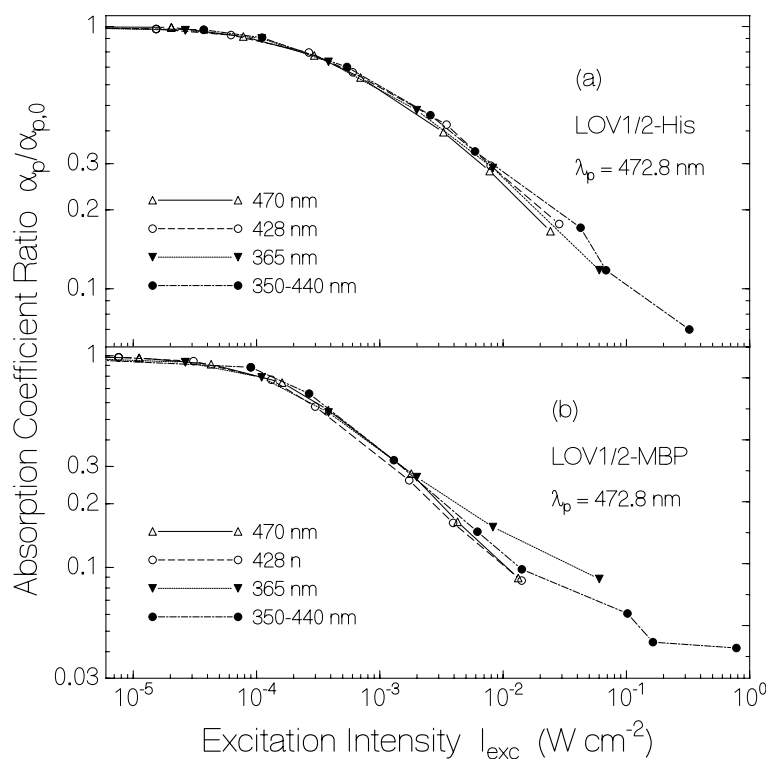

Fig. 4.5   Intensity dependent reduction of absorption coefficient at wavelength λ_p = 472.8 nm. Excitation wavelengths are 470 nm, 428 nm, 365 nm, and 350-440 nm. Each spectrum is normalized. (a) LOV1/2-His. (b) LOV1/2-MBP. Each exposure time is 4 min and the interval time between successive measurements is 5 min. At high intensity, the interval time is 10 min.

The development of the absorption coefficient at 472.8 nm versus excitation intensity is shown in Fig. 4.5. Each absorption coefficient is normalized to its maximum dark state value,

i.e $\alpha_p / \alpha_{p,0} = \dfrac{\alpha_p(I_{exc})}{\alpha_p(I_{exc} = 0)}$ versus excitation intensity, I_{exc}, is plotted. The absorption cross-

section of FMN C(4a)-cysteinyl adduct is very small near to 4×10^{-19} cm^2 at 472.8 nm [24].

The intensity dependent absorption behaviour is similar for the applied different excitation wavelengths. At the highest exposed intensity practically all FMN were converted to the final stage (mainly transferred to cysteinly-adduct).

At the same excitation intensity, the absorption spectral change for LOV1/2-MBP is larger than for LOV1/2-His. Even at maximum excitation intensity, the absorption is not completely depleted. This indicates the presence of a fraction of non-covalently bound FMN, which is not convertible to the adduct state.

The intensity dependent absorption behaviour could be used to determine the quantum efficiency of photo-induced adduct-formation by numerical simulation. The data in Fig 4.5 for $\lambda_{exc} = 428$ nm are re-plotted in Fig. 4.6 and are used to extract the quantum efficiency of adduct-formation.

The intensity dependent absorption change at $\lambda_{exc} = 472$ nm is shown in Fig. 4.6 (a) for LOV1/2-His and in (b) for LOV1/2-MBP. The dots are the experimental data.

Neglecting the small fraction of free FMN, the relevant differential equation system for the number densities, $N_{Ad,f}$ and $N_{Ad,s}$, of fast and slow recovering adduct and for the absorption of the excitation light (intensity I_{exc}) reads [24]

$$\frac{\partial N_{Ad,f}}{\partial t} = \left[\phi_{Ad,0}\left(1 - \frac{N_{Ad}}{N_{con}}\right) + \phi_{Ad,1}\frac{N_{Ad}}{N_{con}} \right]\frac{\sigma_a(\lambda_{exc})I_{exc}}{h\nu_{exc}}(N_{con,f} - N_{Ad,f}) - \frac{N_{Ad,f}}{\tau_{Ad,f}}, \qquad (4.6)$$

$$\frac{\partial N_{Ad,s}}{\partial t} = \left[\phi_{Ad,0}\left(1 - \frac{N_{Ad}}{N_{con}}\right) + \phi_{Ad,1}\frac{N_{Ad}}{N_{con}} \right]\frac{\sigma_a(\lambda_{exc})I_{exc}}{h\nu_{exc}}(N_{con,f} - N_{Ad,s}) - \frac{N_{Ad,s}}{\tau_{Ad,s}}, \qquad (4.7)$$

$$\frac{\partial I_{exc}}{\partial z} = -\sigma_a(\lambda_{exc})(N_0 - N_{Ad})I_{exc} - \sigma_{a,Ad}(\lambda_{exc})N_{Ad}I_{exc}, \tag{4.8}$$

where N_0 is total number density of FMN molecules. The total number density of convertible FMN molecules is defined by

$$N_{con} = N_0 - N_{nc} = N_0(1 - \beta_{nc}),$$

and the total number density of generated adducts is

$$N_{Ad} = N_{Ad,f} + N_{Ad,s}.$$

The number density of convertible FMN molecules with fast adduct recovery time is $N_{con,f} = \beta_f N_{con}$ and the number density of convertible FMN molecules with slow adduct recovery time is $N_{con,s} = \beta_s N_{con}$. In the differential equation system t is the time, and z is the spatial coordinate in the direction of the excitation light propagation. $\sigma_a(\lambda_{exc})$ is the absorption cross-section per non-covalently bound FMN molecule, and $\sigma_{a,Ad}(\lambda_{exc})$ is absorption cross-section per FMN-Cys adduct at the excitation wavelength, λ_{exc}.

The absorption coefficient, $\alpha_p(I_{exc})$ in Fig.4.6 is calculated by the relation

$$\alpha_p(I_{exc}) = \frac{1}{\ell}\int_0^\ell \left[(N_0 - N_{Ad}(I_{exc}, t_e, z))\sigma_a(\lambda_p) + N_{Ad}(I_{exc}, t_e, z)\sigma_{a,Ad}(\lambda_p)\right]dz, \tag{4.9}$$

where ℓ is the sample length, t_e is the time at the end of light exposure, $\sigma_a(\lambda_p)$ is absorption cross-section of FMN at λ_p, and $\sigma_{a,Ad}(\lambda_p)$ is the absorption cross-section of the adduct at λ_p. The adduct absorption cross-section spectrum, LOV-390 was taken in Ref. [24].

The solid curves are calculated for different quantum yields of adduct formation. Comparison with the measured dots shows that the quantum yield of adduct formation decreases with rising excitation intensity.

The estimated quantum efficiencies at low excitation intensity are $\phi_{Ad,0} \approx 0.2$ for LOV1/2-His and ≈ 0.4 for LOV1/2-MBP. At the highest applied excitation intensity one finds $\phi_{Ad} \approx 0.1$
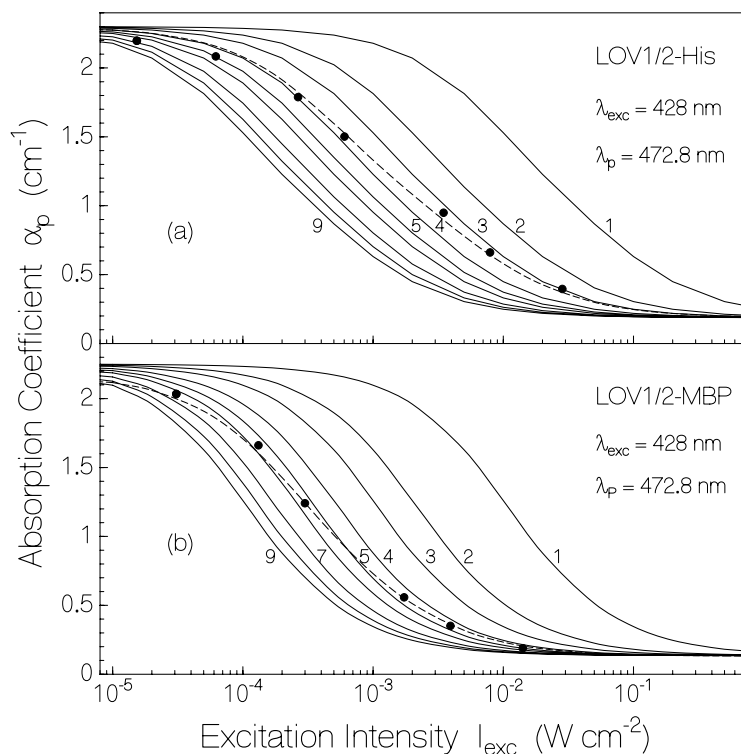
Fig. 4.6 Comparison of experimental intensity dependent absorption coefficients with numerical simulations, where quantum yields of adduct formation, $\phi_{Ad,0}$ and $\phi_{Ad,1}$ are varied. Solid curves indicate the process of initial quantum efficiency, $\phi_{Ad,0}$ same as final experimental $\phi_{Ad,1}$ quantum efficiency. The solid curves belong to $\phi_{Ad,0} = \phi_{Ad,1} = 0.01$ (1), 0.05 (2), 0.1 (3), 0.2 (3) 0.3 (5), 0.6 (7), 0.8 (8), and 1 (9). Dashed curve belongs to $\phi_{Ad,0} = 0.2$ and $\phi_{Ad,1} = 0.1$.
(a) LOV1/2-His. $\lambda_{exc} = 428$ nm, $\lambda_p = 472.8$ nm. Experimental data are taken from Fig. 4.5. Dashed curve belongs to $\phi_{Ad,0} = 0.2$ and $\phi_{Ad,1} = 0.1$.
(b) LOV1/2-MBP. $\lambda_{exc} = 428$ nm, $\lambda_p = 472.8$ nm. Experimental data are taken from Fig. 4.5. Dashed curve belongs to $\phi_{Ad,0} = 0.4$ and $\phi_{Ad,1} = 0.2$.

for LOV1/2-His and $\approx$ 0.2 for LOV1/2-MBP. The decreasing quantum yield of adduct formation suggests that the two FMN molecules in the LOV1/2 full domain do not respond equally. The primary formation of FMN cysteinly-adduct occurs with higher efficiency than the secondary FMN adduct formation when already one adduct is present.

The temporal absorption behaviour during 1 hour of light exposure at the excitation wavelengths 428nm, 470 nm and 350-440 nm is shown in Fig 4.7. The absorption coefficient
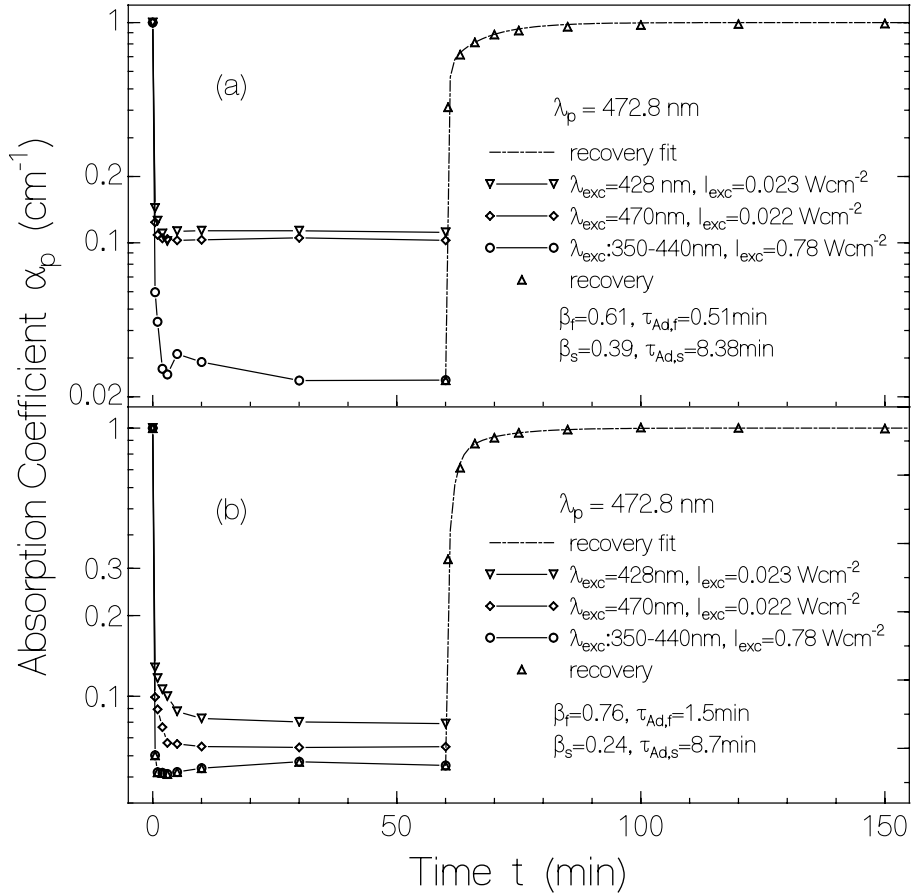
Fig. 4.7   Normalized temporal development of the absorption coefficient for 1 hour exposure and recovery in dark. The results (a) is LOV1/2-His and (b) is LOV1/2-MBP. Dash-dotted curves are bi-exponential fits with parameters listed in the figure.

does not completely drop to zero even at the highest excitation intensity and this indicates that some non-convertible FMN exist in the LOV domain as discussed above (p.54).

After 1 hour of exposure the illumination was switched off. The back-reaction to the dark state is represented as triangle marked curve. The recovery process to the dark state is fitted by Eq. 4.10

$$\alpha_p(t) = \alpha_p(t_0) + [\alpha_p(\infty) - \alpha_p(t_0)] \left\{ \beta_f \left[1 - \exp\left(-\frac{t - t_0}{\tau_{Ad,f}} \right) \right] + \beta_s \left[1 - \exp\left(-\frac{t - t_0}{\tau_{Ad,s}} \right) \right] \right\}, \qquad (4.10)$$

57
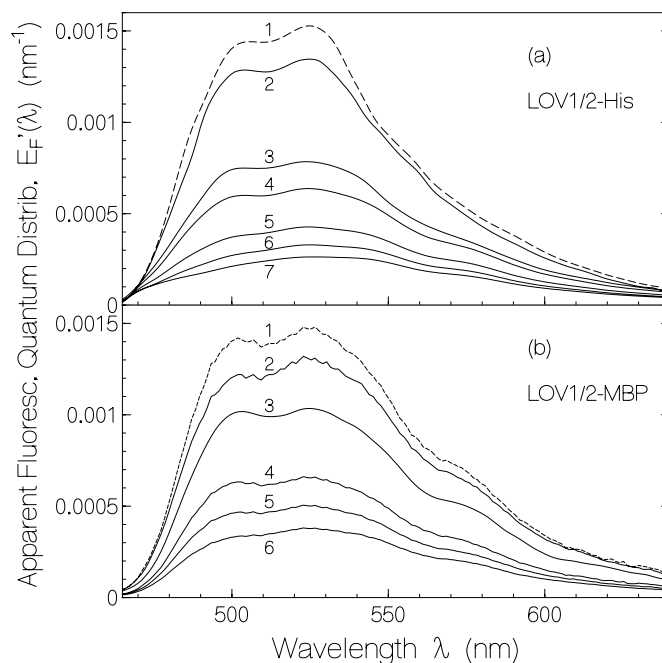
Fig. 4.8   Intensity dependent fluorescence quantum distribution. Exposure time separation between successive measurements was 5 min. Exposure wavelength was 428 nm. (a) LOV1/2-His. Exposure intensity $I_{exc} = 4.8 \times 10^{-6}$ Wcm^{-2} (1), 1.9×10^{-5} Wcm^{-2} (2), 8.7×10^{-5} Wcm^{-2} (3), 2×10^{-4} Wcm^{-2} (4), 1.1×10^{-3} Wcm^{-2} (5), 2.5×10^{-3} Wcm^{-2} (6), and 8.3×10^{-3} Wcm^{-2} (7). (b) LOV1/2-MBP. $I_{exc} = 2.2 \times 10^{-5}$ Wcm^{-2} (1), 9.2×10^{-5} Wcm^{-2} (2), 2.1×10^{-4} Wcm^{-2} (3), 1.2×10^{-3} Wcm^{-2} (4), 2.8×10^{-3} Wcm^{-2} (5), and 1×10^{-2} Wcm^{-2} (6).

where β_f is the mole-fraction of fast recovering adducts, $\beta_s = 1 - \beta_f$ is the mole-fraction of slowly recovering adducts, $\tau_{Ad,f}$ is the time constant of the fast-recovering adducts, and $\tau_{Ad,s}$ is the time constant of the slowly-recovering adducts. The fast component β_f is obtained to be 0.61 for LOV1/2-His and 0.74 for LOV1/2-MBP. The β_f and $\beta_s = 1-\beta_f$ values are collected in Table 1 together with the values of the LOV single-domains.

   The intensity dependences of the fluorescence spectra for LOV1/2-His and LOV1/2-MBP are shown in Fig. 4.8. The excitation wavelength was 428 nm. The fluorescence spectra were recorded during the exposure time of 4 min, and the dark interval time between each measurement was set to 5 min.

58
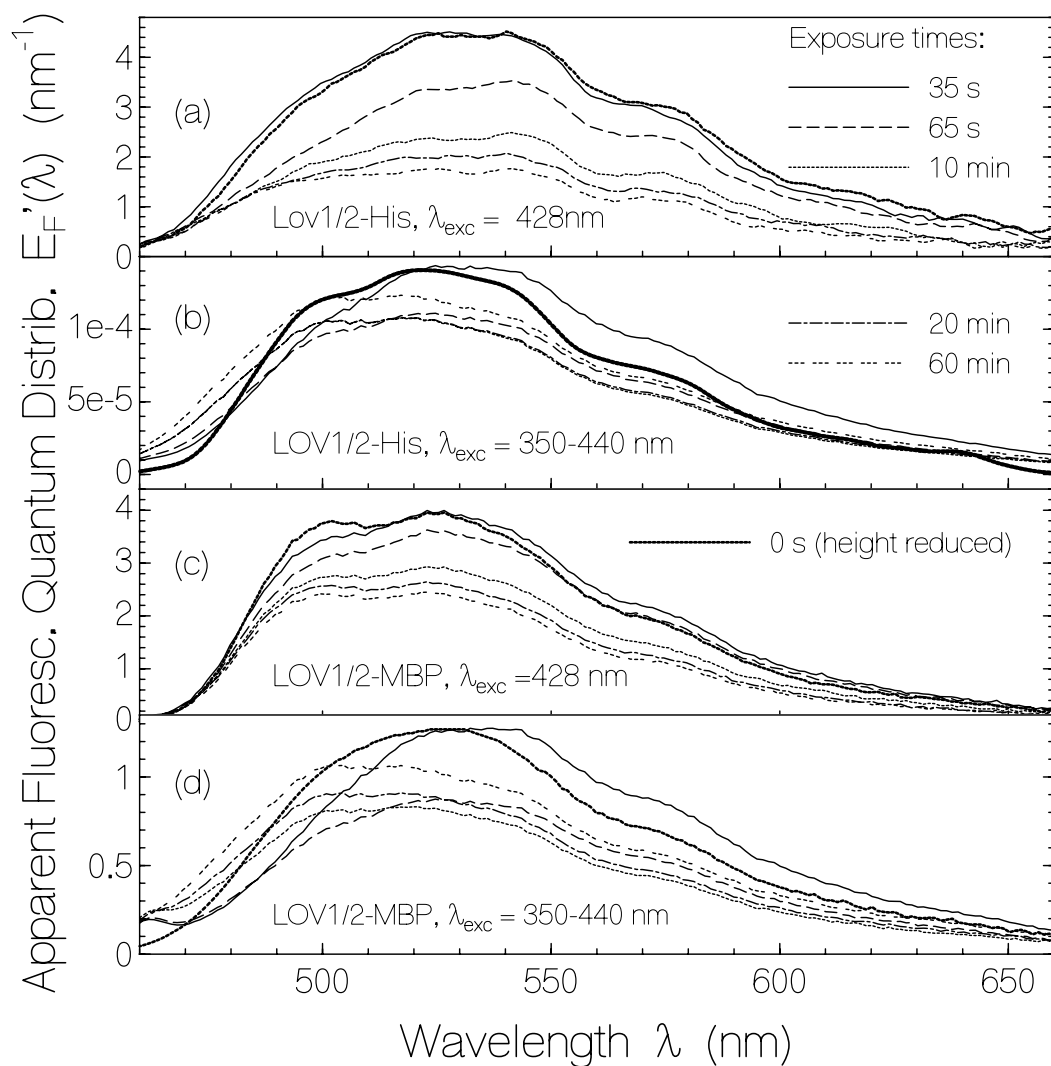
Fig. 4.9 Dependence of apparent fluorescence quantum distributions, $E_F'(\lambda)$, on light exposure time. Applied exposure times are given in the legends. Thick dotted curves were measured with $I_{exc} = 2 \times 10^{-5}$ W cm^{-2} for fluorescence excitation before long-time intense light exposure. Their heights are normalized to the peak height of the curves which were measured after 35 s of light exposure to facilitate pulse-shape comparison.
(a) LOV1/2-His. Exposure wavelength, $\lambda_{exc} = 428$ nm. Exposure intensity $I_{exc} = 0.01$ Wcm^{-2} (b) LOV1/2-His. $\lambda_{exc} = 350\text{-}440$ nm. $I_{exc} = 0.29$ Wcm^{-2}. (c) LOV1/2-MBP. $\lambda_{exc} = 428$ nm. $I_{exc} = 0.01$ W cm^{-2}. (d) LOV1/2-MBP. $\lambda_{exc} = 350\text{-}440$ nm. $I_{exc} = 0.29$ Wcm^{-2}.

59

The spectral shapes are slightly red-shifted with increasing excitation intensity. The fluorescence does not completely disappear even at the highest excitation intensity. The fluorescence of FMN which is unbound to the LOV domain is thought to be responsible for the red-shift.

The photo adduct of the LOV domains is not fluorescent. The amount of free FMN in LOV1/2 sample is estimated to be about 1%. It was reported earlier that 1.7% free FMN exist in LOV1-His samples, 3.8% in LOV2-His samples, 1.7% in LOV2-His samples, and 7% in LOV2-MBP samples [24,136~138].

The temporal development of the fluorescence spectra for LOV1/2-His and LOV1/2-MBP is shown in Fig. 4.9. In (a) and (c) the excitation wavelength was 428 nm with excitation light intensity of 0.01 Wcm^{-2}. In (b) and (d) the excitation was in the wavelength range 350~440 nm, and the excitation intensity was 0.29 Wcm^{-2}.

In order to compare their shapes, the dark-adapted fluorescence spectra were normalized to the spectra, which were measured after 35 seconds of exposure. In (b) and (d), the enhanced red emission after 35 s of exposure is thought to be due to free FMN emission.

A comparison with the fluorescence quantum distribution of free FMN in neutral aqueous solution in Fig 4.2 indicates a mole-fraction of free FMN of $x_2 \approx 0.01$. At high-intensity long-time exposure in (b) and (d) the fluorescence spectra shows a blue-shift. The fluorescence spectral height increases by a small amount. This indicates that a fluorescent photoproduct is formed mainly by photo-degradation of the formed FMN-Cys adducts [145].

In Fig. 4.10 the temporal development of the fluorescence quantum yields of LOV1/2-His and LOV1/2-MBP are shown. The excitation wavelengths (and excitation intensities) were 470 nm ($I_{\mathrm{exc}} = 0.02$ W cm^{-2}), 428 nm ($I_{\mathrm{exc}} = 0.01$ W cm^{-2}), and 350-440 nm ($I_{\mathrm{exc}} = 0.29$ W cm^{-2}). The samples were excited for 2 hours. The fluorescence quantum yield values $\phi_F'(t)$ are normalized to the initial quantum yield $\phi_F(0)$. The initial decrease of fluorescence emission
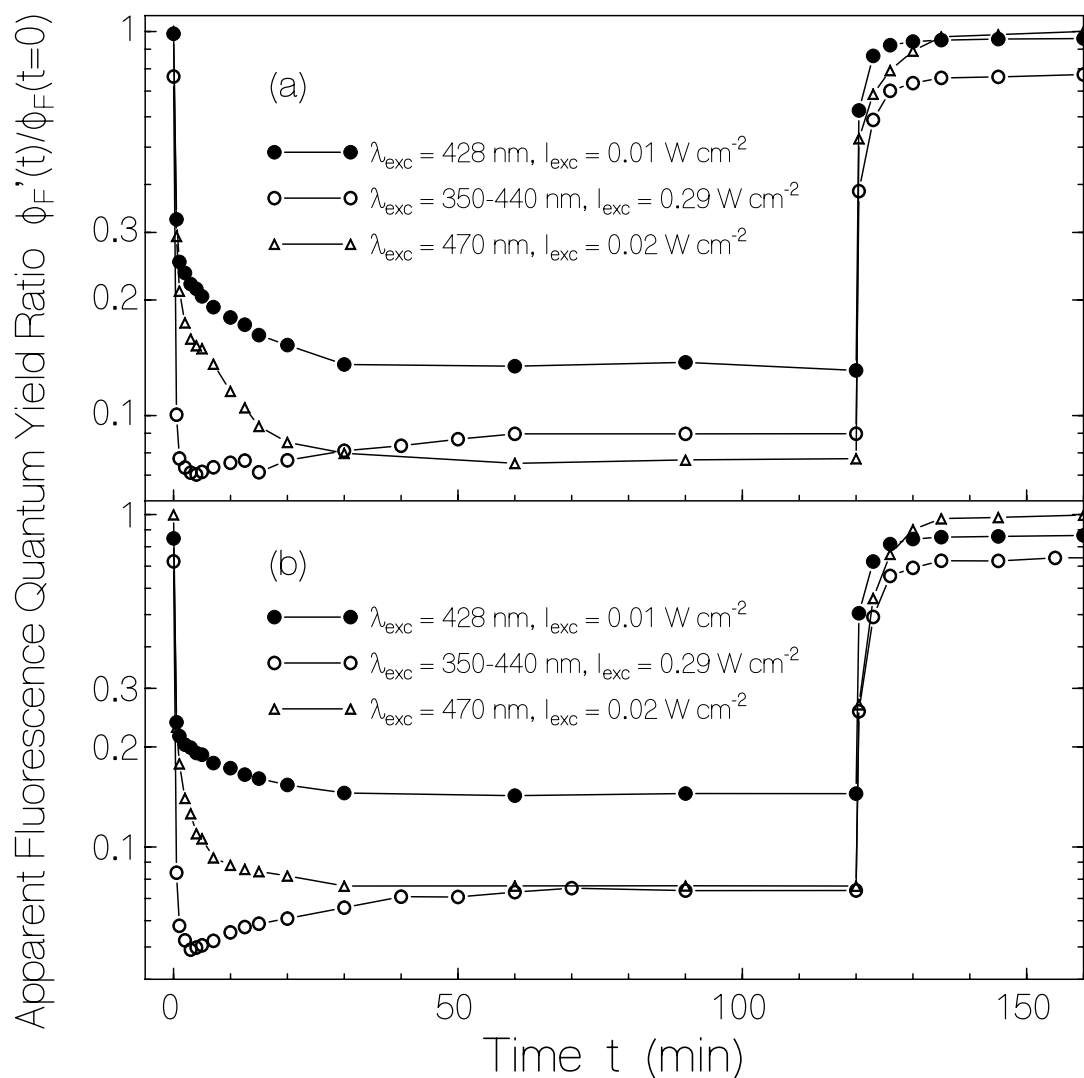
Fig. 4.10   Dependence of normalized apparent fluorescence quantum yield, $\phi_F'(t)/\phi_F(t=0)$, on light exposure time, and normalized apparent fluorescence quantum yield recovery in the dark at room temperature after light exposure. Applied parameters are given in the legends. Fluorescence probing intensities in the recovery regime are $I_{exc,p}(470\ nm) = 1.7 \times 10^{-5}\ W\ cm^{-2}$, $I_{exc,p}(428\ nm) = 2.2 \times 10^{-5}\ W\ cm^{-2}$, and $I_{exc,p}(350\text{-}440\ nm) = 9.9 \times 10^{-5}\ W\ cm^{-2}$. (a) LOV1/2-His. (b) LOV1/2-MBP.

is due to FMN-Cys adduct formation. With the highest intensity the fluorescence quantum yield is slightly increasing with time after the initial sharp decrease indicating the photo-degradation of the formed FMN-Cys adducts to a slightly fluorescing photoproduct [145].

The fluorescence lifetime cycle due to excitation at 428 nm is shown in Fig. 4.11. LOV1/2-His was excited for 42 min (a) and LOV1/2-MBP was excited for 35 min (b). The arrows indicate the start points of light switch-off. The fluorescence lifetime of LOV1/2-His immediately increased to 4.75 ns at light switch on. Since the fluorescence lifetime of free FMN is about 5 ns and the FMN-cysteinyl adduct is not fluorescent, the fluorescence lifetime rise is due to free FMN emission [146]. After light switch-off the lifetime dropped immediately to 1.95 ns and then increased to the initial value. Within the first 15 min after light switch-on the fluorescence lifetime reduces because of photodegradation of the free FMN [138].
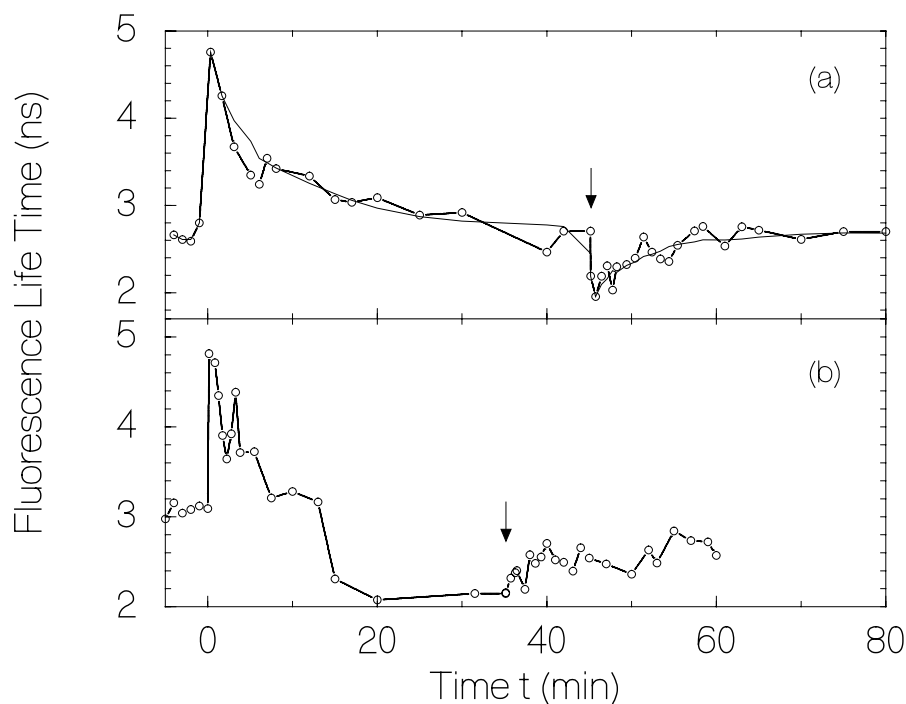
Fig. 4.11   Temporal development of fluorescence lifetime measurement in exposure-dark cycle. Light exposure wavelength at 428 nm.
(a) LOV1/2-His. Experimental data (dotted live) is smoothed (solid line). (b) LOV1/2-MBP. Arrow bars indicate light switch-off point.

4.3 Composition of LOV1/2 domain

Free FMN molecules were found in the LOV1/2 sample. The results of temporal development of absorption and fluorescence spectral measurements in Fig 4.7 and in Fig. 4.10 indicate the presence of free FMN which is not bound in the binding pocket of the LOV domain. The mole-fraction of non-covalently bound FMN and the mole-fraction of free FMN are expressed as x_1 and x_2. In the LOV1/2 domains the mole-fraction of non-covalently bound FMN, x_1, is about 0.99. The mole-fraction of free FMN, x_2, is estimated near to 0.01. As compared to single-domains, the LOV1/2 domain has somewhat smaller fractions of free FMN as shown in Table 1 [24,137,138].

Intensity dependent absorption coefficient measurements and the temporal development of absorption coefficients suggest the existence of not-convertible FMN in the LOV domains. As shown in Fig. 4.4 and Fig. 4.7, in spite of high intensity light-exposure, absorption coefficients were not completely depleted. This finding indicates that not all non-covalently bound FMN molecules is transferred to the flavin-C(4a)-cysteinyl adduct. The flavin-C(4a)-cysteinyl adduct (LOV-390) is practically not absorbing at $\lambda > 473$ nm. From the remaining absorption at $\lambda > 473$ nm, after high-intensity long-time exposure, the fraction of non-convertible FMN, β_{nc}, is determined to be about 0.02 for LOV1/2-His and 0.04 for LOV1/2-MBP.

The LOV1 and LOV2 single-domains possess larger fractions of non-convalently bound FMN not convertible to the adduct state than the LOV1/2 double domain. The results are shown in Table 1. The not convertible FMN in the LOV domains indicates that a protein

conformation exists where the Cys residue is too far away from FMN-C(4a) to be able to form a covalent bond.

The absorption recovery in the dark after light exposure suggests the presence of two non-covalently bound FMN – protein binding pocket conformations in the LOV1/2 domains. One forms blue-light induced adducts with fast adduct recovery time, and the other forms blue-light induced adducts with slow adduct recovery time. The fast recovery times of LOV1/2-His ($\tau_{Ad,f}$ = 30 s, β_f = 61 %) and LOV1/2-MBP ($\tau_{Ad,f}$ = 100 s, β_f = 74 %) are different, while the slow recovery times are similar (both $\tau_{Ad,s}$ slightly above 8 min). It is thought that the two LOV1/2 domain conformations with different adduct recovery times have slightly different barrier energies for the thermal activated back-reaction from the adduct state to the non-covalently bound state.

The absorption spectral reductions for different excitation wavelengths at 470 nm, 428 nm, 365 nm, and 350-440 nm are similar as shown in Fig. 4.5. The generated FMN-C(4a)-Cys adduct is practically not absorbing at λ_{exc} = 470 nm [24].

4.4 Photo-Cycle of LOV1/2 Domain

The photo-cyclic scheme for the LOV1/2 domains, extracted from the experimental studies, is visualized in Fig. 4.12. The mole-fractions and the estimated parameters in this scheme are listed in Table 1. The formational pathway from excited FMN to adduct was not analysed. It is thought that it runs via triplet formation [22,24,137,138] and photo-induced charge-transfer complex formation [24,137,138].

In the dark state, two non-covalently bound FMN molecules in the LOV1/2 domains are in the singlet ground-state. When the FMN molecules absorb light then first one FMN molecule is excited. This FMN molecule combines with the cystein group in LOV domain at C(4a) region of the isoalloxazine ring and forms an adduct with primary quantum efficiency of $\phi_{Ad,0}$. Within the adduct-state lifetime the other FMN in the LOV1/2 domain is excited by the continued light excitation, and this excited FMN molecule reacts with lower quantum efficiency, $\phi_{Ad.1}$, of adduct formation. The primary formed adduct seems to modify the LOV1/2 conformation aggravating FMN-C(4a)-Cys adduct formation for the remaining FMN.

The adducts recover with the fast and slow time constants, $\tau_{Ad,f}$ and $\tau_{Ad,s}$, to non-covalently bound FMN depending on the LOV1/2 domain conformations of LOV1/2$_f$ and LOV1/2$_s$.
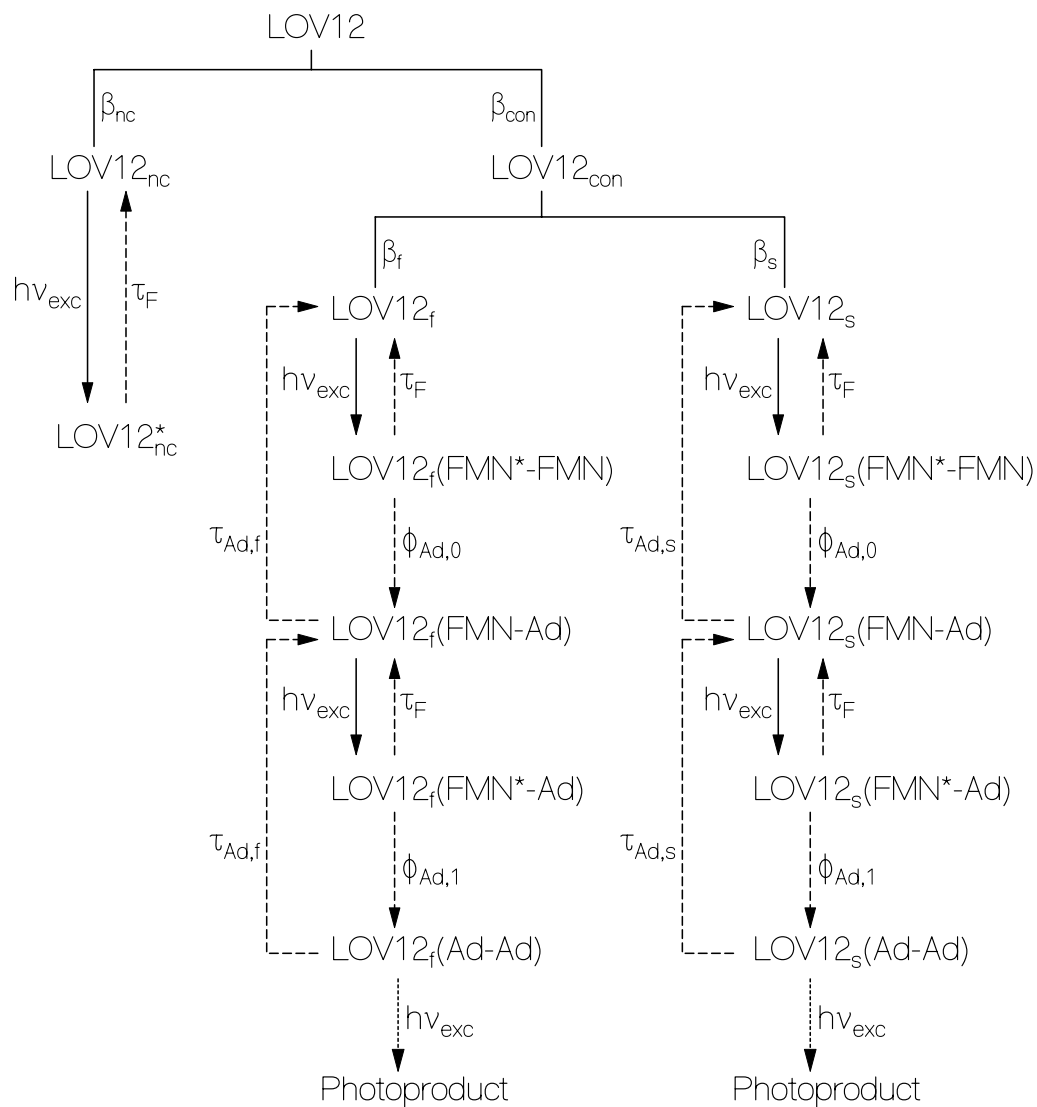
Fig. 4.12   The photo-dynamics of light absorption, fluorescence emission, adduct formation, and adduct recovery of the LOV1/2 domains of phototropin from *Chlamydomonas reinhardtii*. Values of the parameters are given in Table 1.

The quantum yield of primary adduct-formation, $\phi_{Ad,0}$, in the LOV1/2 domains is smaller than the quantum yield of adduct-formation, ϕ_{Ad}, in LOV1 and LOV2 domains. In the protein binding pockets, subtle conformational differences between LOV1/2 double domain and LOV single-domains are thought to be responsible for the smaller quantum yield of adduct-formation in LOV1/2 double domain compared to single LOV1 and LOV2.

5. Results and Discussion II :

Cryptochrome 3

5.1 Absorption spectra

Cry3 contains two important chromophores, one is MTHF as a photoantenna and the other is the catalytic chromophore, FAD. In order to elucidate the characterization of cry3, MTHF and FAD were also studied seperately by absorption spectroscopy.

5.1.1 MTHF and 5-formyl-THF

(6R,S)-5,10-Methenyl-5,6,7,8-tetrahydrofolic acid chloride(MTHF-Cl) was purchased from Schircks-Laboratories, Switzerland. The molar mass is 491.9 g/mol and the chemical structure is shown in Fig. 5.1.

Fig. 5.1 Structural formula of (6R,S)-5,10-Methenyl-5,6,7,8-tetrahydrofolic acid chloride (MTHF-Cl, $C_{20}H_{22}N_7O_6$).

Fig. 5.2 Temporal development of MTHF-Cl in 50 mM Na-phosphate, pH 7.5 50 mM NaCl 10 mM β-mercaptoethanol 10% glycerin (pH 7.5 buffer). The probe wavelength, λ_{pr} is 386 nm.
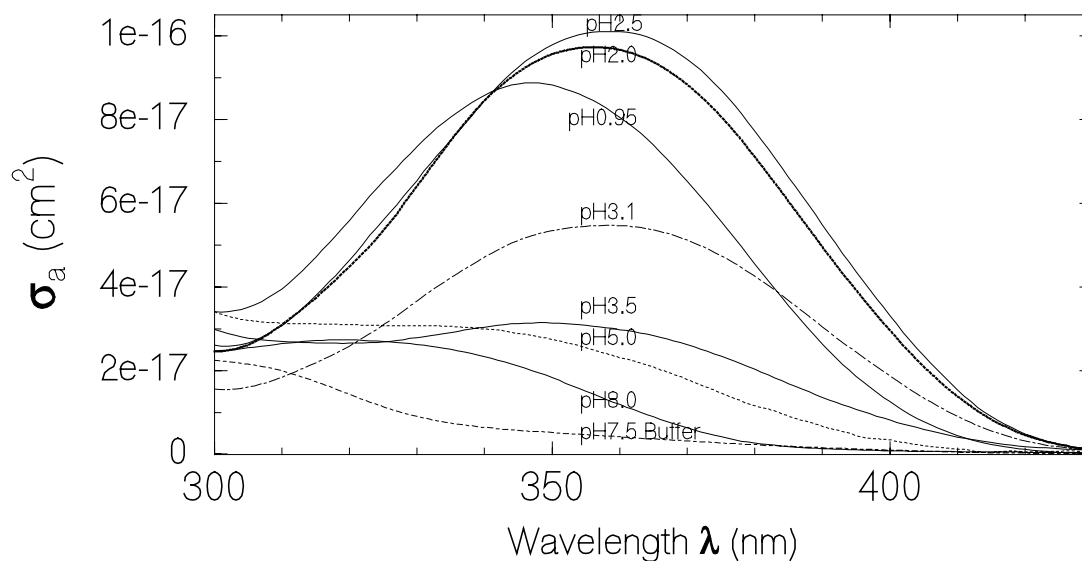
Fig. 5.3 The absorption cross-section spectra of MTHF-Cl in various pH conditions, pH 0.95, pH 2.0, pH 2.5, pH 3.1, pH 3.5, pH 5.0, pH 8.0 aqueous solution and pH 7.5 buffer were measured after one day from dissolution.
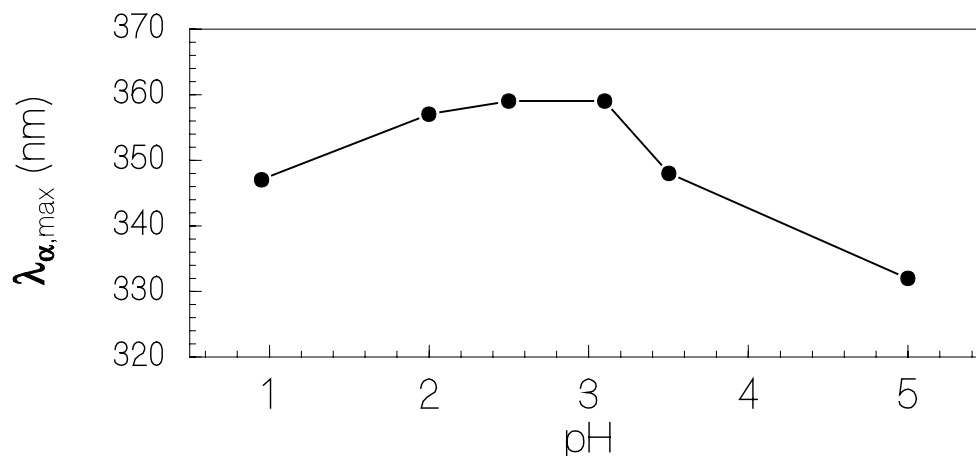
Fig. 5.4　Absorption spectral maximum wavelengths for MTHF-Cl in various pH aqueous solution, $\lambda_{\alpha,max}$ are plotted after one day from dissolution. In pH 2.5 and 3.0 spectra are the most red-shifted.

MTHF-Cl was dissolved into pH 7.5 buffer which was used to dissolve cry3 protein. The pH 7.5 buffer consists of 50 mM Na-phosphate, pH 7.5, 50 mM NaCl, 10 mM β-mercaptoethanol, and 10 % glycerin.

Immediately after dissolution the absorption maximum of MTHF-Cl was at 358 nm, but within 1 hour the absorption peak disappeared. The temporal development of absorption α/N_0 at 386 nm is plotted in Fig. 5.2, where α is the absorption coefficient and N_0 is the initial MTHF-Cl number density. MTHF-Cl converts to another molecule or conformation with time.

MTHF-Cl was dissolved in a variety of pH aqueous solutions. The samples were kept at 4 °C to reduce thermal degradation. The spectra after 24 h of storage are shown in Fig. 5.3. The original absorption at 358 nm remained at pH 2.5.

The wavelength position of maximum absorption after one day of storage at 4 °C is shown in Fig. 5.4. At pH 2.5 aqueous solution the absorption peak is at $\lambda_{\alpha,max} = 360$ nm. For low and high pH the absorption maximum is blue-shifted. MTHF-Cl is reasonably stable at pH 2.5. Therefore further studies on MTHF-Cl were carried out at pH 2.5.

(a)

(b)
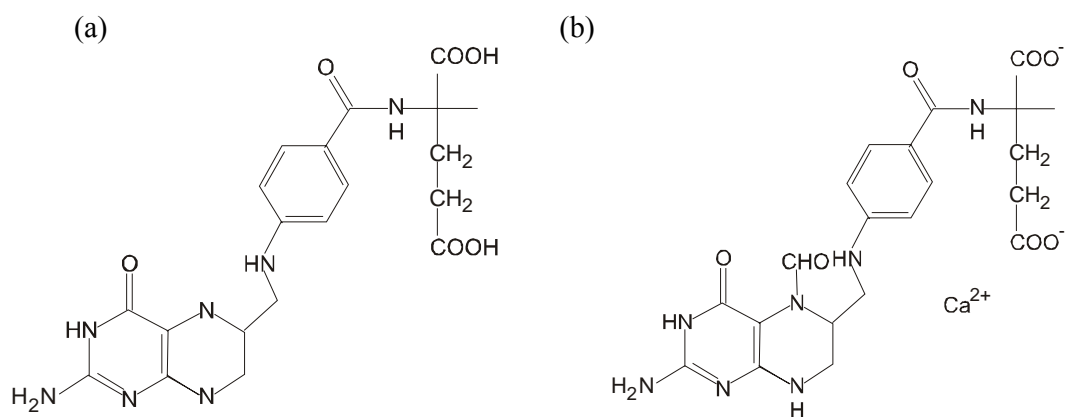
Fig. 5.5   (a) Structural formula of Folic acid ($C_{19}H_{19}N_7O_6$) and (b) chemical structure of (6,R,S)-5-Formyl-5,6,7,8-tetrahydrofolic acid calcium salt (5-formyl-THF-Ca, $C_{20}H_{21}N_7O_7$).
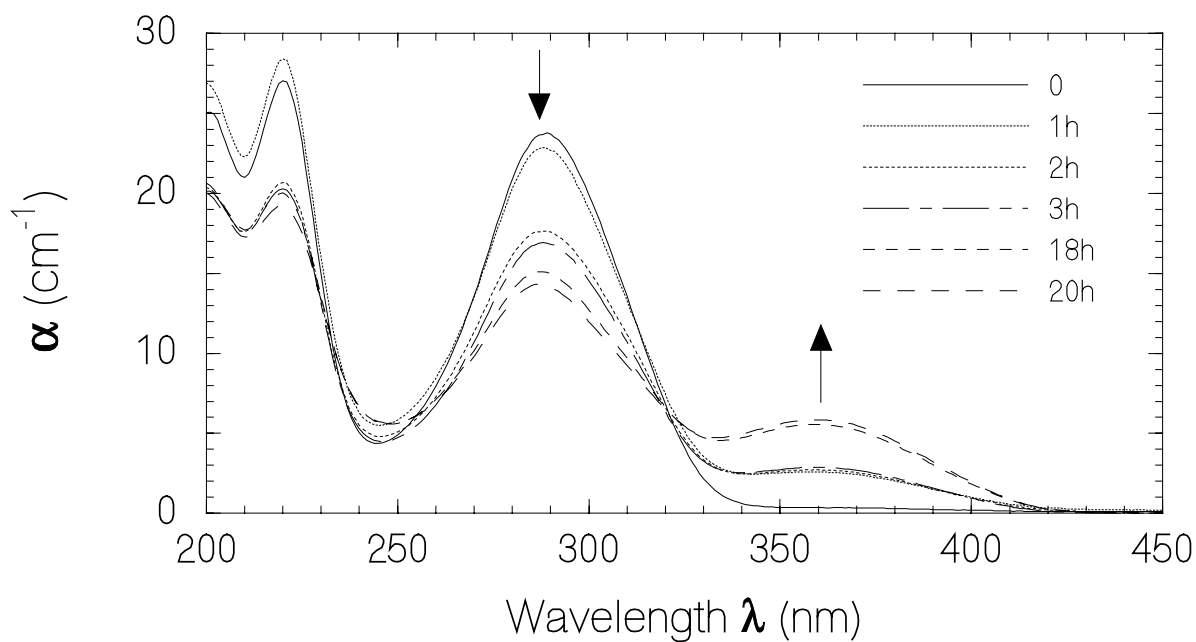
Fig. 5.6   (6,R,S)-5-Formyl-5,6,7,8-tetrahydrofolic acid calcium salt (5-formyl-THF-Ca) 0.77 mg is dissolved into 5 ml pH 2.5 HCl aqueous solution. Sample was kept at 4 °C. Concentration is 3.01×10^{-4} M. The absorption coefficient at 360 nm was increasing with time.

71

For further studies, folic acid and (6,R,S)-5-Formyl-5,6,7,8-tetrahydrofolic acid calcium salt (5-formyl-THF-Ca) were purchased from the commercial company Schircks-Laboratories, Switzerland. The molar mass is 441.4 g/mol for folic acid and 511.5 g/mol for 5-formyl-THF-Ca. Their chemical structures are shown in Fig. 5.5.

Absorption spectra of 5-formyl-THF-Ca in pH 2.5 aqueous solution are shown in Fig. 5.6. The absorption peak of 5-formyl-THF-Ca at 365nm region increased with time, while at 280nm, the absorption decreased with time.

Absorption spectra of folic acid in pH 8.0 aqueous solution are shown in Fig. 5.7. The absorption spectrum was changed little with time.
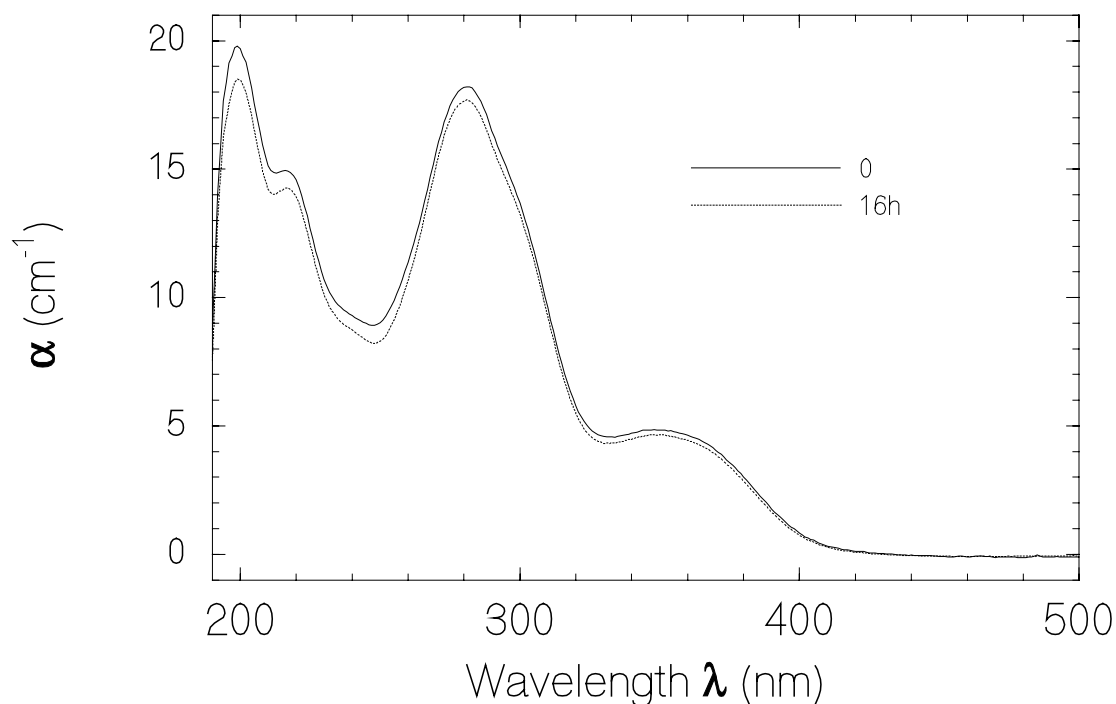
Fig. 5.7   Folic acid 0.62 mg is dissolved into 5 ml pH 8.0 NaP, NaCl aqueous solution. Sample was kept at 4 °C. Concentration is 2.80×10^{-4} M. The absorption spectra of folic acid were stable with time.
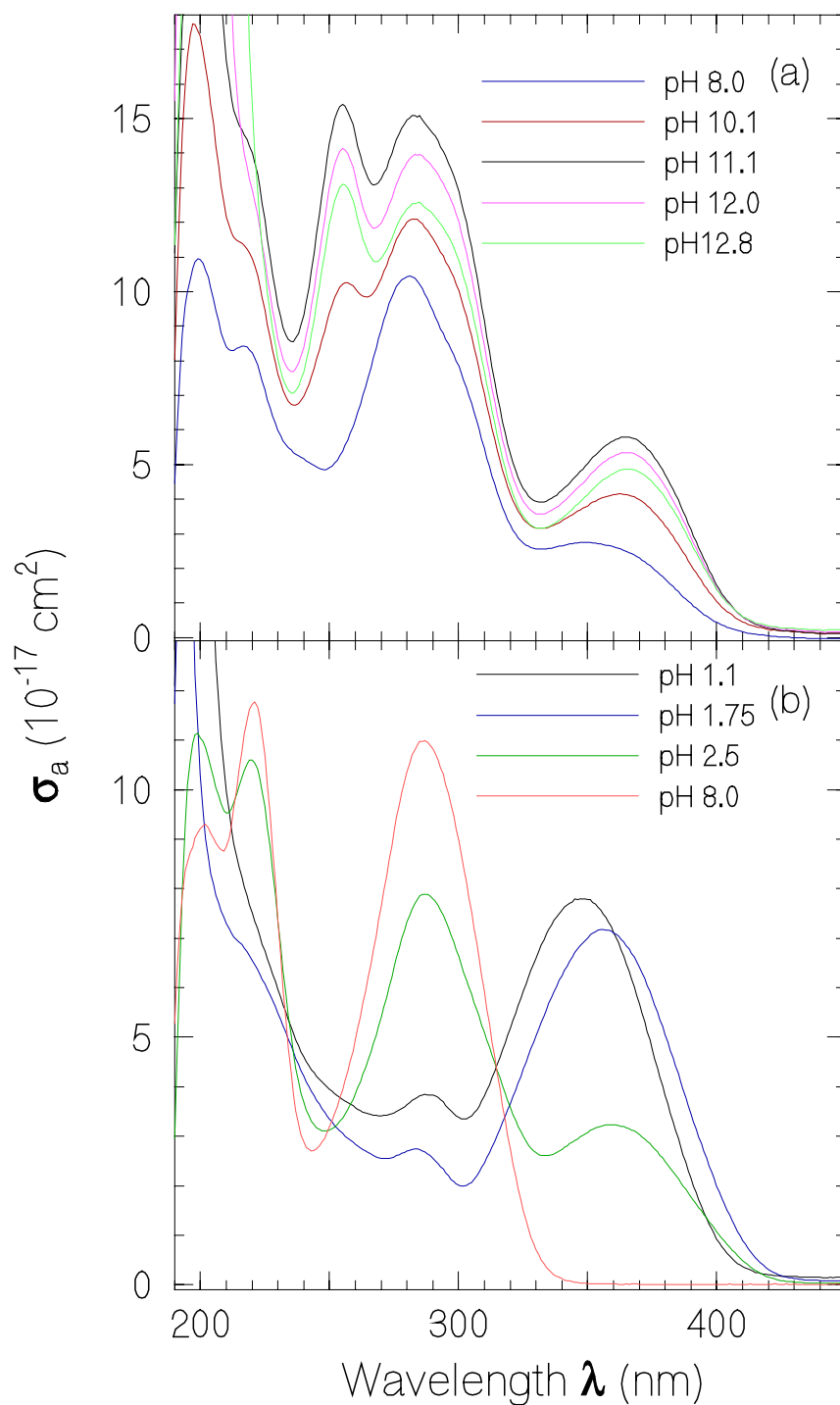
Fig. 5.8 (a) Dark adapted absorption cross-section, σ_a of folic acid in different pH aqueous solution pH 8.0, pH 10.1, pH 11.1, pH 12.0, and pH 12.8.
(b) σ_a of (6,R,S)-5-Formyl-5,6,7,8-tetrahydrofolic acid calcium salt (5-formyl-THF-Ca) at pH 1.1, pH 1.75, pH 2.5 and pH 8.0 aqueous solution.
Samples were kept at 4 °C and data are obtained one day after the dissolution.

Absorption spectra of folic acid and 5-formyl-THF-Ca at different pH values are shown in Fig. 5.8. The spectra were measured after 1 day of storage at 4 °C. Folic acid has its highest absorption at pH 11.1 whereas the absorption peak of 5-formyl-THF-Ca was highest at around 360 nm at pH 1.1.

The absorption spectra of (6,R,S)-5-Formyl-5,6,7,8-tetrahydrofolic acid calcium salt (5-formyl-THF-Ca) at pH 1.1, MTHF at pH 2.5 and folic acid at pH 11.1, measured one day after the preparation, are shown in Fig. 5.9. At these pH values the components are most stable.

The thermal stability of 5-formyl-THF-Ca at pH 1.1 and pH 1.75 is shown in Fig. 5.10. After dissolution, the absorption of the sample kept at 4 °C changed only little within two days (Curve L2). But the absorption of the sample kept at room temperature showed a large decrease of absorption after two days (Curve R2).
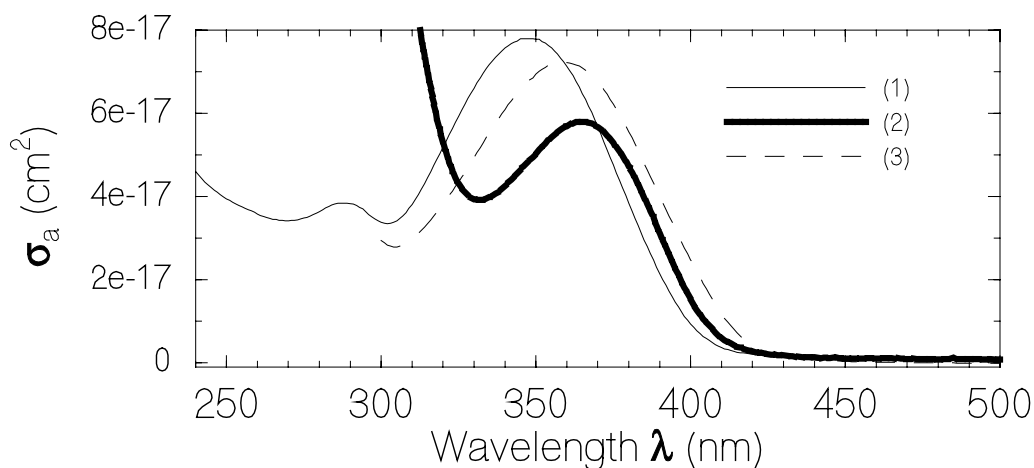

Fig. 5.9   The maximum absorption cross-section spectra of (1) 5-formyl-THF-Ca, (2) Folic acid, and (3) MTHF-Cl are collected. The pH value of aqueous solution is (1) pH 1.1, (2) pH 11.1, and (3) pH. 2.5. The spectra are plotted after one day from dissolution. Samples were kept at 4°C.

74
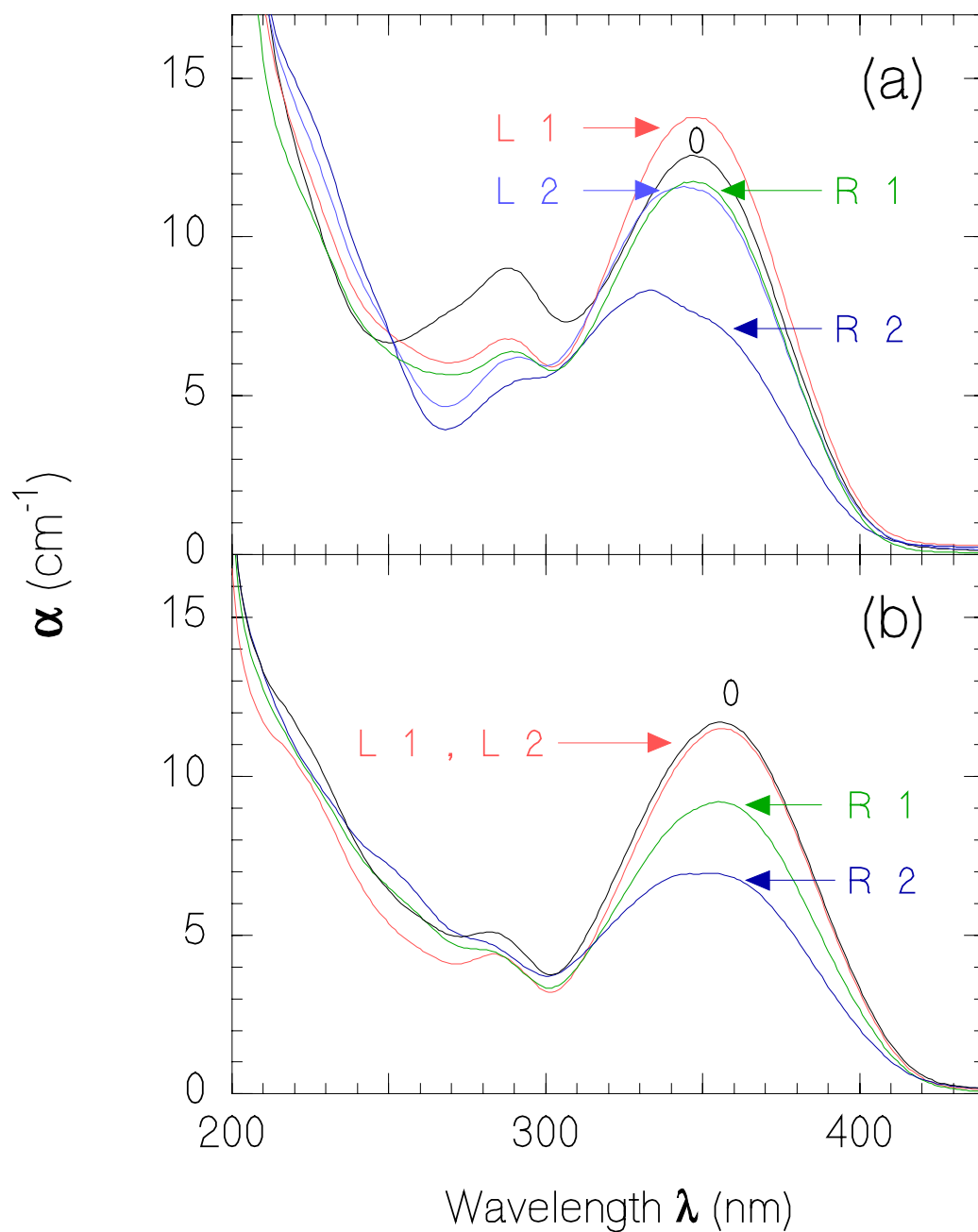
Fig. 5.10   5-formyl-THF-Ca 0.75mg was dissolved in 3 ml (a) pH 1.1 and (b) pH 1.75 HCl
aqueous solution. Curves indicate
0 : obtained directly after preparing sample.
L1 : Sample was kept at low temperature 4°C for 1 day.
L2 : Sample was kept at low temperature 4°C for 2 days.
R1 : Sample was kept at room temperature 22.6°C for 1 day.
R2 : Sample was kept at room temperature 22.6°C for 2 days.

In Fig. 5.11 the spectral changes with the pH-value is checked. Some reversibility is seen. First MTHF-Cl 1.32 mg was dissolved in 5 ml pH 8 aqueous solution. After 3 hours the absorption strength at 360 nm fell down as shown in Fig. 5.11. Then this 1 ml solution was added to 4 ml pH 2.5 HCl water. This solution has a concentration of 0.254 mg MTHF-Cl in pH 3.4 aqueous solution. Samples were kept at room temperature.

The sample was divided into two parts. One half of it was kept under dark conditions
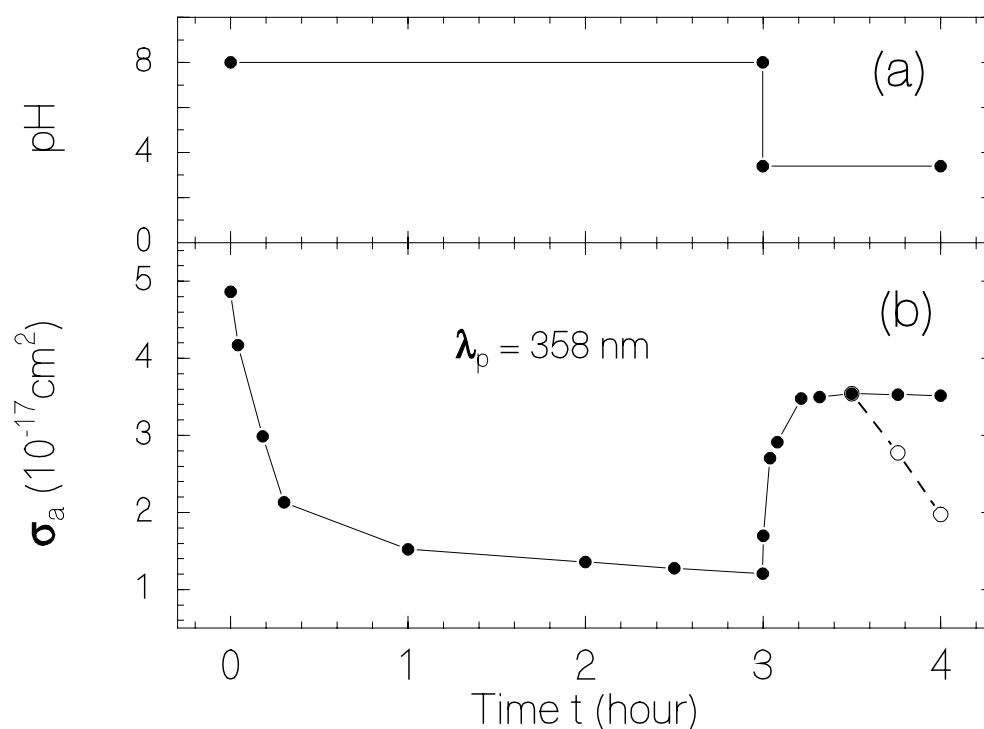
Fig. 5.11   MTHF-Cl was dissolved in pH 8.0 aqueous solution and absorption spectra were measured for 3 hours directly after dissolution. Then the pH value of the solution was changed by mixing pH 2.5 water. Final pH value for the aqueous solution was pH 3.4. Samples were kept at room temperature.
(a) The pH value of aqueous solution.
(b) The change of absorption cross-section. Filled circle curve indicates the change of the sample kept in dark. Open circle curve indicates the change of the sample kept in ambient light conditions after mixing.

(filled-circle) and the other half was kept under ambient light conditions (open-circle). For the sample kept in the dark, the absorption cross-section was found to be more 50 % of the original absorption cross-section even after one day. But for the sample that was kept in the ambient light conditions the spectra first showed a recovery of 50 % of the original absorption cross-section, but fell down to a lower level after 1 hour. These results show that MTHF has a pH-dependent (partial) reversible absorption behaviour (like pH indicator).

5.1.2 FAD and Cry3

The dark-adapted absorption cross-section spectrum, σ_a of cry3 is compared with the absorption cross-section spectra of some flavins (Fig. 5.12). The cross-section spectral peaks for cry3 are in three regimes around 380 nm, 470 nm and 600 nm. The MTHF chromophore is responsible for the absorption peak at 380 nm, the oxidized form of flavin-adenine dinucleotide (FAD) is responsible for the absorption at 470 nm, and the absorption around 600 nm is due to the neutral semiquinone form of FAD.

Additionally in Fig. 5.12 the absorption cross-section spectra of FAD in oxidation form (FAD_{ox}), fully neutral reduced form ($FAD_{red}H_2$), FAD reduced anionic form ($FAD_{red}H^-$) and neutral FAD semiquinone form ($FADH^{\bullet}$) are included. Their chemical structures are shown in Scheme 5.1.

The absorption cross-section spectra of $FAD_{red}H_2$ and $FAD_{red}H^-$ in the blue spectral range are small compared to the absorption cross-section of FAD_{ox} and are therefore hidden in the cry3 spectrum.

The molar mass of cry3 is 60 720 g mol^{-1} and the molar concentration is estimated to be 3.3×10^{-5} mol dm^{-3} by the relation $c = C_w / M_w$, where the applied mass concentration, C_w was 2 mg / ml.
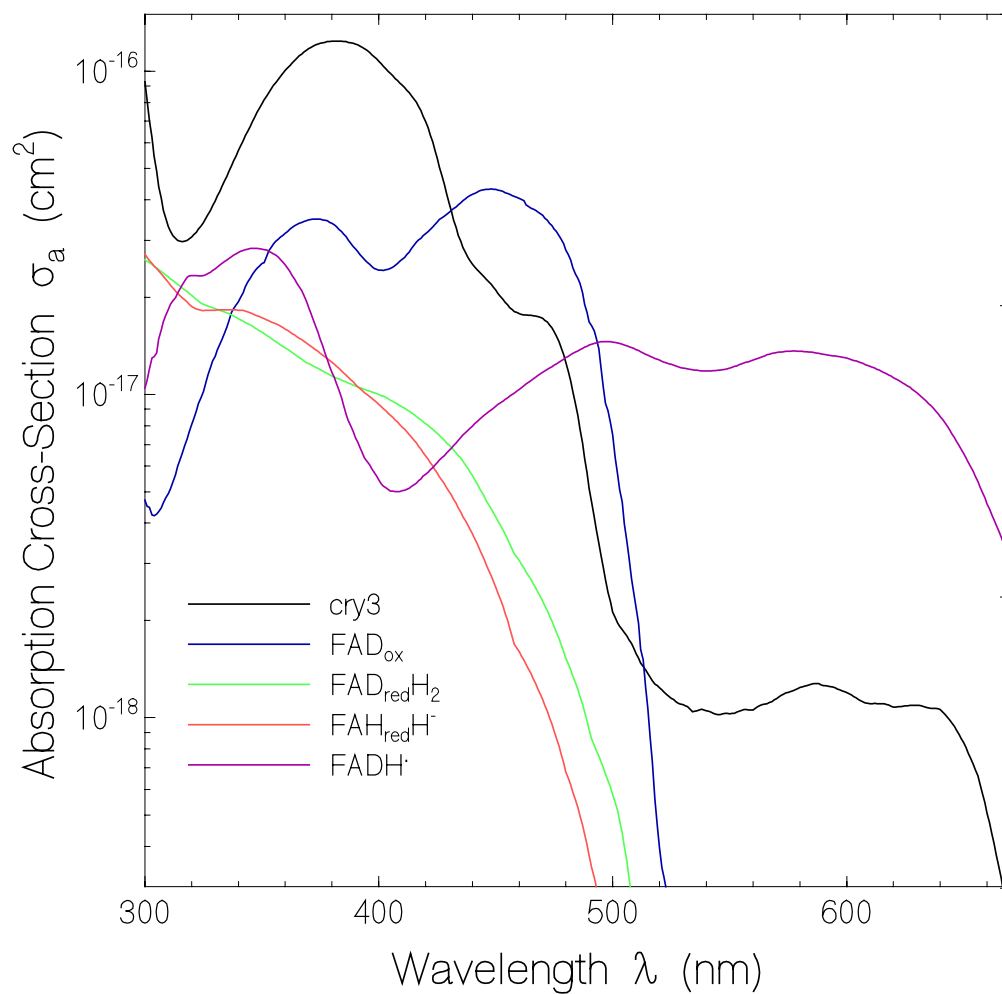
Fig. 5.12   Absorption cross-section of dark-adapted cry3 in pH 7.5 buffer solution, FAD oxidation form FAD_{ox} in aqueous solution at pH 7.0, fully neutral reduced form $FAD_{red}H_2$ [148], FAD reduced anionic form $FAD_{red}H^-$ [148], and neutral semiquinone form $FADH^{\bullet}$ [149].
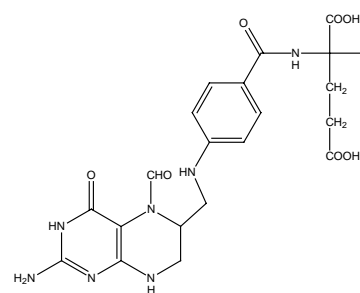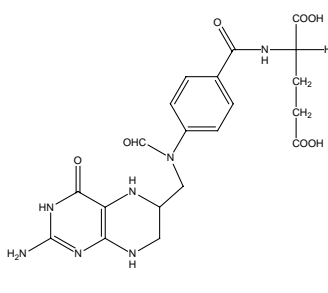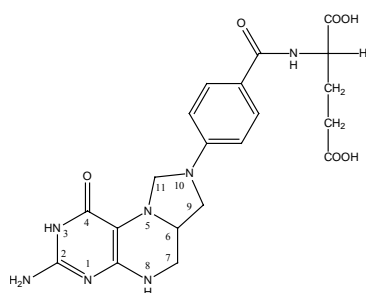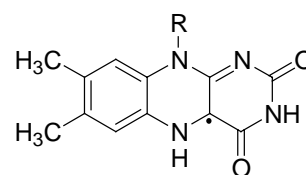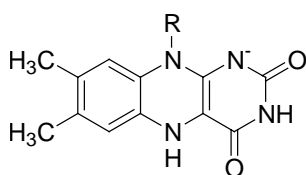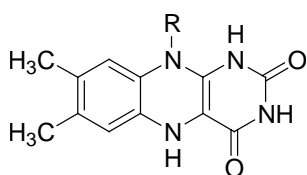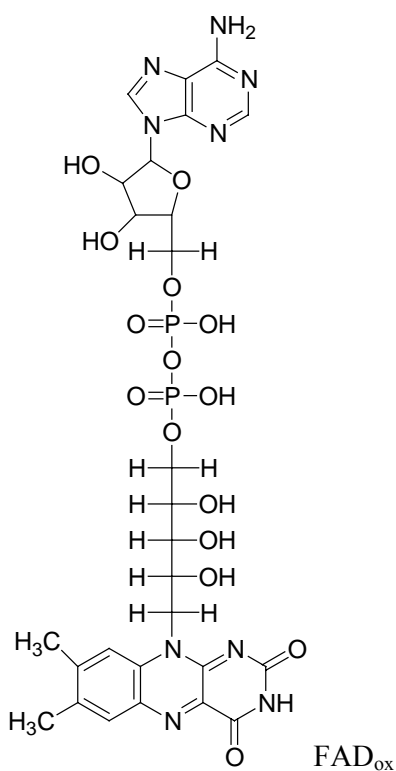
Scheme 5.1 : Structural formulae of FAD in its oxidized form (FAD$_{ox}$), fully reduced neutral form (FAD$_{red}$H$_2$), fully reduced anionic form (FAD$_{red}$H$^-$), neutral semiquinone form (FADH$^\bullet$), and of MTHF-Cl.

The spectral decomposition shown in Fig. 5.13 fits reasonably well to following FAD composition of a mole fraction $x_1 = 0.40$ of FAD_{ox}, a mole fraction $x_2 = 0.55$ of $FAD_{red}H_2$ and a mole fraction $x_3 = 0.05$ of $FADH^\bullet$.

Since the absorption cross-section spectra of $FAD_{red}H_2$ and $FAD_{red}H^-$ are similar, it cannot be distinguished between them. $\sigma_a(cry3) - x_1\,\sigma_a(FAD_{ox}) - x_2\,\sigma_a(FADH^\bullet) - x_3\,\sigma_a(FAD_{red}H_2)$ is shown by the dashed curve in Fig. 5.13. It is attributed to absorption of MTHF.
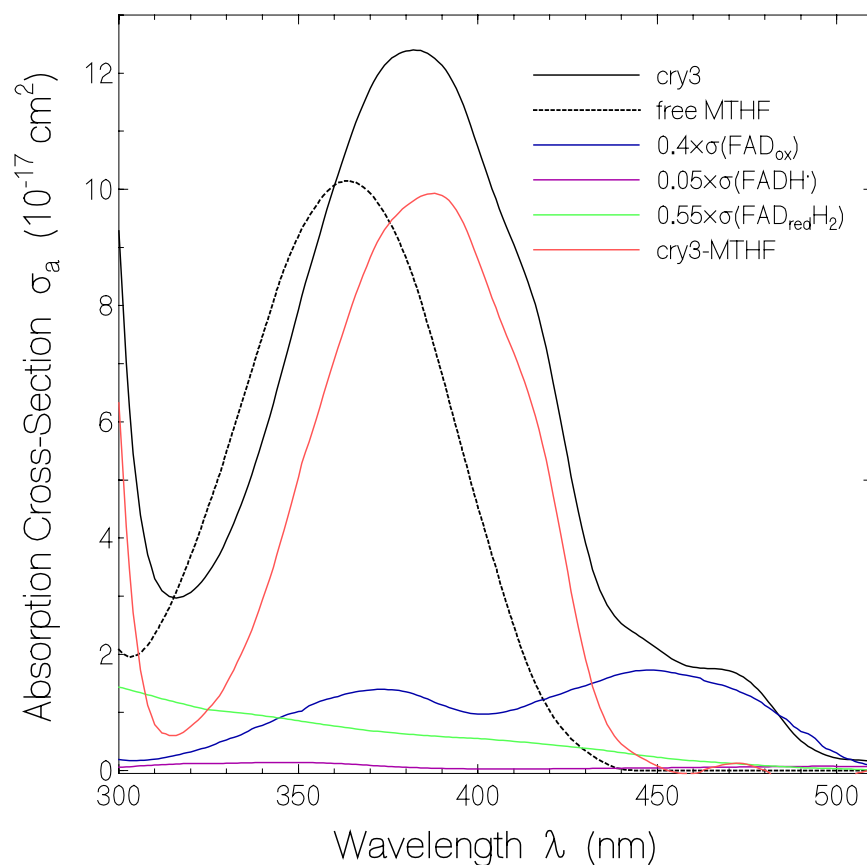
Fig. 5.13 Absorption cross-section spectrum of dark-adapted cry3 in pH 7.5 buffer solution. Absorption cross-section spectra of 40% FAD oxidation form (FAD_{ox}), 5% neutral semiquinone form ($FADH^\bullet$) and 55% fully neutral reduced form ($FAD_{red}H_2$) are shown. The residual spectrum thought to be due to MTHF in the protein (Cry3-MTHF). Cry3-MTHF is obtained by the subtraction of absorption cross-sections contributions of the FAD components, $\sigma_a(cry3) - 0.4 \times \sigma_a(FAD_{ox}) - 0.55 \times \sigma_a(FAD_{red}H_2) - 0.05 \times \sigma_a(FADH^\bullet)$.

In Fig. 5.14 the absorption cross-section spectrum of MTHF released from *E. coli* photolyase [150] (dotted curve) is compared with the absorption cross-section spectrum of MTHF-Cl in aqueous solution at pH 2.5 (dashed curve). There is a small red shift of the released MTHF compared to MTHF-Cl. It should be noticed that bound MTHF in photolyase and in cry3 are strongly red-shifted with absorption maximum around 385 nm. This red-shift is thought to be due to a glutamate interactive mechanism [64].
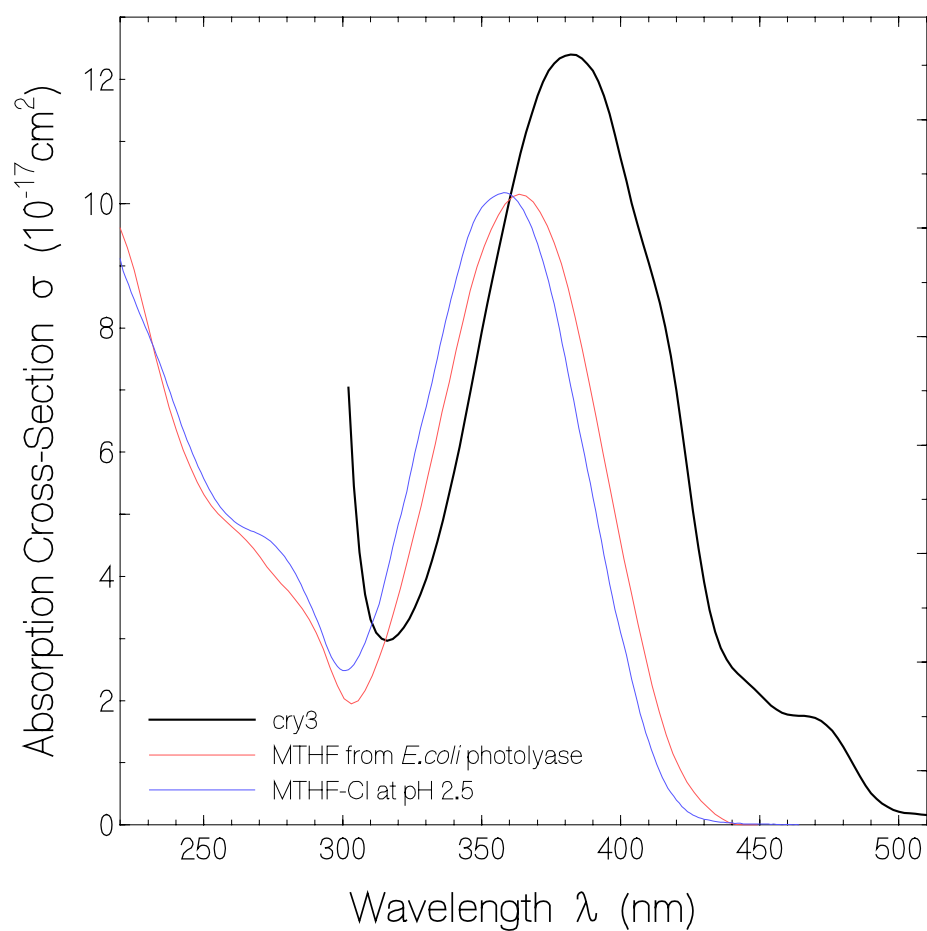

Fig. 5.14   Absorption cross-section spectra for cry3 in pH 7.5 buffer. MTHF released from *Escherichia coli* photolyase [150]. The absorption spectrum of MTHF in photolyase is compared to that of MTHF-Cl in pH2.5 aqueous solution.

5.2 **Fluorescence Studies**

5.2.1. Fluorescence spectra

The fluorescence quantum distribution, $E_F(\lambda)$, for dark-adapted cry3 in pH 7.5 buffer solution is measured by excitation at wavelengths 365nm and 450nm with magic angle polarized light. The fluorescence quantum distribution, $E_F(\lambda)$ of FAD in aqueous solution at pH 7.0 is taken from reference [151]. The fluorescence quantum distribution, $E_F(\lambda)$ of FAD in pH 7.5 buffer was obtained by excitation at 428 nm with polarized light under magic angle condition. The excitation intensity was 2.05×10^{-3} Wcm^{-2}. The fluorescence quantum yield, ϕ_F, of free FAD in neutral aqueous solution is approximately 0.033. That of free FAD in pH 7.5 buffer solution was found to be about 0.07 (see Fig. 5.15).

If FAD is in the stacked form (U-shaped form), then occurs photoinduced electron transfer between the isoalloxazine moiety and the adenine moiety and the fluorescence is quenched. In the unstacked form there occurs no electron transfer and the fluorescence of FAD is similar to that of FMN ($\phi_F \approx 0.26$) [151]. The increase of FAD fluorescence in pH 7.5 buffer indicates that the stacked-unstacked equilibrium is shifted, towards the unstacked form.
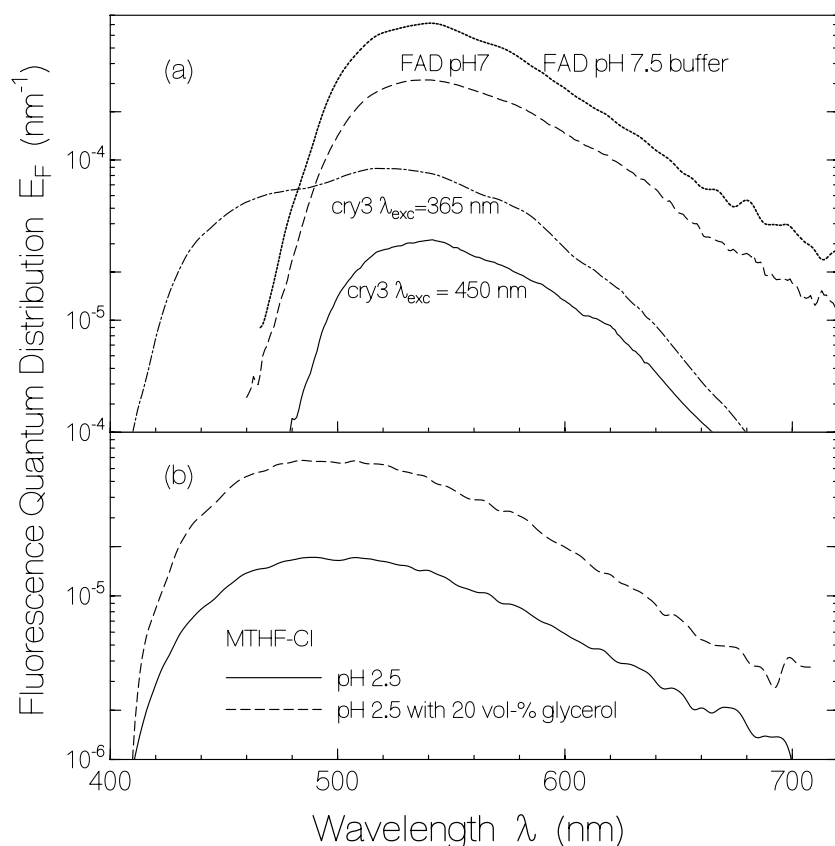
Fig. 5.15   (a) Fluorescence quantum distributions, $E_F(\lambda)$, of dark-adapted cry3 obtained for λ_{exc} = 450 nm (solid line) and 365 nm (dash-dotted line), FAD in pH 7.5 buffer (dotted line), and in aqueous solution at pH 7.0 (dashed line, from [151]).
(b) Fluorescence quantum distribution, $E_F(\lambda)$, of MTHF-Cl dissolved in pH 2.5 aqueous solution is shown as solid line. MTHF-Cl in aqueous solution at pH 2.5 with 20 vol-% glycerin is shown as dash line.

As described above pH 7.5 buffer solution is 50 mM Na-phosphate, pH 7.5, 50 mM NaCl, 10 mM β-mercaptoethanol, and 10 % glycerin. The β-mercaptoethanol might cause some more unstacked arrangement of the isoalloxazine-adenine moiety in pH 7.5 buffer.

The fluorescence quantum distributions of FAD and cry3 are shown in Fig. 5.15 (a). The fluorescence quantum yield, $\phi_F = \int E_F(\lambda)d\lambda$, of cry3 at excitation wavelength 365 nm is about 0.012. Upon excitation at 365 nm the light is absorbed about 80 % by MTHF, about 10 % absorbed by FAD_{ox}, and the rest by $FAD_{red}H_2$ and $FADH^\bullet$. The fluorescence emitted by

exposure at 365 nm is dominated by MTHF absorption. Excitation light at 450 nm is only absorbed by FAD and the emission is due to FAD_{ox} fluorescence. The quantum yield, ϕ_F is about 3×10^{-3}.

The shape of $E_F(\lambda)$ caused by 365 nm excitation exhibits two peaks : one is located at 450 nm is due to MTHF emission and the other at 520nm is due to FAD_{ox} emission. This 520 nm emission is larger than expected from directly absorbed FAD_{ox}. Energy transfer occurs from MTHF to FAD_{ox}.

The fluorescence quantum distribution of MTHF-Cl in pH 2.5 aqueous solution, and in pH 2.5 aqueous solution with 20 vol-% glycerin is shown in Fig. 5.15 (b). The excitation wavelength was 365 nm. The fluorescence quantum yield, ϕ_F, of MTHF-Cl at pH 2.5 HCl water is about 2.5×10^{-3} and that ϕ_F of MTHF-Cl with 20 % glycerin in pH 2.5 HCl aqueous solution is about 9.2×10^{-3}. Glycerin increases the viscosity. Therefore internal conversion is reduced and the fluorescence quantum yield is increased.

The degree of fluorescence polarization was measured by vertical polarized excitation light and detection of the parallel polarized, $S_{F,\parallel}(\lambda)$ and perpendicular polarized fluorescence light, $S_{F,\perp}(\lambda)$. The normalized fluorescence spectra $S_{F,\perp}(\lambda)/S_{F,\parallel,max}(\lambda)$ and $S_{F,\parallel}(\lambda)/S_{F,\parallel,max}(\lambda)$ are shown in the top row of Fig. 5.16. Cry3 in pH 7.5 buffer was excited at 365 nm and 450 nm. The degree of fluorescence polarization, P_F is calculated by $P_F = (S_{F,\parallel} - S_{F,\perp})/(S_{F,\parallel} + S_{F,\perp})$.

The diagram (d) belongs to the degree of polarization, P_F of cry3 in pH 7.5 buffer solution with excitation at 365 nm. In the wavelength regime below 470 nm P_F is larger than in the regime above 470 nm. The emission below 470 nm is caused by MTHF. There occurs no molecular reorientation within the fluorescence lifetime above 470 nm. P_F is reduced by the excitation energy transfer from MTHF to FAD_{ox}.
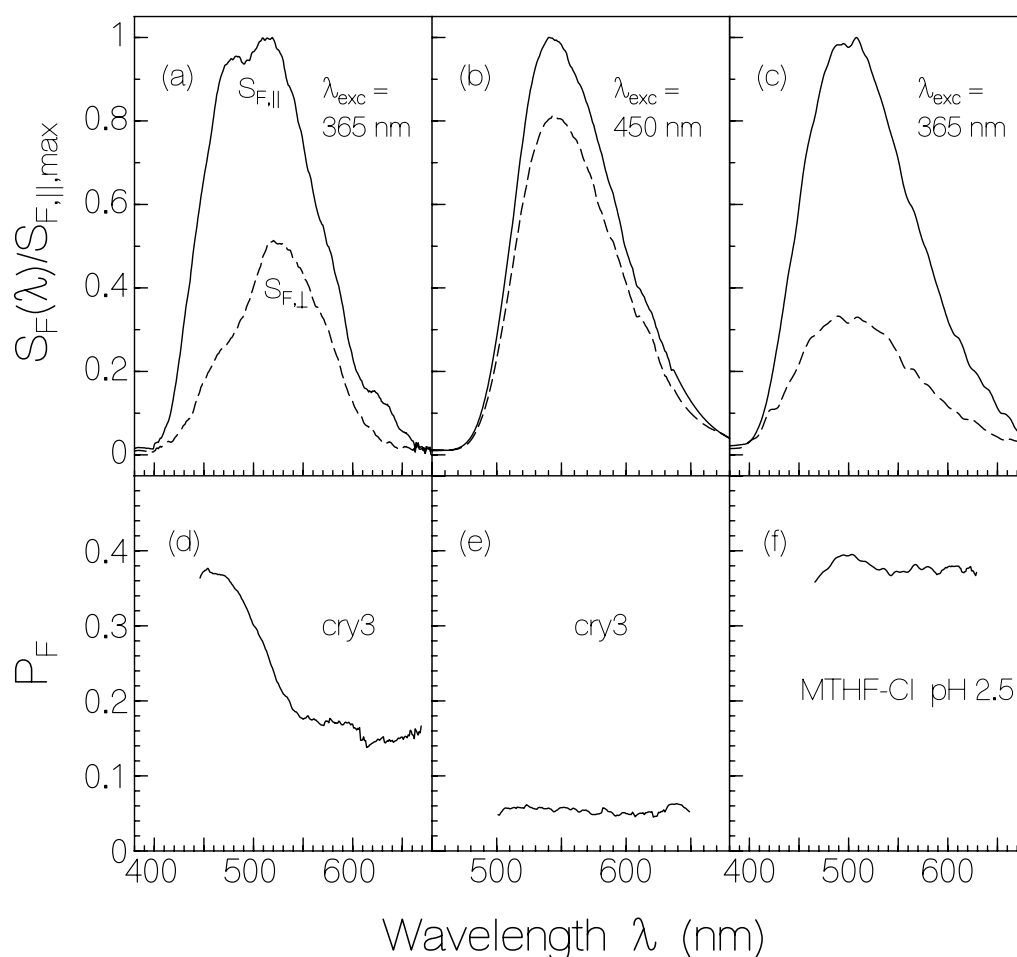
Fig. 5.16 (a)(b)(c) Normalized fluorescence quantum distribution signals, versus wavelength. The fluorescence emission signals are normalized to maximum value of parallel polarized fluorescence emission. Parallel polarized signal is $S_{F,\parallel}(\lambda)$ and perpendicular polarized signal is $S_{F,\perp}(\lambda)$. Cry3 is exposed with wavelength (a) 365nm and (b) 450nm. Panel (c) shows that of MTHF-Cl in pH 2.5 aqueous solution at 365 nm exposure.

(d)(e)(f) The degree of fluorescence polarization, P_F, versus wavelength. The graphs (d), (e), and (f) correspond to degrees of fluorescence polarization of respectively (a), (b), and (c).

In diagram (e), cry3 is exposed at 450 nm where only FAD_{ox} is absorbing and emitting. The shape of P_F is flat nearly to zero. The fluorescence is dominated by emission from free FAD in unstacked conformation with long fluorescence lifetime. The free molecules reorient

with the fluorescence lifetime and therefore the degree of fluorescence polarization is low. In cry3 FAD is in the U-shaped conformation and therefore practically non-fluorescent.

In diagram (c) is shown $S_{F,\parallel}(\lambda)$ and $S_{F,\perp}(\lambda)$ of MTHF-Cl in pH 2.5 aqueous solution with excitation wavelength at 365 nm. The resulting $P_F(\lambda)$ is shown in panel (f). It is rather high and wavelength independent. The fluorescence quantum yield, ϕ_F for MTHF-Cl in pH 2.5 aqueous solution is about 0.0048. This results in very short lifetime of $\tau_F = \phi_F \, \tau_{rad} \approx 93$ ps. Within this short lifetime the molecules reorient only partially.

5.2.2. Fluorescence Lifetime

Temporal fluorescence signal traces of free MTHF and cry3 are shown in Fig. 5.17. The samples were excited with the second harmonic pulses of a mode-locked Ruby laser of wavelength 347.15 nm and 35 ps pulse duration. The fluorescence was detected with a micro-channel-plate photomultiplier.

Probe wavelength was selected to be 470 nm. MTHF-Cl in pH 2.5 aqueous solution was kept in a 4.0 mm × 10 mm × 35 mm cell. During the measurement the solution was circulated with a magnetic stirrer to replace the excited volume after each shot and thereby retain the
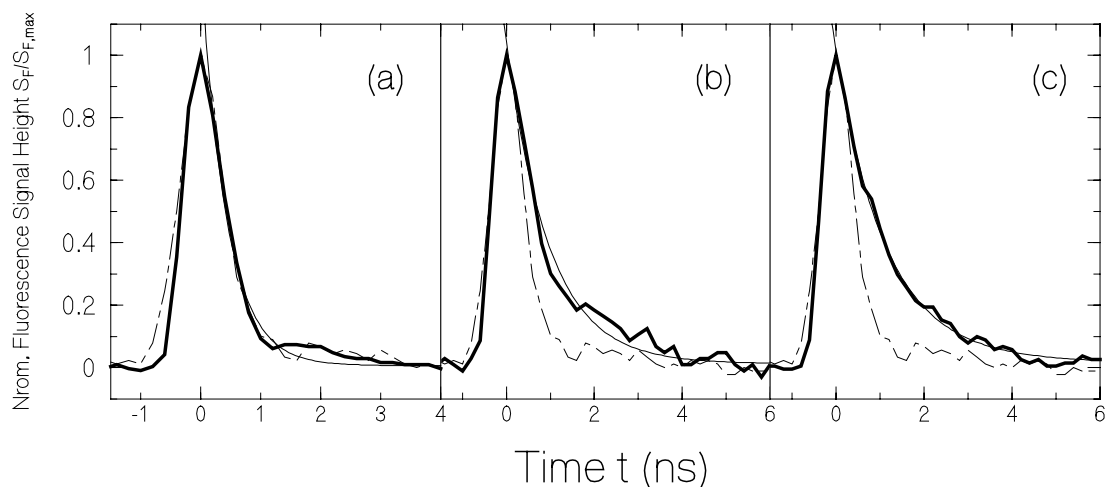
Fig. 5.17   The temporal fluorescence signal trace of MTHF and cry3 by Ruby laser. The pump wavelength is at 347.15 nm. The thick solid curve line is experimental emission signal and thin solid curves are exponential fitting curve.
(a) Dark-adapted MTHF-Cl in pH 2.5 aqueous solution and detection at 470 nm.
(b) Dark-adapted cry3 in pH 7.5 buffer and detection at 455 nm.
(c) Dark-adapted cry3 in pH 7.5 buffer and detection at 550nm.
Thin solid curves for (a) and (b) follow as single exponential function and that for (c) follows as bi-exponential function.
Dashed-Dot lines indicate a response function.

dark-adapted state. The obtained fluorescence trace is shown in Fig. 5.17 (a). For cry3 a 1.5 mm × 1.5 mm × 5 mm cell was used and the cell was filled with a volume of 40 μl. The probing wavelength was set with an interference filter to 455 nm in panel (b) and to 550 nm in panel (c).

In Fig. 5.17 (a) the fluorescence decay nearly follows the response function. The real fluorescence decay time could not be extracted.

The fluorescence trace in Fig 5.17 (c) (cry3 probed at wavelength 550 nm) is fitted with a bi-exponential curve and the paramaters $\tau_{F1} = 1$ ns (fraction $x_1 = 0.96$) and $\tau_{F2} = 5$ ns (fraction $x_2 = 0.04$). The slow component is due to the presence of free unstacked FAD.

Further temporal fluorescence signals of dark-adapted cry3 are shown as solid lines in
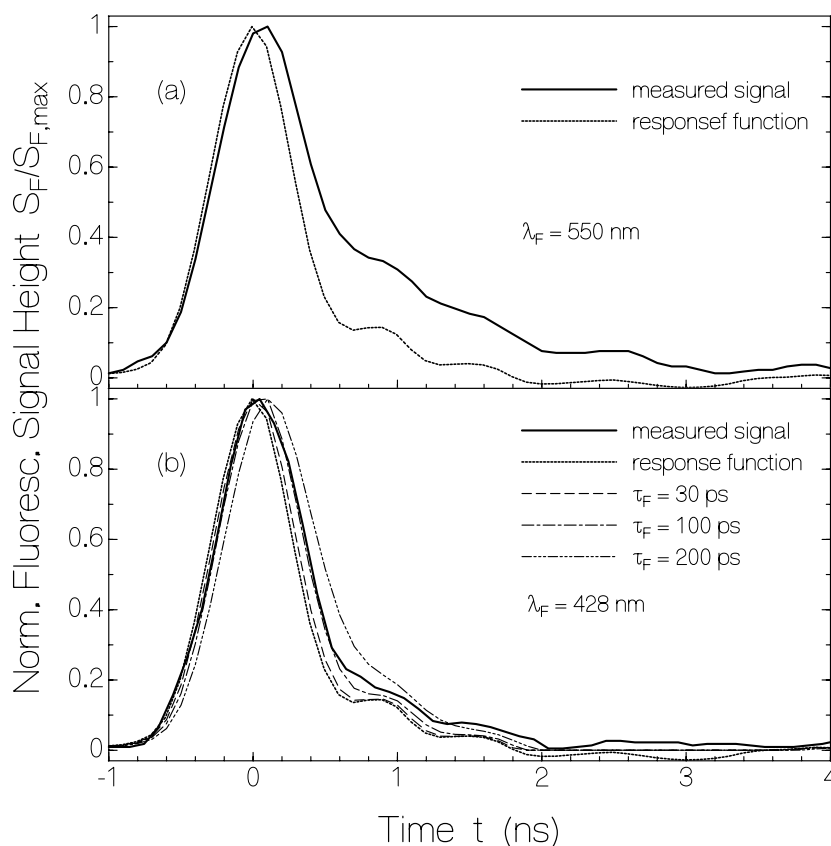
Fig. 5.18   Temporal fluorescence signals of dark-adapted cry3 are shown as sold curve. Transmission was 0.952. Dotted curve line shows response function.
(a) Detection at 550nm (MTHF and FAD emission). (b) Detection at 428 nm (MTHF emission). Three convolution fits are included.

Fig. 5.18. The excitation wavelength was 400 nm and the pulse duration was 3.5 ps (Ti:sapphire laser system). The sample transmission at the laser wavelength was set to T = 0.952. The response function, $g(t)$ is shown as dotted line. The diagram in (a) with fluorescence detection at wavelength 550 nm results from MTHF and FAD_{ox} emission. Fluorescence emission from MTHF alone, recorded by detection at wavelength 428 nm, is displayed in diagram (b).

In order to extract the fluorescence lifetimes from the measured signal curves, convolution curves were calculated. In the case of shorter decay time than response time the convolution procedure may extract the decay time [151]. In the convolution procedure the experimental response function, $g(t)$ was used.

The true fluorescence signal due to δ-function excitation is called, $S_{F,\delta}$. The experimental fluorescence signal, $S_F(t)$, is fitted by the convoluted fluorescence function $S_{F,con}(t)$ which is given by

$$S_{F,con}(t) = \int_{-\infty}^{t} g(t')S_{F,\delta}(t-t')dt' , \qquad (5.1)$$

where the response function $g(t)$ is given by the dotted curves in Fig. 5.18.

For single-exponential excitation decay, the true fluorescence signal function is

$$S_{F,\delta}(t) = S_0 \exp(-t/\tau_F), \qquad (5.2)$$

where S_0 is the peak signal value and τ_F is the fluorescence lifetime.

From Fig. 5.18 (b) the convolution fit gives τ_F = 100±50 ps. It belongs to the excited state lifetime of MTHF in cry3. The fluorescence signal in Fig. 5.18 (a) is due to MTHF and FAD_{ox} emission, and it indicates a fast and a slow relaxation. The slow lifetime of $\tau_{F,sl}$ is determined to be about 1.1 ns by non-linear regression fit. It is attributed to not correctly fixed FAD_{ox} or free FAD_{ox}. If the fluorescence quantum yield by exposure at 450 nm of ϕ_F = 0.003 would

result completely from not correctly bound (free) FAD_{ox}, then the fraction of free FAD_{ox} to total FAD_{ox}, β_{free} would be

$$\beta_{free} = \frac{\phi_F(cry3,450nm)}{\phi_F(FAD_{ox})}.$$

(5.3)

The relation (5.3) gives $\beta_{free} \leq 0.037$. Since the composition of FAD_{ox} in cry3 is 40 % of the mole fraction of the not correctly bound FAD_{ox}, in the relation to the total amount of FAD, β_{free} is less than or equal to 1.5%.

If the fluorescence quantum yield of cry3 at 450 nm excitation, ϕ_F of about 0.003 would be due to non-covalently bound FAD_{ox}. The fluorescence lifetime of the non-covalently bound FAD_{ox}, τ_F would be estimated to be 59 ps by the relation $\tau_F = \phi_F \tau_{rad}$, where the radiative lifetime of FAD_{ox}, $\tau_{rad} = 19.5$ ns from reference [152] is used. The presence of free FAD_{ox} indicates that fluorescence lifetime of non-covalently bound FAD_{ox} is considerably less than 59 ps.

5.3 Thermal stability

The absorption spectrum of MTHF-Cl did not change very much at 50 °C (sample was kept for 5 min in thermal chamber). But under same condition the transmission spectrum of cry3 was shown serious a light scattering caused by a protein denaturation.

The thermal stability of cry3 was measured at 20 °C and 26 °C. At 20 °C cry3 begins to show light scattering (decrease of transmission in transport region) after 12~16 h. At 26 °C cry3 the light scattering begins already after 3 hours as shown in Fig. 5.19. Light scattering is due to protein denaturation (protein unfolding).
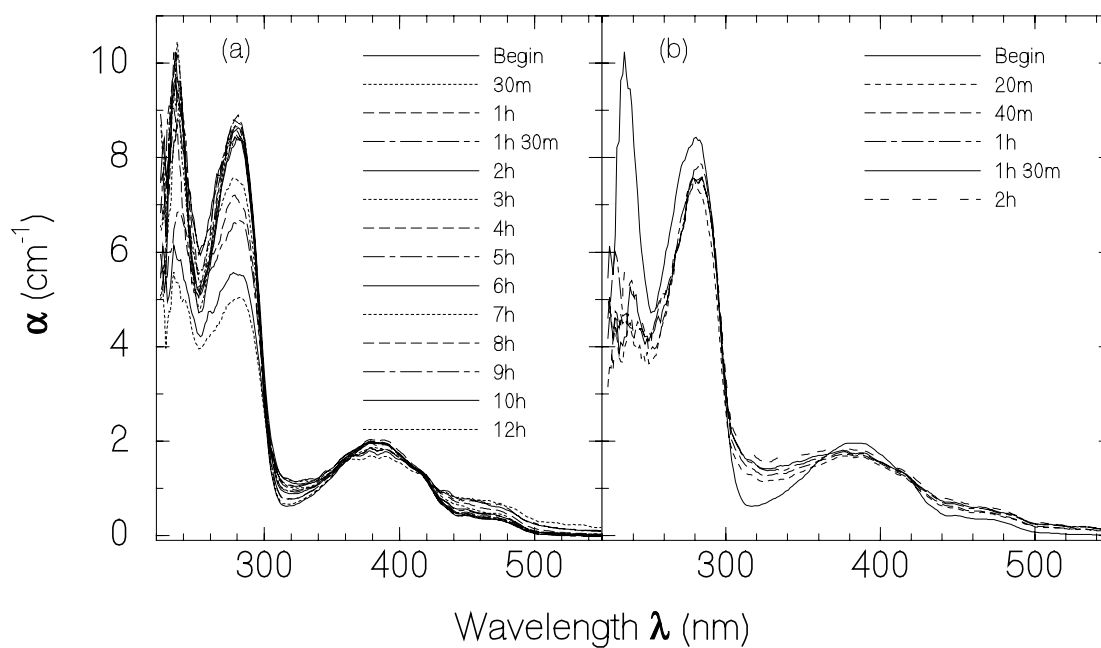

Fig. 5.19 Thermal stability test of cry3 in pH 7.5 aqueous buffer. The samples were thermostated. (a) Cry3 was kept at 20 °C. After 12 hours light-scattering initiated. (b) At 26 °C cry3 shows light-scattering after 20 min.

5.4 Light-Induced Behaviour

The transmission spectra for MTHF-Cl 1.98mg in 10 ml pH2.5 aqueous solution, estimated concentration $c = 4.03 \times 10^{-4} M$, were measured.
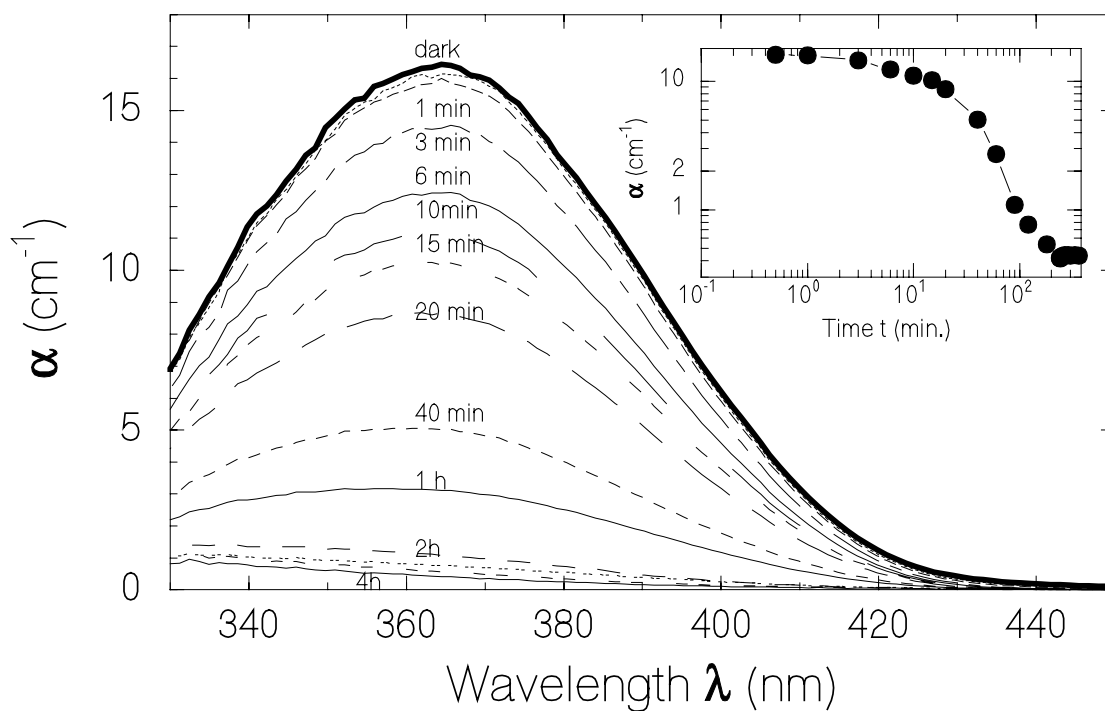

Fig. 5.20 MTHF-Cl 1.98 mg was dissolved in 10 ml pH 2.5 aqueous solution and transmission spectra were measured with exposure at 365 nm for 4 hours at room temperature. Exposure intensity, $I = 2.37 \times 10^{-2} Wcm^{-2}$.
The insert shows absorption coefficient versus time at λ_p=386 nm.
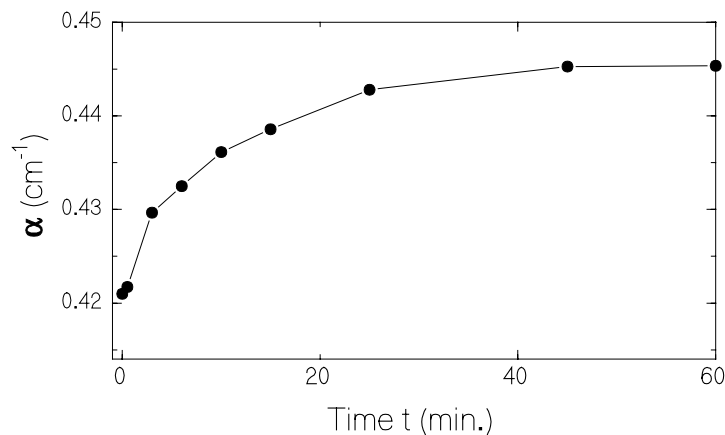
Fig. 5.21   Absorption recovery after light exposure λ_{exc}=365 nm for 4 hours. Exposure intensity, I = $2.37 \times 10^{-2} Wcm^{-2}$. Curve is plotted at λ_p=386 nm.
The spectrum of MTHF-Cl after light switch-off little recovered.

A 1.5 mm × 1.5 mm × 4 mm sample was excited for 4 h at 365 nm with an intensity of 2.37×10^{-2} W cm^{-2}. In Fig. 5.20 the absorption decrease with time is shown. The insert in Fig. 5.20 shows the temporal development of absorption coefficient at 386 nm. After light switch-off there occurred practically no absorption recovery as is seen in Fig. 5.21. This shows that an irreversible photo-degradation of MTHF-Cl has occurred.

The change of the absorption spectra of cry3 due to the exposure at 4 different excitations wavelengths is shown in Fig. 5.22. The exposure time, t_{exp}, was fixed to 20 min and the excitation intensity was varied. For $I_{exc} \geq 10^{-3}$ W cm^{-2} the sample was replaced by fresh one for each measurement. The transmission spectra were probed with an attenuated tungsten lamp. At excitation wavelength 470 nm in Fig. 5.22 (a), only FAD in cry3 is excited. The absorption decreases in the 440 to 490 nm region. FAD_{ox} is converted to the neutral fully reduced form ($FAD_{red}H_2$) or to the anionic fully reduced form ($FAD_{red}H^-$). In Fig. 5.22 (b) both FAD and MTHF chromophores are excited by light at 428 nm. The FAD_{ox} band and the MTHF band are decreased. Excitation at 407 nm (Fig. 5.22 (c)) and 365 nm (Fig. 5.22 (d))

94

causes a stronger decrease of the MTHF absorption band around 380 nm. At these wavelength the initial absorption is dominated by the absorption of MTHF.
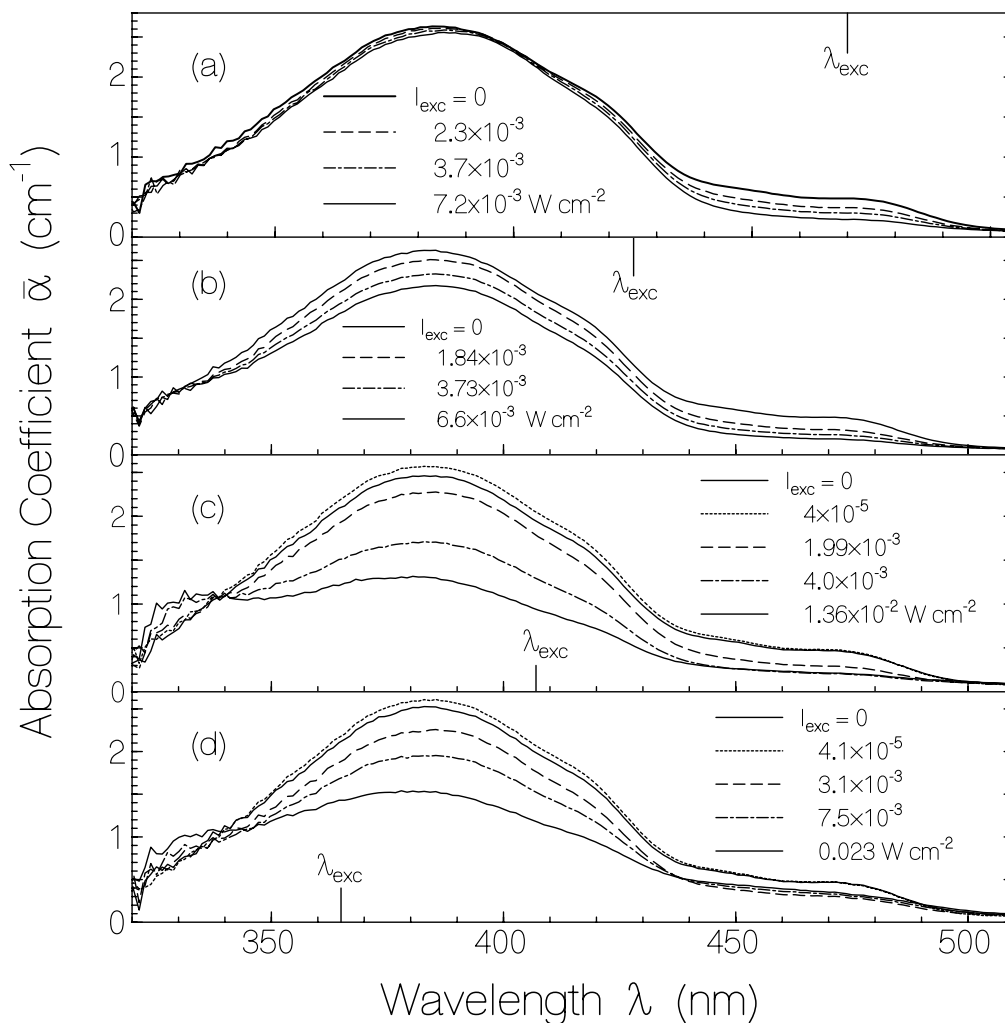
Fig. 5.22   Change of absorption spectra due to light exposure at different wavelengths and different excitation intensities. In all cases, spectra were recorded after 20 min of exposure. Transmission spectra were measured in succession. For excitation intensities $I_{exc} \geq 10^{-3}$ W cm^{-2} each time sample was replaced by fresh one.
(a) The exposure wavelength $\lambda_{exc} = 470$ nm, (b) $\lambda_{exc} = 428$ nm, (c) $\lambda_{exc} = 407$ nm, and (d) $\lambda_{exc} = 365$ nm.
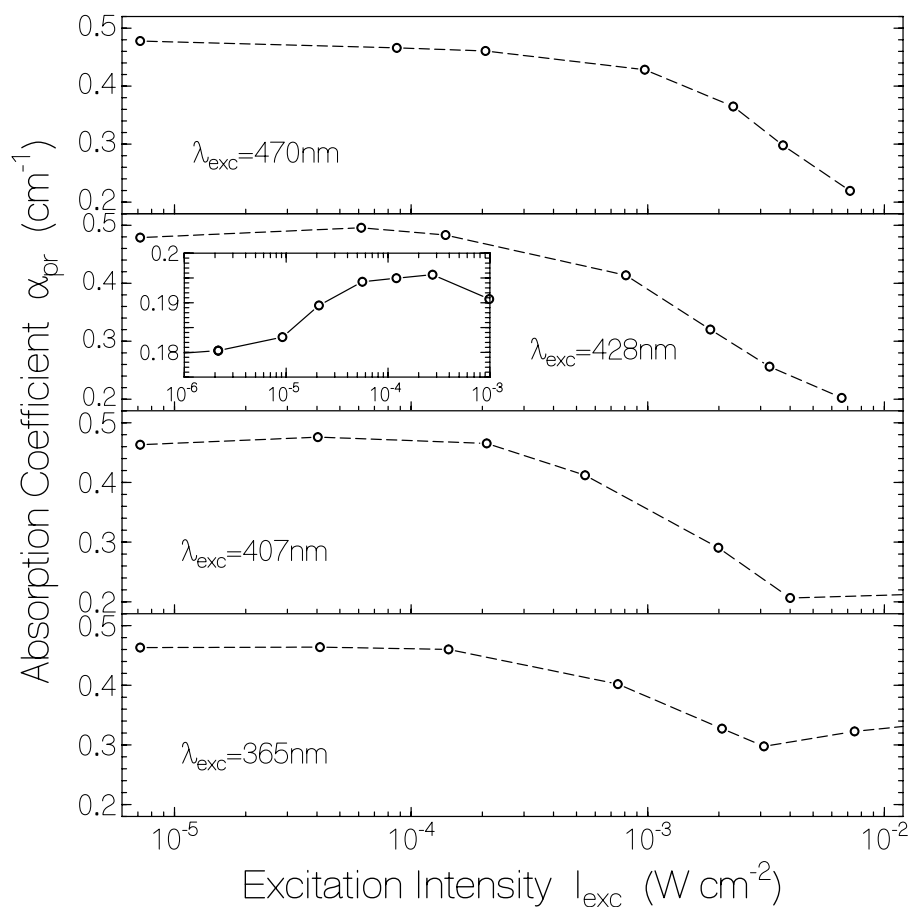
Fig. 5.23 (a)   Intensity dependent reduction of absorption coefficient of cry3 at λ_{pr} = 473 nm.
Exposure time was 20 min and the insert shows cry3 with λ_{exc} = 428 nm for 5 min exposure (sample concentration: 0.75 mg/ml).

The intensity dependent absorption behaviour at λ_{pr} = 473 nm (dominant absorption of FAD_{ox}) is shown in Fig. 5.23 (a) for the different excitation wavelength. The same is done in Fig 5.23 (b) for the probe wavelength λ_{pr} = 386 nm (dominant absorption of MTHF).

At low excitation intensity there occurs a slight rise in absorption both at λ_{pr} = 473 nm (FAD_{ox} absorption) and λ_{pr} = 386 nm (dominant MTHF absorption) as is more clearly seen by the inserts in Fig. 5.23. It is thought that the photo-excitation causes a structural conformation

96
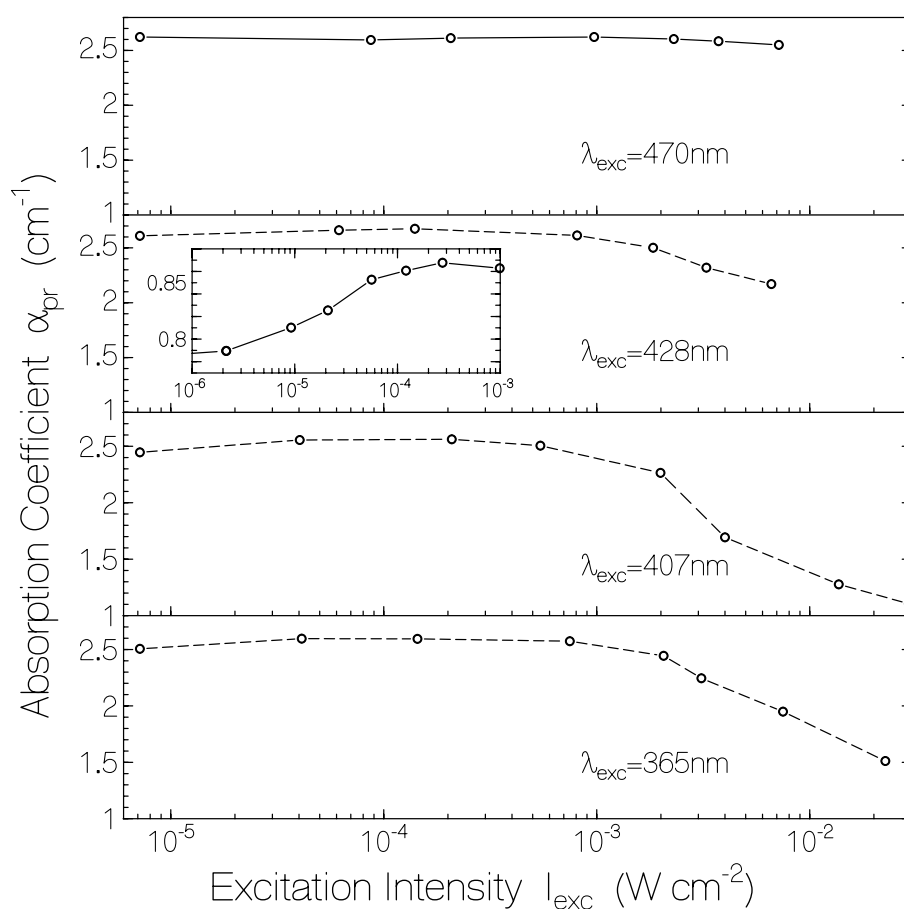
Fig. 5.23 (b) Intensity dependent reduction of absorption coefficient of cry3 at $\lambda_{pr} = 386$ nm. Exposure time was 20 min and the insert shows cry3 with $\lambda_{exc} = 428$ nm for 5 min exposure (sample concentration: 0.75 mg/ml).

change of the protein, which leads to a slight change of the absorption strength of FAD_{ox} and MTHF in the S_0-S_1 absorption bands.

At excitation intensities $> 10^{-4}$ W cm^{-2} the FAD_{ox} and MTHF absorption decreased. These decreases are due to FAD_{ox} reduction to $FAD_{red}H_2$ or $FAD_{red}H^-$, and due to photo-conversion of MTHF to a species which is not absorbing in the original 380 nm band region.

At high excitation intensities $> 10^{-2}$ W cm^{-2} some rise of absorption was observed. This rise was caused by light scattering due to protein unfolding probably due to sample heating [164].
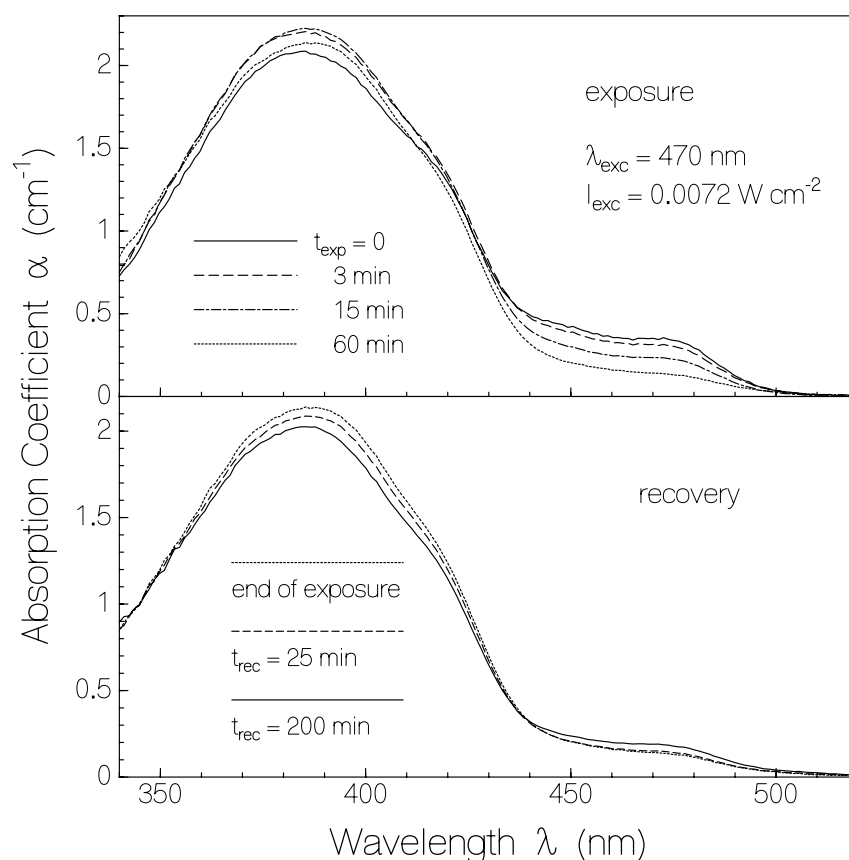
Fig. 5.24 (a) Top part: Absorption change due to excitation for 1 hour. Excitation wavelength, λ_{exc} = 470 nm; excitation intensity, I_{exc} = 0.0072 W cm^{-2}. The exposure times, t_{exp}, are given in the figure.
Lower part: Absorption recovery in the dark after 1 h of exposure. The times in darkness, t_{rec}, are given in the figure.

The photo-cyclic behaviour of cry3 was studied by exciting samples at high intensity for some period and then following the recovery in the dark. In Fig 5.23 (a) cry3 was excited at 470 and for 1 hour, and the absorption changes were measured. During the exposure the S_0-S_1 absorption of FAD_{ox} decreased due to photo-reduction. The absorption of the MTHF band changed slightly. The S_0-S_1 absorption band of MTHF first increased and then decreased. The rise in absorption is thought to be due to protein conformation changes what increase the MTHF absorption strength. The latter absorption decrease is thought to be due to the absorption decrease of FAD.

98
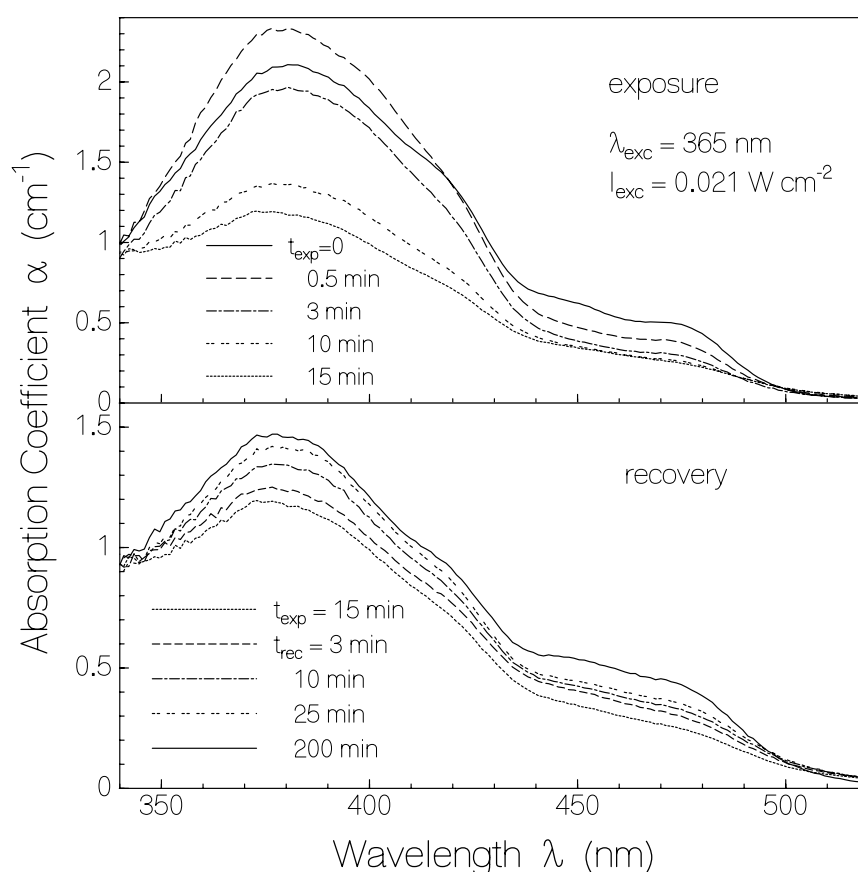
Fig. 5.24 (b) Top part: Absorption change due to excitation for 15 min. Excitation wavelength, λ_{exc} = 365 nm; excitation intensity, I_{exc} = 0.021 W cm^{-2}. The exposure times, t_{exp}, are given in the figure.
Lower part: Absorption recovery in the dark after 15 min of exposure. The times in darkness, t_{rec}, are given in the figure.

After light switch-off the absorption recovery is shown in the down part of Fig. 5.24 (a). The absorption band of FAD_{ox} is not completely recovered. It is thought that some permanent reduced FAD ($FAD_{red}H_{2,per}$) in cry3 has been formed during the long time of exposure. No oxidizing partner seems to be in the vicinity of $FAD_{red}H_2$. Also some irreversible photoproduct formation may be present [145].

In Fig. 5.24 (b) the photo-cyclic dynamics is shown for excitation at 365 nm. Both FAD_{ox} and MTHF are excited and undergo photo cycles. FAD_{ox} is reduced during exposure and recovers in the dark. MTHF first increases in absorption by protein conformation change then decreases by conversion to another folate moiety, and partly recovers in the dark.

99
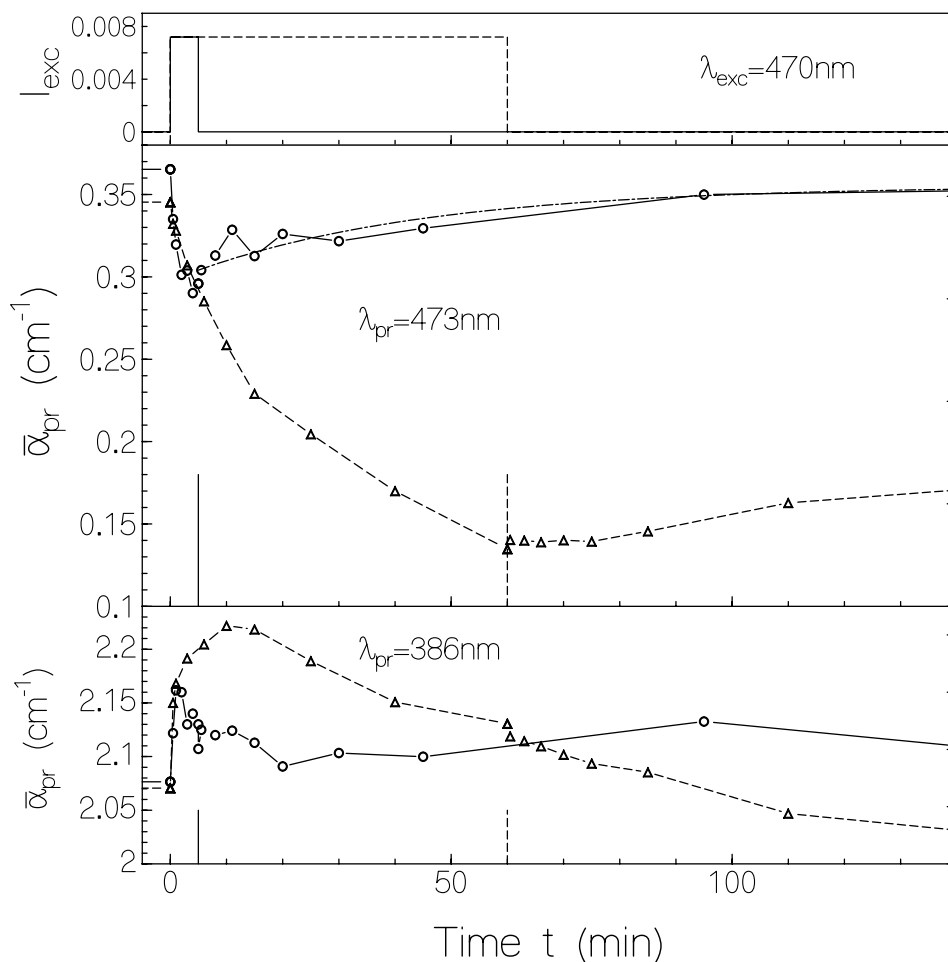
Fig. 5.25 (a)   Temporal photo-cyclic behaviour of cry3. λ_{exc}=470 nm. Solid lines belong to 5 min exposure and dashed lines belong to 60 min exposure. The absorption recovery with exposure time for 5 min is fitted as dashed-dotted curve.

The temporal development at the probe wavelengths λ_{pr} = 473 nm and λ_{pr} = 386 nm in the case of excitation at 470 nm are shown in Fig. 5.25 (a). In the middle part of Fig. 5.25 (a) the FAD_{ox} absorption recovery after 5 min exposure is fitted by the following single-exponential function :

$$\alpha_{pr}(t) = (\alpha_{pr,\infty} - \alpha_{pr,e})\{1 - \exp[-(t - t_e)/\tau_{rec}]\} + \alpha_{pr,e}, \qquad (5.4)$$

where t_e is the end of light exposure, $\alpha_{pr,\infty}$ is the final absorption coefficient after long time recovery, and $\alpha_{pr,e}$ is the absorption coefficient at t_e. The fit gives a recovery time of τ_{rec} = 42

100

min. The absorption difference between $\alpha_{pr}(0)$ and $\alpha_{pr}(\infty)$ indicates the permanent formation of $FAD_{red}H_2$ or $FAD_{red}H^-$.

Quantum efficiencies of protein and chromophore modification, ϕ_{mod}, may be determined by

$$\phi_{mod} = \frac{\Delta N_{mod}}{\Delta n_{ph,abs}} \tag{5.5}$$

where ΔN_{mod} is the number (density) of modified species, and $\Delta n_{ph,abs}$ is the number (density) of absorbed photons by the considered species. For the determination of the quantum efficiency of FAD_{ox} photo-reduction, ΔN_{mod} is given by

$$\Delta N_{mod} = \Delta N_{FAD_{ox}} \ell = x_1 N_0 \ell [\alpha_{pr}(t_{exp}) - \alpha_{pr}(0)]/\alpha_{pr}(0), \tag{5.6}$$

and $\Delta n_{ph,abs}$ is given by

$$\Delta n_{ph,abs} = I_{exc} t_{exp} \{1 - [T_{pr}(0) + T_{pr}(t_{exp})]/2\}/(h\nu_{exc}), \tag{5.7}$$

N_0 is the initial number density of cry3 molecules, x_1 is the mole-fraction of FAD_{ox}, and ℓ is the sample length ($l = 0.15$ mm in the experiments). Analysing the experimental data in the early part of light exposure in the middle part of Fig. 5.25 (a) delivers a quantum efficiency of FAD_{ox} reduction of $\phi_{FAD,red} \approx 0.0018$.

The quantum efficiency of permanent reduced FAD formation, $\phi_{FAD,red,per}$, is estimated from incomplete absorption recovery after photo-excitation as shown in the middle part of Fig. 5.25 (a). Using Eq. 5.5 with

$$\left. \begin{aligned} \Delta N_{mod} &= \Delta N_{FAD_{red,per}} \ell = x_1 N_0 \ell [\alpha_{pr,\infty} - \alpha_{pr}(0)]/\alpha_{pr}(0), \\ \text{and} \\ \Delta n_{ph,abs} &= I_{exp} t_e \{1 - [T_{pr}(0) + T_{pr}(t_e)]/2\}/(h\nu_{exc}), \end{aligned} \right\} \tag{5.8}$$

applied to the situation of 60 min light exposure in the middle part of Fig. 5.25 (a) gives $\phi_{FAD,red,per} \approx 4.3 \times 10^{-4}$.

The absorption spectral development at 386 nm in the case of excitation at 470 nm is shown in the down part of Fig. 5.25 (a). During beginning of exposure the absorption increases and then decreases. At light switch-off a small fast absorption reduction is seen followed by a slow absorption decrease or practically constant absorption. As described above, some structural change of the surrounding protein induces a modification of the MTHF absorption. The quantum efficiency of FAD light absorption induced MTHF absorption rise by protein reconformation, $\phi_{a,rise,MTHF}$, is given by the length-integrated number density of modified MTHF molecules to the absorbed photons according to Eq 5.5. ΔN_{mod} and $\Delta n_{ph,abs}$ are

$$
\left.
\begin{aligned}
\Delta N_{mod} &= \Delta N_{MTHF}\ell = N_0\ell[\alpha_{pr}(t_{exp}) - \alpha_{pr}(0)]/[\alpha_{pr,max} - \alpha_{pr}(0)], \\
\text{and} \\
n_{ph,abs} &= [1 - \overline{T}(\lambda_{exc})]t_{exp}I_{exc}/(h\nu_{exc}),
\end{aligned}
\right\} \quad (5.9)
$$

where $\overline{T} = [T(t_{exp}) + T(0)]/2$. Using the parameters from Fig. 5.25 (a) with t_{exp} = 30 s, $\alpha_{pr}(t_{exp})$ - $\alpha_{pr}(0)$ = 0.0796 cm^{-1}, $\alpha_{pr,max}$ - $\alpha_{pr}(0)$ = 0.151 cm^{-1}, I_{exc} = 0.0072 Wcm^{-2}, λ_{exc} = 470 nm, and $\overline{T}(\lambda_{exc})$ = 0.95, a value of $\phi_{a,rise,MTHF}$ = 0.1 is obtained.

The absorption changes at λ_{pr} = 473 nm (FAD$_{ox}$ absorption) and λ_{pr} = 386 nm (dominant MTHF absorption) in the case of 365 nm excitation are shown in Fig 5.24 (b). The S$_0$-S$_1$ absorption of FAD$_{ox}$ continuously decreases during exposure. The MTHF absorption at 386 nm increases the first 30 seconds and then drops.

As described above, this initial increasing MTHF absorption is thought to be caused by photo-induced protein restructuring. After 30 seconds of continuous light exposure the photo-conversion of MTHF to reversible MTHF′ (likely 5,10-methylene-THF) begins to dominate and the absorption decreases.
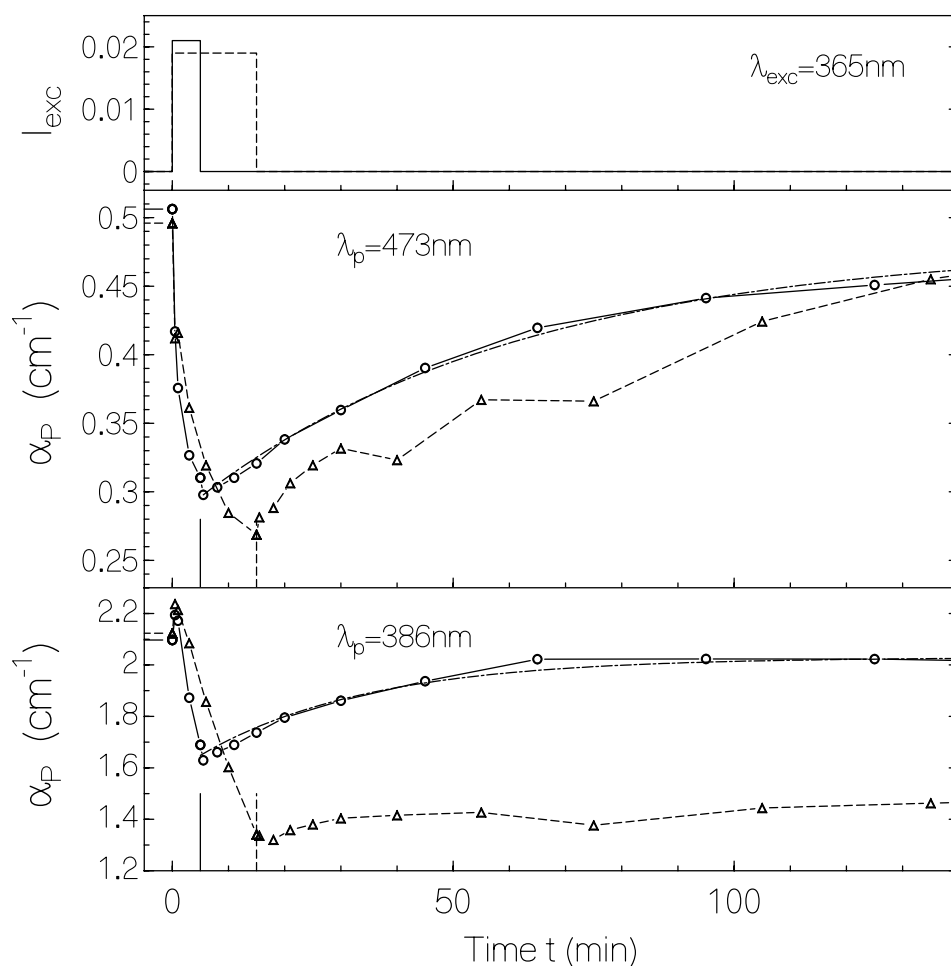
Fig. 5.25 (b) Temporal photo-cyclic behaviour of cry3. λ_{exc}=365 nm. Solid lines belong to 5 min exposure and dashed lines belong to 15 min exposure. The absorption recovery with exposure time for 5 min is fitted as dashed-dotted curve.

The MTHF absorption recovers partly in the dark (MTHF photo-cycle). Part of MTHF forms an irreversible photoproduct (MTHF´´ likely 5-formyl-THF or 10-formyl-THF).

For the short time exposure of 5 min, the absorption recovery at 386 nm is fitted by Eq. 5.4 and gives a recovery time of τ_{rec} (MTHF´) $\approx$ 30 min.

The decrease of the MTHF absorption band upon continuous light exposure is caused by reversible MTHF conversion (MTHF´) and irreversible MTHF degradation (MTHF´´). It is likely the MTHF´ is equal to 5,10-methylene-THF, and that MTHF´´ is equal to 10-formyl-

THF or 5-formyl-THF (hydrolysis of MTHF [165]). In the dark recovery MTHF´ (likely 5,10-methylene-THF) is converted back to MTHF.

The quantum efficiency of conversion of MTHF to MTHF´, $\phi_{MTHF´}$ is calculated to be about 2.9×10^{-4} by application of Eq. 5.5 with

$$\left. \begin{aligned} \Delta N_{mod} &= \Delta N_{MTHF} \ell = N_0 \ell \Delta \alpha_{pr} / \alpha_{pr}(0), \\ \text{and} \\ \Delta n_{ph,abs} &= \delta t_{exp} I_{exc}[1 - \overline{T}(\lambda_{exc})]/(h\nu_{exc}), \end{aligned} \right\} \quad (5.10)$$

where δt_{exp} is the considered time interval of exposure, and $\overline{T}(\lambda_{exc})$ is the average transmission at the excitation wavelength during the exposure interval (t_e = 5 min, $\alpha_{pr}(0)$ = 2.09 cm^{-1}, $\Delta \alpha_{pr}$ = 0.318 cm^{-1}, I_{exc} = 0.021 Wcm^{-2}, λ_{exc} = 365 nm, and $\overline{T}(\lambda_{exc})$ = 0.758).

The quantum efficiency for the formation of MTHF´´, $\phi_{MTHF´´}$ is extracted from the not complete recovery at 386 nm absorption after excitation switch-off. Application Eq. 5.5 with

$$\left. \begin{aligned} \Delta N_{mod} &= \Delta N_{MTHF,ox} \ell = N_0 \ell [\alpha_{pr,\infty} - \alpha_{pr}(0)] / \alpha_{pr}(0), \\ \text{and} \\ \Delta n_{ph,abs} &= t_e I_{exc} \{1 - \overline{T}(\lambda_{exc},0) + T(\lambda_{exc},t_e)]/2\}/(h\nu_{exc}), \end{aligned} \right\} \quad (5.11)$$

gives $\phi_{MTHF´´} \approx 3.7 \times 10^{-5}$ (t_e = 15 min, $\alpha_{pr,\infty} - \alpha_{pr}(0)$ = 0.148 cm^{-1}, $\alpha_{pr}(0)$ = 2.12 cm^{-1}, I_{exc} = 0.019 Wcm^{-2}, λ_{exc} = 365 nm, and $\overline{T}(\lambda_{exc})$ = 0.81).

The dark-adapted cry3 includes 5 % FAD in the semiquinone state ($FADH^\bullet$). The photo-cyclic absorption behaviour of $FADH^\bullet$ in cry3 is shown in Fig. 5.26. Since the S_0-S_1 absorption cross-section of $FADH^\bullet$ is rather small (see Fig. 5.13), a highly concentrated sample was used ($c = C_w / M_w = 1.4 \times 10^{-3}$ mol dm^{-3}, C_w = 85 mg / ml).

(a)

(b)
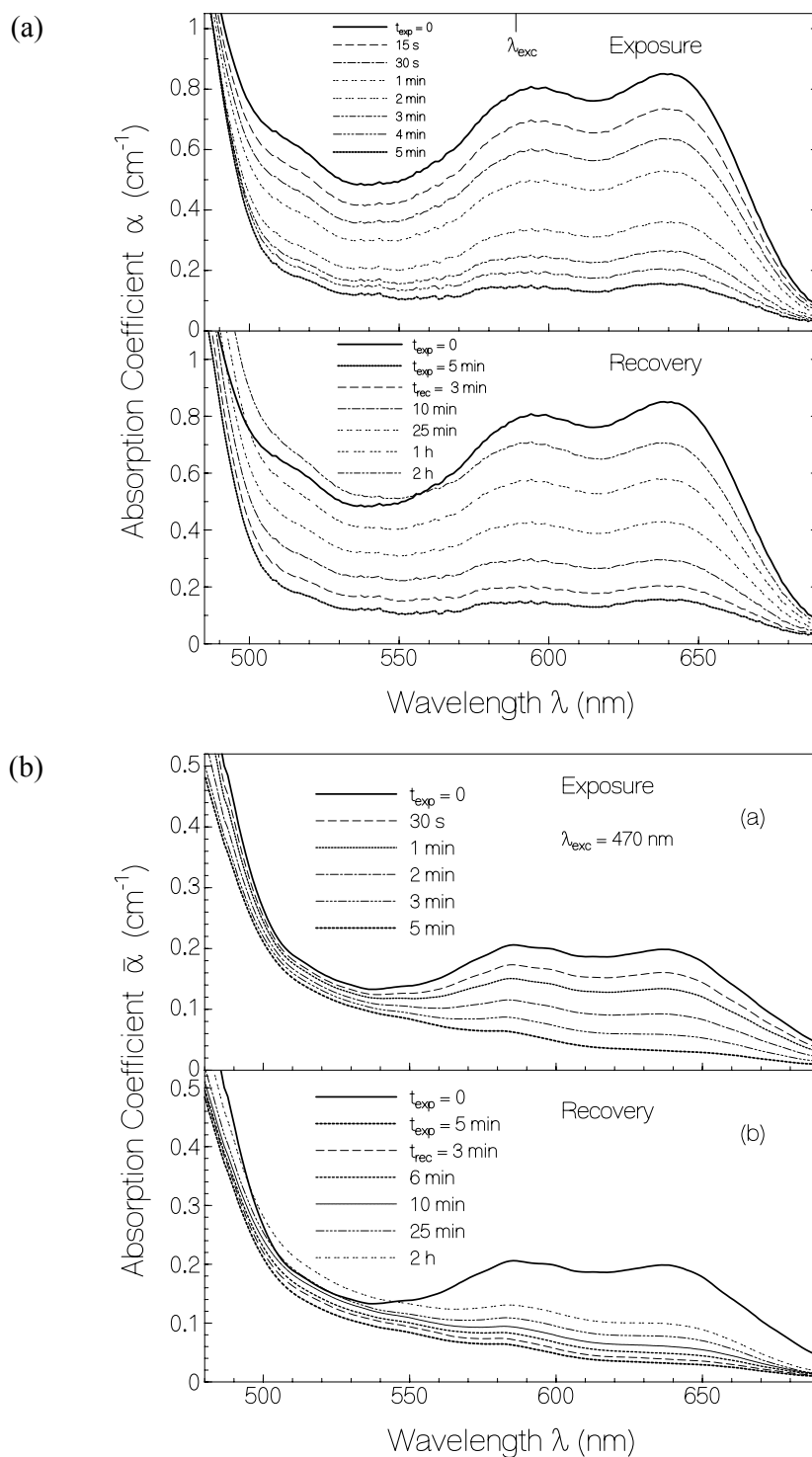
Fig. 5.26 The spectral change of neutral FAD-semiquinone (FADH$^\bullet$) with exposure (top) and their recovery (down). Exposure time was 5 min.
(a) Exposure wavelength, λ_{exp} = 589 nm and exposure intensity, $I_{exc,589}$ = 2.55×10^{-3} W cm^{-2}.
(b) Exposure wavelength 470 nm and exposure intensity, $I_{exc,470}$ = 1.05×10^{-2} W cm^{-2}.

The FADH$^\bullet$ was excited at 589 nm with intensity 2.55×10^{-3} Wcm^{-2}. In Fig. 5.26 (a) the FADH$^\bullet$ absorption spectra decreased with time. They fully recovered in the dark with a time constant of τ_{rec} = 60 min.

The quantum efficiency, $\phi_{sq,red}$, of FAD-semiquinone reduction to FAD-hydroquinone was calculated by application of Eq. 5.5 to the experimental situation with

$$\Delta N_{mod} = \Delta N_{FADH^\bullet} \cdot \ell = x_2 N_0 \ell [\alpha_{pr}(0) - \alpha_{pr}(t_{exp})/\alpha_{pr}(0)],$$
and
$$\Delta n_{ph,abs} = t_{exp} I_{exc}[1 - \overline{T}(\lambda_{exc})]/(h\nu_{exc}).$$

$$\left. \right\} \quad (5.12)$$

The analysis gives $\phi_{sq,red} \approx 0.07$ (t_{exp} = 5 min, $\alpha_{pr}(0) - \alpha_{pr}(t_{exp})$ = 0.697 cm^{-1}, $\alpha_{pr}(0)$ = 0.850 cm^{-1}, I_{exc} = 0.0025 Wcm^{-2}, λ_{exc} = 589 nm, and $\overline{T}(\lambda_{exc})$ = 0.92).

The temporal absorption behaviour of FADH$^\bullet$ in the case of excitation of FAD$_{ox}$ at 470 nm is shown in Fig. 5.26 (b) (sample concentration C_w = 8.5 mg / ml). During light exposure FADH$^\bullet$ reduces. No measurable FADH$^\bullet$ formation occurs in the photo-reduction of FAD$_{ox}$. Only the photo-reduction of FAD$_{ox}$ to FAD$_{red}$H$_2$ or FAD$_{red}$H$^-$ is detectable. After light switch-off the absorption of FADH$^\bullet$ recovers partly similar to the absorption recovery of FAD$_{ox}$ (thermodynamic equilibrium between both).

Reduction of FAD$_{ox}$* to to FAD$_{red}$H$_2$ via excited FADH$^\bullet$ (FADH$^\bullet$*) might occur according to Scheme 5.2.

$$FAD_{ox} \xrightarrow{h\nu} FAD_{ox}* \xrightarrow{e^-} FADH^\bullet* \xrightarrow{e^-} FAD_{red}H_2$$
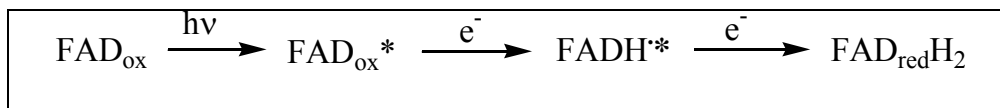
Scheme 5.2 Photo-induced transfer from FAD$_{ox}$ in cry3.
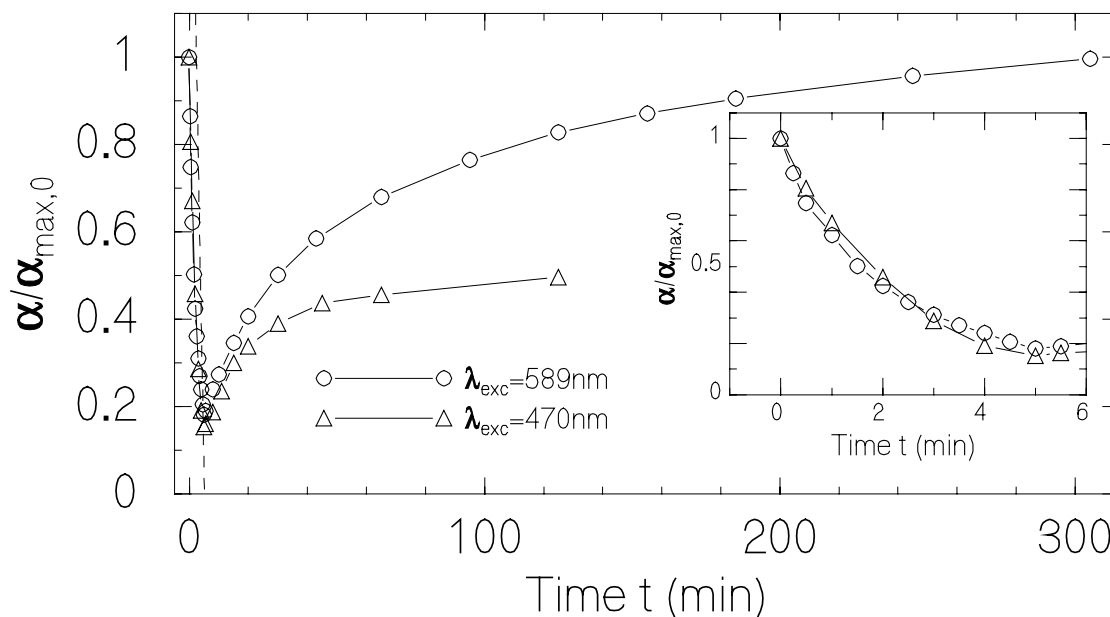
Fig. 5.27   Temporal development of neutral FAD-semiquinone ($FADH^\bullet$) with exposure wavelength 589 nm (circle) and 470 nm (triangle). Spectral probe wavelength, λ_{pr} is 640 nm. Insert shows the exposure part for initial 5 min. Exposure intensity, $I_{exc,589} = 2.55 \times 10^{-3}$ W cm^{-2} and $I_{exc,470} = 1.05 \times 10^{-2}$ W cm^{-2}.

The photo-cyclic dynamics of $FADH^\bullet$ probed at 640 nm by exposure wavelength 589 nm and 470 nm are shown in Fig. 5.27.

The temporal development of the fluorescence quantum distributions, E_F (λ), of cry3 during light exposure at 365 nm, is shown in Fig. 5.28. The E_F (λ) signal is shown for magic-angle fluorescence detection. The excitation intensity was 4.5×10^{-3} Wcm^{-2}. The fluorescence quantum efficiency of cry3 in the dark state was measured by fluorescence excitation with intensity 1.0×10^{-4} Wcm^{-2} for 990 ms. The fluorescence quantum distribution, E_F (λ), increases quickly with exposure time. Since the excitation wavelength is 365 nm, E_F (λ) is dominated by MTHF emission. The rise in E_F (λ) is thought to be due to the reduction of photo-induced electron-transfer by light induced protein structural change. It is known that electron transfer is strongly dependent on the distance between donor-acceptor [141,159,166~168].

107

The fluorescence peak around 520 nm is due to FAD_{ox} emission. It clearly indicates the Förster-type energy transfer from MTHF to FAD_{ox}. At longer times the FAD_{ox} contribution is reduced because of non-fluorescent $FAD_{red}H_2$ formation. In the dark the MTHF fluorescence reduces back towards the dark-adapted signal situation.
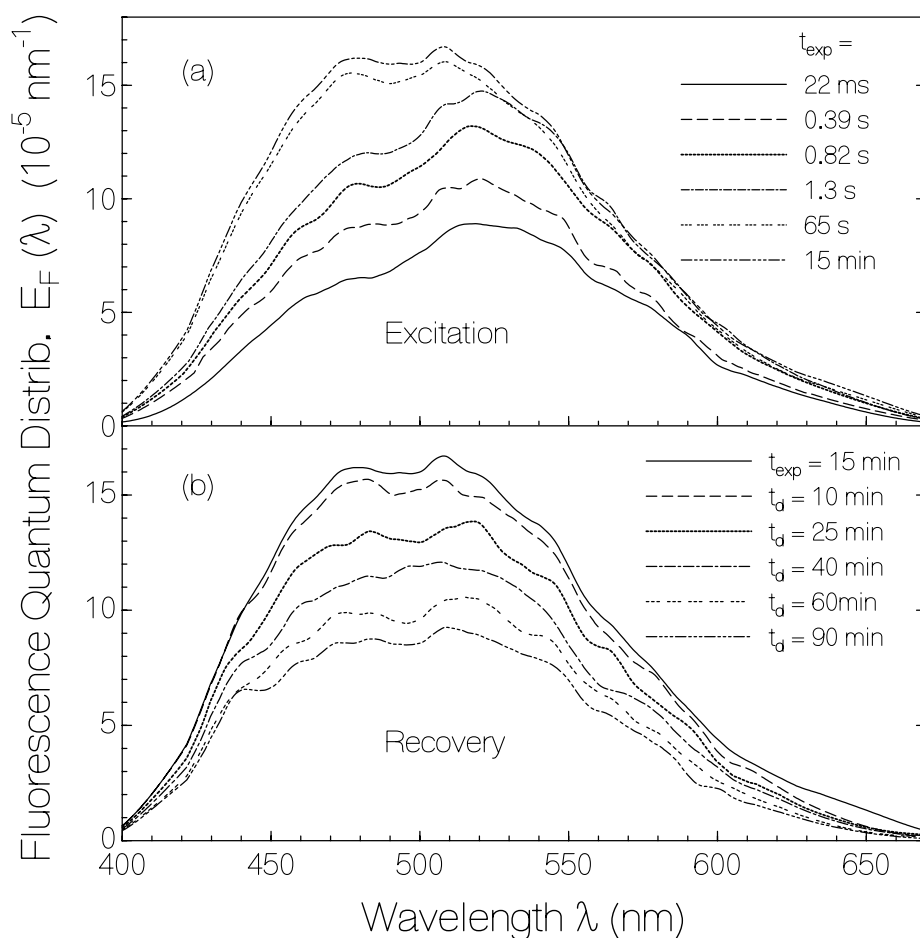
Fig. 5.28   Fluorescence quantum distribution of cry3 in pH 7.5 buffer at several times, t_{exp}, during light exposure at λ_{exc} = 365 nm with I_{exc} = 4.5×10^{-3} W cm^{-2} (a), and at several times, t_d, in the dark after light switch-off (b). Magic angle polarized light was recorded to detector.
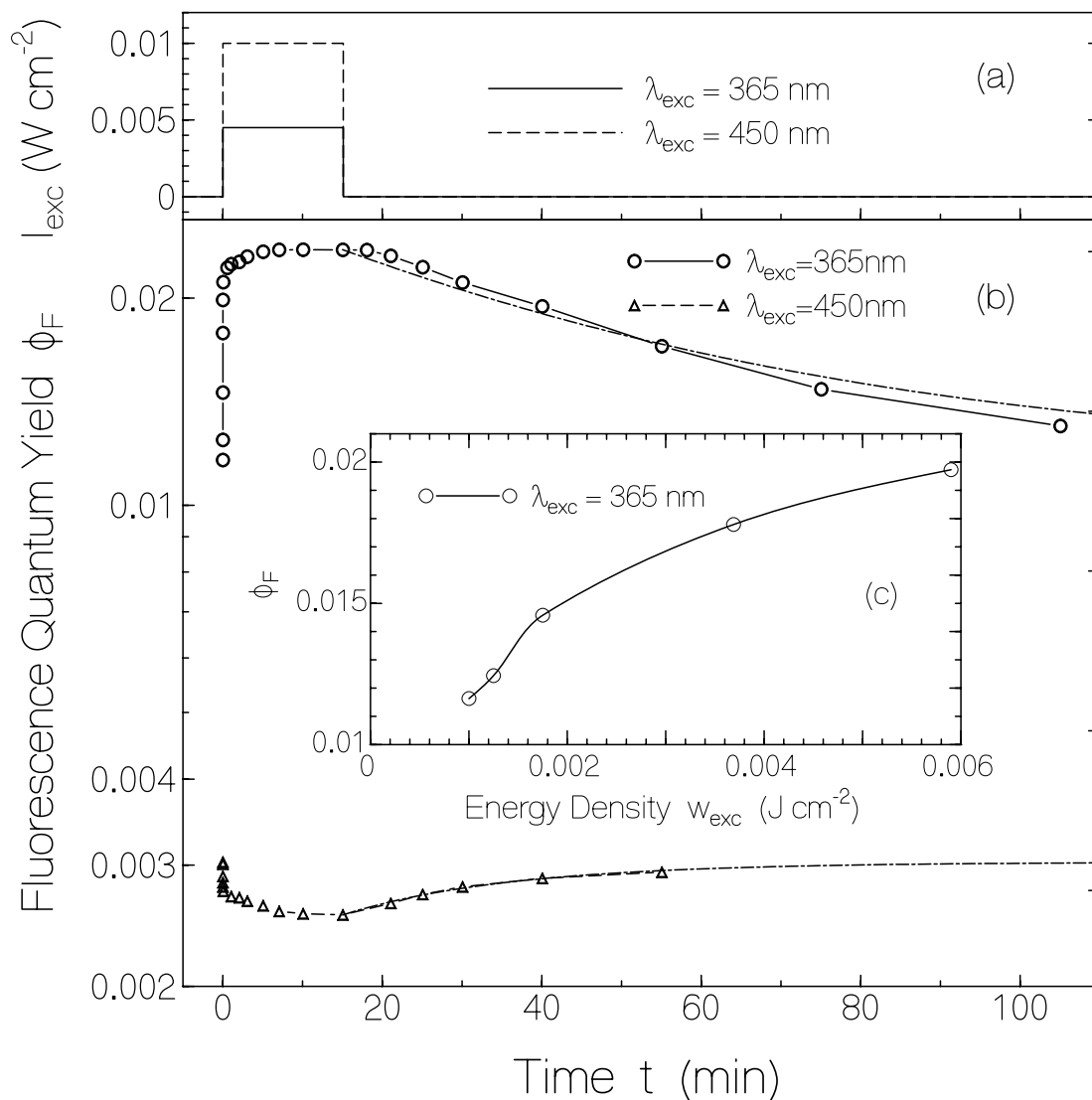
Fig. 5.29 (a) Light excitation profiles.
(b) Temporal development of fluorescence quantum yield during light exposure and recovery. Circle marked curve is with exposure wavelength 365 nm and triangle curve shows that of exposure 450 nm. Dash-Dotted lines indicate single-exponential fitting. The recovery time $\tau_{F,rec} \approx 52$ min at $\lambda_{exc} = $ 365 nm and $\tau_{F,rec} \approx$ 23 min at $\lambda_{exc} = $ 450 nm.
(c) Intensity dependent fluorescence quantum yield measurement. Exposure time was 990 ms.

The FAD$_{ox}$ fluorescence is not fully recovered. This seems to be due to some permanent FAD$_{red}$H$_2$ formation and not complete re-structuring to the original protein structure, leading to less efficient Förster-type energy transfer to FAD$_{ox}$.

The temporal development of the fluorescence quantum yield of cry3 in pH 7.5 buffer is shown in Fig. 5.29. The light exposure versus time is shown in part (a). The excitation wavelengths at 365 nm and 450 nm were used.

The open circle curve in part (b) belongs to the temporal fluorescence quantum yield development in the case of exposure at 365nm. At light switch-on the fluorescence quantum yield belonging to MTHF and FAD emission rises quickly by a factor of two.

The triangle marked curve displays the temporal fluorescence efficiency development in the case of exposure at 450 nm. The fluorescence quantum yield belonging to FAD$_{ox}$ steeply decreases a little bit at the onset of exposure. This is thought to be caused by protein re-conformation (signaling state formation with increased efficiency of photo-induced electron transfer). In the dark the fluorescence quantum yield recovers back to the initial behaviour. The time constants of single-exponential fluorescence recovery, $\tau_{F,rec}$ are about 52 min for λ_{exc} = 365 nm, and $\tau_{rec} \approx 23$ min for λ_{exc} = 450 nm.

The intensity dependent rise of fluorescence quantum yield with increasing exposure intensity for an exposure time of 990 ms is shown in the Fig 5.29 (c) for an excitation wavelength of 365 nm. The excitation energy density, w_{sat}, where the rise in fluorescence quantum yield reaches half of its maximum value, is $w_{sat} \approx 4.2 \times 10^{-3}$ J cm^{-2}. The saturation energy density, for the photo-induced MTHF fluorescence increases, is estimated from reference [169] as follows,

$$w_{sat} = h\nu_{exc} / (\sigma_{a,exc} \phi_{F,rise,MTHF}), \tag{5.13}$$

where $\sigma_{a,exc}$ is the absorption cross-section of cry3 at the excitation wavelength $\lambda_{exc} = c_0/\nu_{exc}$ (c_0 is speed of light in vacuum) and $\phi_{F,rise,MTHF}$ is the quantum efficiency of photo-induced

charge transfer reduction. The experimental parameters are $\lambda_{exc} = 365$ nm, $\sigma_{a,exc} = 1.24 \times 10^{-16}$ cm^2, and $w_{sat} \approx 4.2 \times 10^{-3}$ J cm^{-2}. Comparison of Eq. 5.8 with the experimental w_{sat} value gives $\phi_{F,rise,MTHF} \approx 1$.

This result implies that each absorbed photon in cry3 modifies the protein structure to have larger distance between charge transfer partners.

The temporal development of fluorescence signal of cry3 was also measured by the picosecond laser pulse fluorescence probing as shown in Fig. 5.30. The laser pump wavelength was at 400 nm and exposure wavelengths were at 365 nm and at 470 nm. The fluorescence emission was probed at 428 nm.
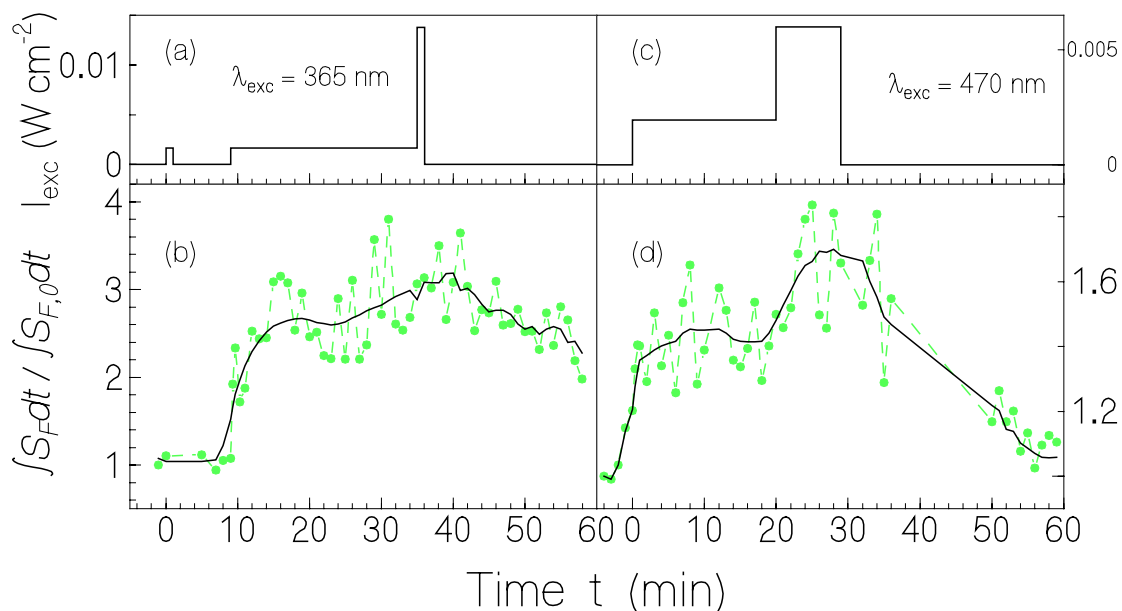
Fig. 5.30   The development of fluorescence emission signal by light exposure with a time and its recovery in dark. The probing wavelength is 428 nm.
(a) and (b) with exposure wavelength 365 nm.
(c) and (d) with exposure wavelength 470 nm.
In down part, circle-dashed lines indicate experimental results and solid curve lines are its smoothed curve.

The integral of fluorescence signal by exposure of wavelength 365 nm quickly increased more than two times. After light switch-off the fluorescence signal slowly decreased.

In the case of exposure at 470 nm the integral value of the fluorescence signal of cry3 showed a similar behaviour as in the case of 365 nm excitation increased. It is thought that the FAD_{ox} excitation causes a protein conformation change which increases the distance between the MTHF and acid residue charge-transfer pair. After light switch-off again the fluorescence integral recovered to the original dark adapted situation.

5.5 Förster-Type Energy Transfer

The radiative lifetime of MTHF is calculated from the S_0-S_1 absorption cross-section spectrum and the shape of the fluorescence quantum distribution using the Strickler-Berg formula [170~172]

$$\tau_{rad}^{-1} = \frac{8\pi c_0 n_F^3}{n_A} \frac{\int_{em} E_F(\lambda)d\lambda}{\int_{em} E_F(\lambda)\lambda^3 d\lambda} \int_{abs} \frac{\sigma_a(\lambda)}{\lambda} d\lambda \,, \tag{5.14}$$

where c_0 is the vacuum light velocity, n_A and n_F are the average refractive indices in the S_0-S_1 absorption region (*abs*) and the S_1-S_0 emission region (*em*).

The radiative lifetime of MTHF, τ_{rad}, is estimated to be 7.6 ns (upper border of absorption wavelength λ_u = 303 nm, n_A = 1.3475, n_F = 1.337). From the relation $\tau_F = \phi_F \tau_{rad}$, the fluorescence lifetime, τ_F, is estimated to be about 19 ps. On comparing with results in Ref [173], the τ_F value determined here is similar to the τ_F value determined there. But a higher fluorescence quantum yield of MTHF was reported in Ref. [173].

The Förster-type energy transfer in two-chromophore-systems occurs from the short-wavelength absorbing component (donor) to the long-wavelength absorbing component (acceptor). In cry3, the electron donor is MTHF and the acceptor is FAD (FAD$_{ox}$, FAD$_{red}$H$_2$, and FADH$^\bullet$) [44]. In the following the quantum efficiencies of Förster-type energy transfer, ϕ_{ET}, between MTHF and FAD$_{ox}$, FAD$_{red}$H$_2$, and FADH$^\bullet$ are estimated.

The Förster-type energy transfer quantum efficiency is given by

$$\phi_{ET} = \frac{k_{ET}}{k_{tot}} = \frac{k_{ET}}{k_{ET} + k_{F,0,d}} = \frac{k_{ET}}{k_{ET} + (\phi_{F,0,d}\tau_{rad,d})^{-1}} , \tag{5.15}$$

where k_{ET} is the rate of energy transfer, k_{tot} is the total rate constant of the donor relaxation, and $k_{F,0,d} = \tau_{F,0,d}^{-1}$ is the rate of S_1-S_0 relaxation of the donor in the absence of energy transfer. $\phi_{F,0,d}$ is the fluorescence quantum yield of the donor in the absence of energy transfer, and $\tau_{rad,d}$ is the radiative lifetime of the donor.

The rate of Förster-type energy transfer is defined by [142,143],

$$k_{ET} = k_{F,0,d}\left(\frac{R_0}{R_d}\right)^6 = k_{rad,d}\left(\frac{R_0'}{R_d}\right)^6 , \tag{5.16}$$

where R_0 is the critical Förster distance ($k_{ET} = k_{F,0,d}$). R_0' is the critical Förster distance where $k_{ET} = k_{rad,d}$, and R_d is the distance between the energy transfer partners. The Förster distance, R_0', is given by the relation [142~144]

$$R_0'^6 = \frac{9\overline{\kappa^2}}{128\pi^5 n^4}\int E_F'(\lambda)\sigma_a(\lambda)\lambda^4 d\lambda , \tag{4.4}$$

where n is the average refractive index in the overlap region of absorption and emission, and $\sigma_a(\lambda)$ is the absorption cross-section of the acceptor. $E_F'(\lambda)$ is the normalized fluorescence quantum distribution of the donor according to

$$E_F'(\lambda) = E_F(\lambda)/\int E_F(\lambda')d\lambda' = E_F(\lambda)/\phi_F .$$

The orientation factor, κ, is determined by the orientation of the transition dipole moments of the interacting donors (D) and acceptors (A) [142]. The orientation factor is given by [142]

$$\kappa = \cos(\varphi_{DA}) - 3\cos(\varphi_D)\cos(\varphi_A) , \tag{5.17}$$

where φ_D and φ_A are the angles of the donor and acceptor transition dipole moments to the connection line between D and A. φ_{DA} is the mutual angle between the transition dipole moments. Depending on the orientation of transition dipole moments, the range of κ may be

114

between 0 and 2. $\overline{\kappa^2}$ is 2/3 for a statistical isotropic orientation of the transition dipole moments [142].

The critical Förster distances are calculated to be R'_0 (MTHF-FAD$_{ox}$) = 3.93 nm, R'_0 (MTHF-FAD$_{red}$H$_2$) = 2.68 nm, and R'_0 (MTHF- FADH$^{\bullet}$) = 3.84 nm. For the considered situations of energy transfer from MTHF to FAD, the distance between donor and acceptor is R_d = 1.5247 nm. The angles of a transition dipole moments are φ_D = 38.91°, φ_A = 69.44°, and φ_{DA} = 86.40° [174], with $\overline{\kappa^2}$ = 0.573. The calculated energy transfer rates are k_{ET}(MTHF $\rightarrow$FAD$_{red}$H$_2$) $\approx$ 4×10^9 s^{-1}, k_{ET}(MTHF $\rightarrow$FAD$_{ox}$) $\approx$ 3.9×10^{10} s^{-1}, and k_{ET}(MTHF $\rightarrow$FADH$^{\bullet}$) $\approx$ 3.6×10^{10} s^{-1} with τ_{rad} = 7.6 ns.

The quantum efficiencies of Förster-type energy transfer, ϕ_{ET}, by Eq. 5.15, can not be exactly determined since the fluorescence quantum yield, $\phi_{F,0}$, of MTHF in cry3 in the absence of FAD in cry3 is not known. Assuming as a lower limit $\phi_{F,0} = \phi_F \approx 0.012$ for dark-adapted cry3, and $\phi_{F,0} = \phi_F \approx 0.024$ for light-adapted cry3, the lower limits of quantum efficiencies of Förster-type energy transfer are ϕ_{ET} (MTHF-FAD$_{ox}$) $\approx$ 0.78 for dark adapted cry3, and ϕ_{ET} (MTHF-FAD$_{ox}$) $\approx$ 0.87 for light-adapted cry3.

5.6 Photo-Cycles of Cry3

The photo-cyclic behaviour was investigated by absorption and fluorescence spectroscopy. The results are presented by the schemes 5.3 to 5.6. These photo-cycles consider protein conformation changes, FAD-semiquinone reduction, oxidized FAD reduction, and MTHF conversion. Additionally the conversion of oxidable reduced FAD to permanent reduced FAD and the conversion of MTHF to permanent conversion of MTHF (MTHF´´) was observed.

$$\text{MTHF-Cry3}_{da}\text{-FAD}_{ox} \underset{\text{dark}}{\overset{h\nu,\ \phi_{protein}}{\rightleftharpoons}} \text{MTHF-Cry3}_{la}\text{-FAD}_{ox}$$
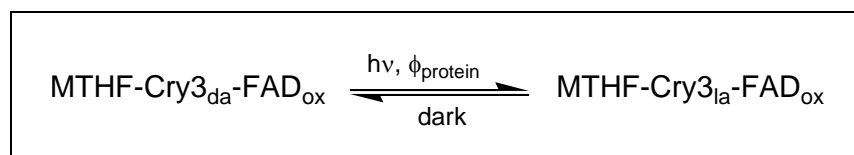
Scheme 5.3 : The photo-cyclic dynamics of dark-adapted cry3 to light-adapted cry3 form.

The cycle of the protein conformational change follows the general Scheme 5.3. When cry3 absorbs a photon, the dark-adapted cry3 (MTHF-Cry3$_{da}$-FAD) is converted to the light-adapted form (MTHF-Cry3$_{la}$-FAD). The quantum efficiency of this modification, $\phi_{protein} \approx \phi_{F,rise,MTHF} \approx \phi_{F,decrease,FAD} \approx 1$ is obtained. In dark, after light switched off, cry3 is back-recovered to the primary dark state. The back-reaction occurs with rather slow recovery time

constant, $\tau_{protein,rec} \approx 60$ min. Upon weak light-illumination, small absorption changes of MTHF and FAD_{ox} were observed, with a quantum efficiency of $\phi_{a,rise,MTHF} \approx \phi_{a,rise,FAD} \approx 0.1$.

$$\text{MTHF-Cry3-FADH}^{\bullet} \underset{\text{dark}}{\overset{h\nu,\ \phi_{sq,red}}{\rightleftharpoons}} \text{MTHF-Cry3'-FAD}_{red}\text{H}_2$$
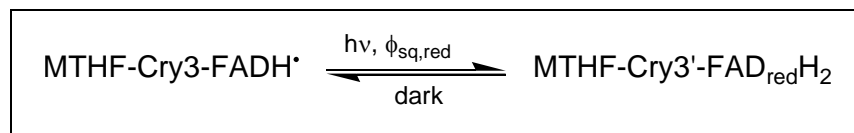
Scheme 5.4 : The photo-cyclic dynamics of FAD-semiquinone reduction form in cry3.

The photo-cyclic dynamics of FAD-semiquinone reduction follows Scheme 5.4. MTHF-Cry3- $FADH^{\bullet}$ is modified to MTHF-Cry3′-$FAD_{red}H_2$. The apoprotein Cry3 changes its structure to Cry3′ because of the electron transfer to $FADH^{.}$. The quantum yield of FAD-semiquinone reduction to FAD-hydroquinone, $\phi_{sq,red}$ is about 0.07. After the light switch-off, $FAD_{red}H_2$ is recovered to $FADH^{\bullet}$ in the dark. The time constant of recovery was found to be $\tau_{sq,rec} \approx 60$ min.

$$\text{MTHF-Cry3-FAD}_{ox} \underset{\text{dark}}{\overset{h\nu,\ \phi_{FAD,red}}{\rightleftharpoons}} \text{MTHF-Cry3''-FAD}_{red}\text{H}_2$$
$$\downarrow \begin{array}{c} h\nu \\ \phi_{FAD,red,per} \end{array}$$
$$\text{MTHF-Cry3''-FAD}_{red}\text{H}_{2,per}$$
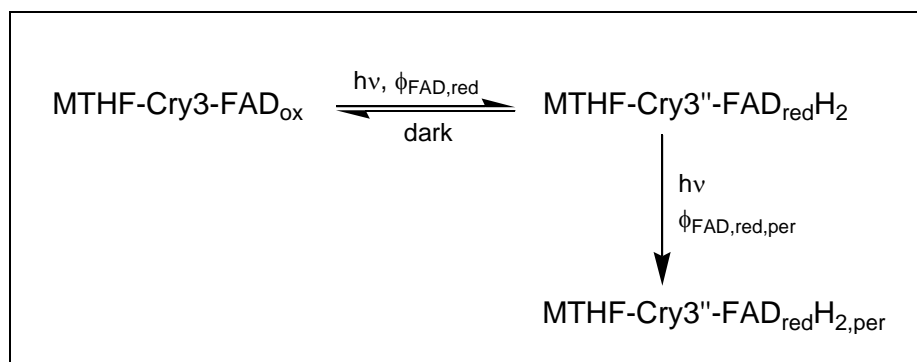
Scheme 5.5 : The photo-cyclic dynamics of reversible reduction of bound FAD_{ox} to $FAD_{red}H_2$ and the modification of re-oxidable $FAD_{red}H_2$ to permanent $FAD_{red}H_2$.

Scheme 5.5 exhibits the photo-cyclic dynamics of FAD_{ox} reduction, and the conversion of reversible $FAD_{red}H_2$ to permanent $FAD_{red}H_2$. MTHF-Cry3-FAD_{ox} is converted to MTHF-

Cry3′′-FAD$_{red}$H$_2$. The quantum efficiency for this photo-conversion, $\phi_{FAD,red}$ was estimated above to be about 1.8×10^{-3}. The recovery time of back re-oxidation was obtained to be, $\tau_{rec} \approx$ 50 min. Prolonged excitation converts the re-oxidable FAD$_{red}$H$_2$ to non-oxidable FAD$_{red}$H$_{2,per}$. Some unique protein conformation change is thought to be responsible for this conversion. The quantum efficiency of the conformation to permanent reduced FAD was determined to be, $\phi_{FAD,red,per} \approx 4\times10^{-4}$ by the not complete absorption recovery after photo-excitation.

MTHF-Cry3-FAD $\xrightleftharpoons[\text{dark}]{h\nu,\ \phi_{MTHF'}}$ MTHF'-Cry3'''-FAD

$h\nu$
$\phi_{MTHF''}$
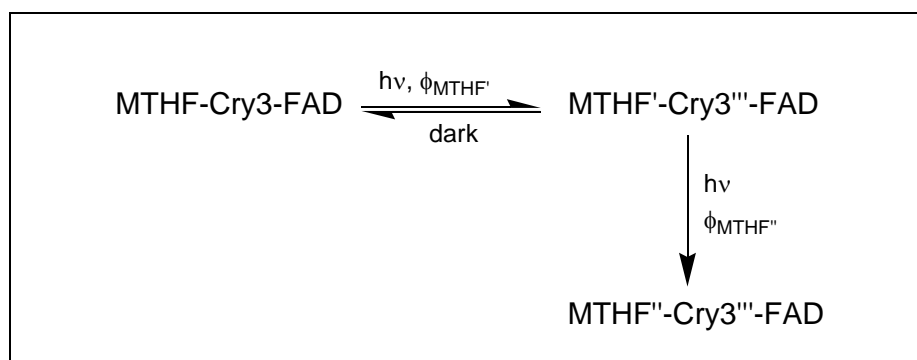
MTHF''-Cry3'''-FAD

Scheme 5.6 : The reversible formation of a MTHF species (MTHF′, MTHF photo-cycle) and the formation of an irreversible photoproduct (MTHF′′).

Scheme 5.6 shows the photo-cyclic dynamics of conversion of MTHF-Cry3-FAD to MTHF′-Cry3′′′-FAD and its back-recovery after light switch-off. The conversion quantum efficiency, $\phi_{MTHF'} \approx 2.9\times10^{-4}$, was obtained. In the dark the back-recovery time, $\tau_{MTHF,rec}$, was found to be about 30 min. Prolonged light exposure caused irreversible MTHF conversion to MTHF′′ with low quantum efficiency of $\phi_{MTHF''} \approx 3.7\times10^{-5}$.
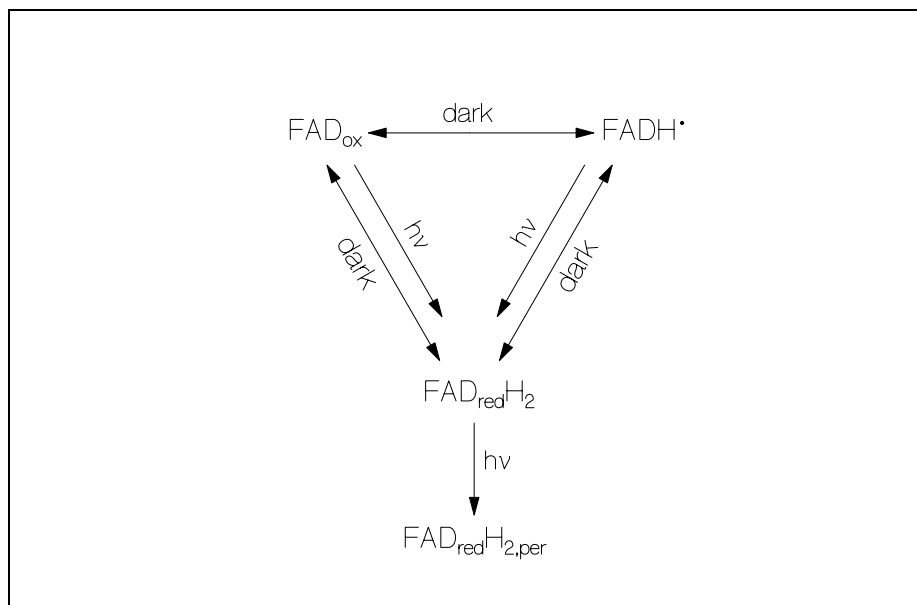
Fig. 5.32 FAD state compositions in cry3.

A reaction and equilibration scheme for FAD in cry3 is illustrated in Fig. 5.32. FAD_{ox}, $FADH^{\bullet}$, and $FAD_{red}H_2$ are in equilibrium in the dark state. FAD_{ox} is reduced to $FAD_{red}H_2$ and $FADH^{\bullet}$ is reduced to $FAD_{red}H_2$ upon light absorption. With prolonged light exposure, re-oxidable $FAD_{red}H_2$ is modified to non-oxidable $FAD_{red}H_{2,per}$.

6. Summary

The investigation of blue-light photoreceptors is an active field of research. They are the newest discussed group of photoreceptors. Biologist and biochemist made enormous progress in expression of some members of these photoreceptor proteins and opened the possibility of the investigation of their structure, response, and function. The study and analysis of the photo-cyclic behaviour of the blue-light photoreceptors became possible and is still in progress. The signal transduction from the receptor part (light signaling part) of the blue-light photoreceptor proteins to their biological functional part (kinase part) is yet unknown. Till now three classes of blue-light photo-receptors with flavin cofactor have been found, the phototropins, the cryptochromes, and the BLUF-proteins.

In this dissertation the photodynamic behaviour of a phototropin and a cryptochrome was studied by absorption and emission spectroscopic methods. First the blue-light receptor part of the phototropin, phot, from the green algae *Chlamydomonas reinhardtii* was studied. This photoreceptor part consists of two LOV domains, LOV1 and LOV2. The protein piece consisting of both LOV domains (called LOV1/2) was investigated. Each LOV domain contains a non-covalently bound FMN molecule as chromophore.

The photocyclic dynamics of LOV1/2 was compared with the photocyclic dynamics of the separated LOV1 and LOV2 domains. The behaviour of LOV1/2 domain was not found as the simple sum of the behaviours of the separated LOV1 and LOV2 domains. The two chromophores are too near together so that they have mutual influence. The relevant

absorption and emission spectroscopic parameters and dynamical parameters have been determined, so that the complete photocyclic-dynamics of the LOV1/2 double domain could be revealed.

The LOV1/2 domain contains free FMN and non-covalently bound FMN. The non-covalently bound FMN consists of not convertible FMN to adduct state and of convertible FMN to adduct state. The convertible FMN is distinguished by fast and slow recovery time to the dark state. The quantum efficiency of adduct formation gradually reduces with increasing intensity. When one FMN molecule in the LOV1/2 domain is already converted to the adduct state then the other FMN molecule in the LOV1/2 domain is less efficiently converted to the adduct state.

In the second part of this dissertation the photo cyclic dynamics of the cryptochrome 3 from the plant *Arabidopsis thaliana* was studied. This cryptochrome could be recently expressed from *E. coli*. The analysis of the photodynamics is aggravated by the presence of two chromophores in the PHR (photolyase homology region) of this protein. The two chromophores are MTHF and FAD.

To entangle the complex dynamics, the separate spectroscopic behaviour of MTHF and FAD was studied. FAD in cry3 was found to be presented in different redox forms, the oxdized form (FAD_{ox}), the reduced form ($FAD_{red}H_2$), and the half-reduced semiquinone form ($FADH^{\bullet}$). The light response of cry3 turned out to be complex due to the presence of two chromophores and the presence of the FAD chromophore in three different redox states.

A detailed steady-state absorption and emission spectroscopic investigation and a time-resolved fluorescence spectroscopic analysis succeeded in the clarification of the photocycle dynamics involving a variation of the protein conformation by light absorption, the photocycle of FAD_{ox} reduction and reoxidation, the photo-cycle of $FADH^{\bullet}$ reduction and reoxidation, as well as the photocycle of reversible MTHF conversion. The chromophore-

protein interaction showed up in an efficient photo-induced electron transfer from amino acid donor to the FAD acceptor. The presence of MTHF and FAD showed up an efficient Förster-type energy transfer from MTHF to FAD.

For the studied systems, the LOV1/2 double domain of phot from *Chlamydomonas reinhardtii* and the cry3 protein from *Arabidopsis thaliana*, the photo-cyclic behaviour could be clarified to a certain degree of detail. Other methods like crystal structure analysis, NMR spectroscopy, FT-IR spectroscopy, Raman spectroscopy, and ultrafast time resolved pump probe spectroscopy may help to refine the photo response processes and may lead to an atomistic understanding of the light signaling.

Work on LOV domains in other organism and on other cryptochromes in different expressions from different biological systems may help to get a further understanding of the biochemical, biophysical, biological mechanisms and functions of blue–light photoreceptors.

7. References

[1] C. Darwin, The Power of Movement in Plants. (1881) New York: D. Appleton and Company.

[2] G. Lasceve, J. Leymarie, M. Olney, E. Liscum, J.M. Christie, A. Vavasseur, W.R. Briggs, *Plant Physiol.* (1999) **120**: 605-614.

[3] W.R. Briggs, C. Beck, A.R. Cashmore, J.M. Christie, J. Hughes, J.A Jarillo, T. Kagawa, H. Kanegae, E. Liscum, A. Nagatani, *Plant Cell* (1999) **13**: 993-997.

[4] W.R. Briggs, C.F. Beck, A.R. Cashmore, J.M. Christie, J. Hughes, J.A. Jarillo, T. Kagawa, H. Kanegae, E. Liscum, A. Nagatani, K. Okada, M. Salomon, W. Rüdiger, T. Sakai, M. Takano, M. Wada, J.C. Watson, *Plant Cell* (2001) **13**: 993-997.

[5] E. Huala, P.W. Oeller, E. Liscum, I.-S. Han, E. Larsen, W.R. Briggs., *Science* (1997) **278**: 479-487.

[6] M. Wada, F. Grolig, W. Haupt, *J. Photochem. Photobiol. B* (1993) **17**: 3-25.

[7] H. Yatsuhashi, *J. Plant Res.* (1996) **109**: 139-146.

[8] W. Haupt, R. Scheuerlein, *Plant Cell Environ.* (1990) **13**: 595-614.

[9] T. Sakai, T. Kagawa, M. Kashara, T.E. Swartz, J.M. Christie, W.R. Briggs, M. Wada, K. Okada, *Proc. Natl. Acad. Sci. U.S.A.* (2001) **98**: 6969-6974.

[10] S.M. Miller, V. Massey, D. Ballou, C.H. Williams, M.D. Distefano, M.J. Moore, C.T. Walsh, *Biochemistry* (1990) **29**: 2831-2841.

[11] Jarillo JA, Ahmad M Cashmore AR, *plant physiol.* (1998) **117**: 719-725.

[12] B.L. Taylor, I,B. Zhulin, *Mol. Biol. Rev.* (1999) **63**: 479-506.

[13] J.M. Christie, T.E. Swartz, R.A. Bogomolni, W.R. Briggs, *The Plant Journal* (2002) **32**: 205-219.

[14] M. Salomon, J.M. Christie, E. Knieb, U. Lempert, W.R. Birggs, *Biochem.* (2000) **39**: 9401-9410.

[15] T.E. Swartz, S.B. Corchnoy, J.M. Christie, J.W. Lewis, I. Szundi, W.R. Briggs, R.A. Bogomolni, *J. Biol. Chem.* (2001) **276**: 36493-36500.

[16] S.M. Miller, V. Massey, D. Ballou, C.H. Williams, M.D. Distefano, M.J. Moore, C.T. Walsh, *Biochem.* (1990) **29**: 2831-2841.

[17] S. Crosson, K. Moffat, *Proc. Natl. Acad. Sci. U.S.A.* (2001) **98**: 2995-3000.

[18] D. Matsuoka, S. Tokutomi, *Proc. Natl. Acad. Sci. U.S.A.*(2005) **102**: 13337-13342.

[19] T. Iwata, D. Nozaki, S. Tokutomi, T. Kagawa, M. Wada, H. Kandori, *Biochem.* (2003) **42**: 8183-8191.

[20] G.E. Borgstahl, D.R. Williams, E.D. Getzoff, *Biochem.* (1995) **34**: 6278-6287.

[21] S. Crosson, S. Rajagopal, K. Moffat, *Biochem.* (2003) **42**: 2-10.

[22] T. Kottke, J. Heberle, D. Hehn, B. Dick, P. Hegemann, *Biophys. J.* (2003) **84**: 1192-1201.

[23] H. Guo. T. Kottke, P. Hegemann, B. Dick, *Biophys. J.* (2005) **89**: 402-412.

[24] W. Holzer, A. Penzkofer, T. Susdorf, M. Alvarez, Sh.D.M. Islam, P. Hegemann, *Chem. Phys*. (2004) **302**: 105-118.

[25] T.A. Schüttrigeit, C.K. Kompa, M. Salomon, W. Rüdiger, M.E. Michel-Beyerle, *Chem. Phys.* (2003) **294**: 501-508.

[26] M. Kasahara, T. E. Swartz, M. A. Olney, A. Onodera, N. Mochizuki, H. Fukuzawa, E. Asamizu, S. Tabata, H. Kanegae, M. Takano, J.M. Christie, A. Nagatani, W.R. Briggs, *Plant Physiol*. (2002), **129**: 762-773.

[27] R. Fedorov, I. Schlichting, E. Hartmann, T. Domaratcheva, M. Fuhrmann, O. Hegemann. *Biophys. J.* (2003) **84**: 2474-2482.

[28] E. Schleicher, R.M. Kowalczyk, C.W. Kay, P. Hegemann, A. Bacher, M. Fischer, R. Bittl, G. Richter, S. Weber, *J. A. Chem. Soc.* (2004) **126**: 11067-11076.

[29] C.W.M. Kay, E. Schleicher, A. Kuppig, H. Hofner, W. Rüdiger, M. Schleicher, M. Fischer, A. Bacher, S. Weber, G. Richter, *J. Biol. Chem.* (2003) **278**: 10973-10982.

[30] M. Sakai, H. Takahashi, *J. Mol. Struct*. (1996) **379**: 9-18.

[31] P.F. Heelis, B.J. Parsons, G.O. Phillips, *Biochim. Biophys. Acta* (1979) **587**: 455-462.

[32] S. Schreiner, H.A.E. Kramer, Influence of pH on flavins in the triplet state. In *Flavins and Flavoproteins*; Singer, T. P., Ed.; Elsevier Scientific Publishing Company: Amsterdam, 1976; p 793.

[33] C. Neiss, P. Saalfrank, *Photochem. Photobiol.* (2003) **77**: 101-109.

[34] W.A. Phillips, J. Low Temp. Phys. (1972) 7: 351-361.

[35] M.W. Klein, *Phys. Rev. B* (1985) **31**: 1114-1121.

[36] G. Deutscher, K.A. Müller, *Phys. Rev. Lett.* (1987) **59**: 1745-1747.

[37] R. Bittl, C.W.M. Kay, S. Weber, P. Hegemann, *Biochem*. (2003) **42**: 806-8512.

[38] T. Kottke, B. Dick, R. Fedorov, I. Schlichting, R. Deutzmann, P. Hegemann, *Biochem*. (2003) **42**: 9854-9862.

[39] P.F. Heelis, G.O. Philips, *Photobiochem. Photobiophys.* (1979) **1**: 63-70.

References

[40] K. Lanzl, Search for intermediates in the photoadduct formation of a LOV domain, *'Sensory Blue Light Receptors' Workshop*, (2006), Marburg.

[41] V. Massey, G. Palmer, *Biochem.* (1966) **5**: 3181-3189.

[42] A.R. Cashmore, J.A. Jarillo, Y.J. Wu, D. Liu, *Science* (1999) **284**: 760-765.

[43] A. Sancar, *Annu. Rev. Biochem.* (2000) **69**: 31-67.

[44] C.L. Partch, A. Sancar, *Photochem. and Photobiol.* (2005) **81**: 1291-1304.

[45] M.P. Vreeswijk, A. Hoffen, B.E. Westland, H. Vrieling, A.A. Zeeland, L.H. Mullenders, *J. Biol. Chem.* (1994) **269**: 31858-31863.

[46] H. Wang, C. Saxena, D. Quan, A. Sancar, D. Zhong, *J. Phys. Chem. B* (2005) **109**: 1329-1333.

[47] C. Saxena, H. Wang, I.H. Kavakli, A. Sancar, D. Zhong, *J. Am. Chem. Soc*. (2005) **127**: 7984-7985.

[48] C. Saxena, D. Zhong, *J. Phys. Chem. B* (2004) **108**: 18026-18033.

[49] H. Daiyasu, T. Ishikawa, K.-I. Kuma, S. Iwai, T. Todo, H. Toh, *Genes to Cells* (2004) **9**: 479-495.

[50] T. Kleine, P. Lockhart, A. Batschauer, *Plant J.* (2003) **35**: 93-103.

[51] S. Kanai, R. Kikuno, H. Toh, H. Ryo, T. Todo, *J. Mol. Evol.* (1997) **45**: 535-548.

[52] A. Yasui, A.P. Eker, S. Yasuhira, *EMBO J.* (1994) **13**: 6143–6151.

[53] A. Mees, T. Klar, P. Gnau, U. Hennecke, A.P. Eker, T. Carell, L.-O. Essen, *Science* (2004) **306**: 1789-1793.

[54] A.J. Ramsey, J.L. Alderfer, M.S. Jorns, *Biochem.* (1992) **31**: 4-11.

[55] H.W. Park, S.T. Kim, A. Sancar, J. Deisenhofer, *Science* (1995) **268**, 1866-1872.

[56] T.K. Tamada, Y. Kitadokoro, K. Higuchi, A. Inaka, P.E. Yasui, A. Ruiter, K. Miki, *Nat. Struct. Biol.* (1997) **4**: 887-891.

[57] H. Komori, R. Masui, S. Kuramitsu, *Proc. Natl. Acad. Sci. USA,* (2001) **98**: 13560–13565.

[58] C.A. Brautigam, B.S. Smith, Z. Ma, M. Palnitkar, D.R. Tomchick, M. Machius, J. Deisenhofer, *Proc. Natl. Acad. Sci. U.S.A*. (2004) **101**: 12142-12147.

[59] R.K. Brudler, H. Hitomi, H. Daiyasu, H. Toh, K. Kucho, M. Ishiura, M. Kanehisa, V.A. Roberts, T. Todo, J.A. Tainer, E.D. Getzoff, *Mol. Cell* (2003) **11**: 59-67.

[60] A. Sancar, G.B. Sancar, *J. Mol. Biol*. (1984) **172**: 223-229.

[61] G. Payne, P.F. Heelis, B.R Rohrs, A. Sancar, *Biochem.* (1987) **26**: 7121-7127.

[62] M.S. Jorns, G.B. Sancar, A. Sancar, *Biochem*. (1984) **23**: 2673-2679.

[63] G.B. Sancar, F.W. Smith, P.F. Heelis, *J. Biol. Chem*. (1987) **262**: 15457-15465.

References

[64] A.A. Henry, R. Jimenez, D. Hanway, F.E. Romesberg, *ChemBioChem*. (2004) **5**: 1088-1094.

[65] A.P.M. Eker, J.K.C. Hessels, J. Velde, *Biochem.* (1988) **27**: 1758-1765.

[66] C.T. Walsh, *Acc. Chem. Res*. (1986) **19**: 216-224.

[67] V. Massey, P. Hemmerich, *Biochem.* (1978) **17**: 9-18.

[68] A.P.M. Eker, P. Kooiman, J.K.C. Hessels, A. Yasui, *J. Biol. Chem*. (1990) **265**: 8009-8015.

[69] I. Husain, A. Sancar, *Nucleic Acids Res*. (1987) **15**: 1109-1115.

[70] J. Hahn, M.E. Michel-Beyerle, N. Rosch, *J. Mol. Model* (1998) **4**: 73-81.

[71] J. Antony, D.M. Medvedev, A.A. Stuchebrukhov, *J. Am. Chem. Soc.* (2000) **122**: 1057-1062.

[72] A. Sancar, *Biochem.* (1994) **33**: 2-9.

[73] M. Ahmad, C. Lin, A.R. Cashmore, *Pant J.* (1995) **8**: 653-658.

[74] H.-Q. Yang, Y.-J. Wu, R-H. Tang, D. Liu, Y. Liu, *Cell* (2000) **103**: 815-827.

[75] C. Lin, D. E. Robertson, M. Ahmad, A.A. Raibekas, M.S. Jorns, P.L. Dutton, A.R. Cashmore, *Science* (1995) **269**: 968-970.

[76] C. Lin, *The Plant Cell* (2002) **14**: S207-S225.

[77] A. Batschauer, (Ed.), Photoreceptors and Light Signalling, Comprehensive Series in Photochemical & Photobiological Sciences, (2003) The Royal Society of Chemistry, Cambridge, UK.

[78] T. Imaizumi, A. Kadota, M. Hasebe, M. Wada, *Plant Cell* (2002) **12**: 81-96.

[79] B.M. Parks, K.M. Folta, *Curr. Opin. Plant Biol.* (2001) **4**: 436-440.

[80] T.C. Mockler, H. Guo, H. Yang, H. Duong, C. Lin, *Development* (1999) **126**: 2073-2082.

[81] C. Lin, H. Yang, H. Guo, T. Mockler, J. Chen, A.R. Cashmore, *Proc. Natl. Acad. Sci. U.S.A*. (1998) **95**: 2686-2690.

[82] M. Ahmad, C. Lin, A.R. Cashmore, *Plant J.* (1995) **8**: 663-658.

[83] G.I. Jekins, *Plant Cell Environ*. (1997) **20**: 773-778.

[84] M. Ahmad, J.A. Jarillo, O. Smirnova, A.R. Cashmore, *Nature* (1998) **392**: 720-723.

[85] S.E. El-Assal, C.A. Blanco, A.J.M. Peeters, V. Raz, M Koornneef, *Natl. Genet.* (2001) **29**: 435-440.

[86] D.J. Bagnall, R.W. King, R.P. Hangarter, *Planta* (1996) **200**: 278-280.

[87] P. Mas, P.F. Devlin, S. Panda, S.A. Kay, *Natur*e (2000) **408**: 207-211.

[88] Jarillo JA, Ahmad M Cashmore AR, *plant physiol*. (1998) **117**: 719-725.

[89] P. Emery, W.V. So, M. Kaneko, J.C. Hall, M. Rosbash, *Cell* (1998) **95**: 669-679.

[90] G.T. Horst, *Nature* (1999) **398**: 627-630.

[91] J.C. Dunlap, *Cell* (1999) **96**: 271-290.

[92] M.F. Ceriani, T.K. Darlington, D. Staknis, P, Mas, A.A. Petti, C.J. Weitz, S.A. Kay, *Science* (1999) **285**: 553-556.

[93] M.H. Vataterna, C.P. Selby, T. Todo, H. Niwa, C. Thompson, E.M. Fruechte, K. Hitomi, R.J. Thresher, T. Ishikawa, J. Miyazaki, J.S. Takahashi, A. Sancar, *Proc. Natl. Acad. Sci. U.S.A.* (1999) **96**: 12114-12119.

[94] R. Pokorny, T. Klar, L.-O. Essen, A. Batschauer, *Acta Cryst.F* (2005) **61**: 935-938.

[95] B. Giovani, M. Byrdin, M. Ahmad, K. Brettel, *Nat. Struct. Biol.* (2003) **10**: 489-490.

[96] C. Lin, S.T. Kim, A. Batschauer, I. Dawut, A. Sancar, *Biochem.* (1995) **34**: 6892-6899.

[97] T. Kottke, A. Batschauer, M. Ahmad, J. Heberle, *Biochem.* (2006) **45**: 2472-2479.

[98] M. Gomelsky, G. Klug, *Trends Biol. Sci.* (2002) **27**: 497-500.

[99] S. Masuda, C.E. Bauer, *Cell* (2002) **110**: 613-623.

[100] A. Jung, T. Domratcheva, M. Tarutina, Q. Wu, W-H. Ko, R.L. Shoeman, M. Gomelsky, K.H. Gardner, I. Schlichting, *Proc. Natl. Acad. Sci. U.S.A* (2005) **101**: 12306-12311.

[101] M. Iseki, S. Matsunaga, A. Murakami, K. Ohno, K. Shiga, K. Yoshida, M. Sugai, T. Takahashi, T. Hori, M. Watanabe, *Nature* (2002) **415**: 1047-1051.

[102] S. Masuda, K. Hasegawa, A. Ishii, T. Ono, *Biochem.* (2004) **43**: 5304-5313.

[103] M. Gomelsky, S. Kaplan, *J. Biol. Chem*. (1998) **273**: 35319-35325.

[104] K. Okajima, S. Yoshihara, Y. Fukushima, X. Geng, M. Katayama, S. Higashi, M. Watanabe, S. Sato, S. Tabata, Y. Shibata, S. Itoh, M. Ikeuchi, *J. Biochem*. **137**: 741-750.

[105] K. Hasegawa, S. Masuda, T.-A. Ono, *Biochem*. (2006) **45**: 3785-3793.

[106] A.J. Schimidt, D.A. Rvjenkov, M. Gomelsky, *J. Bacteriol*. (2005) **187**: 4774-4781.

[107] M. Gomelsky, S. Kaplan, *J. Bacteriol.* (1997) **179**: 128-134.

[108] W. Laan, M.A. Horst, I.H. Stokkum, K.J. Hellingwerf, *Photochem. Photobiol* (2003) *78*: 290-297.

[109] M. Gauden, S. Yeremenko, W. Laan, I.H.M. Stokkum, J.A. Ihalainen, R. Grondelle, K.J. Hellingwerf, J.T.M. Kennis, *Biochem*. (2005) **44**: 3653-3662.

[110] K.C. Toh, J.T.M. Kennis, *The Gordon Research Conference on Photosensory Receptors & Signal Transduction* (2006).

[111] R. Kort, W.D. Hoff, M. West, A.R. Kroon, S.M. Hoffer, K.H. Vlieg, W. Crielaand, J.J. Beeumen, K.J. Hellingwerf, *EMBO J.* (1996) **15**: 3209-3218.

References

[112] J.-L. Pellequer, K.A. Wager-Smith, S.A. Kay, E.D. Getzoff, (1998) *Proc. Natl. Acad. Sci. USA* **95**: 5884-5890.

[113] T.E. Meyer, E. Yakali, M. Cusanovich, G. Tollin, *Biochem.* (1987) *26*: 418-423.

[114] M. Baca, G.E. Borgstahl, M. Boissinot, P.M. Burke, D.R Williams, K.A. Slater, E.D. Getzoff, *Biochem.* (1994) **33**: 14369-14377.

[115] W.D. Hoff, P. Dux, K. Hard, B. Devreese, I.M. Nugteren-Roodzant, W. Crielaard, R. Boelens, R. Kaptein, J. Beeumen, K.J. Hellingwerf, *Biochem.* (1994) **33**: 13959-13962.

[116] W.W. Sprenger, W.D. Hoff, J.P. Armitage, K.J. Hellingwerf, *J. Bacteriol* (1993) **175**: 3096-3104.

[117] Y.-Z. Gu, J.B. Hogenesch, C.A. Bradfield, *Annu. Rev. Pharmacol. Toxicol.*(2000) **40**: 519-561.

[118] K.J. Hellingwerf, *J. Photochem. Photobiol. B:Biol.* (2000) **54**: 94-102.

[119] L. Ujj, S. Devanathan, T.E. Meyer, M.A. Cusanovich, G. Tollin, G.H. Atkinson, G. H. *Biophys. J.* (1998) **75**: 406-412.

[120] W. Hoff, I.H. Stokkum, H.J. Ramesdonk, M.E. Brederode, A.M. Brouwer, J.C. Fitch, T.E. Meyer, R. Grondelle, K.J. Hellingwerf, *Biophys. J.* (1994) **67**: 1691-1705.

[121] T. Gensch, C. Gradinaru, I. Stokkum, J. Hendriks, K. Hellingwerf, R. Grondelle, *Chem. Phys. Lett.* (2002) **356**: 347-354.

[122] T.E. Meyer, E. Yakali, M.A. Cusanovich, G. Tollin, *Biochem*. (1987) **26**: 418-423.

[123] J. Hendriks, T. Gensch, L. Hviid, M.A. Horst, K.J. Hellingwerf, J.J.Thor, *Biophys. J.* (2002) **82**: 1632-1643.

[124] A. Xie, L. Kelemen, J. Hendriks, B.J. White, K.J. Hellingwerf, W.D. Hoff, *Biochem.* (2001) **40**: 1510-1517.

[125] M.E. Brederode, W.D. Hoff, I.H. Stokkum, M.L. Groot, K.J. Hellingwerf, *Biophys. J.* (1996) **71**: 365-380.

[126] U.K. Genick, S. Devanathan, T.E. Meyer, I.L. Canestrelli, E. Williams, M.A. Cusanovich, G. Tollin, E.D. Getzoff, *Biochem.* (1997) **36**: 8-14.

[127] Z. Jiang, L.R. Swem, B. Rushing, S. Devanathan, G. Tollin, C. Bauer, *Science*, (1999) **285**: 406-409.

[128] C.R. Martin, *Int. Rev. Cytol*. (1993) **147**: 233-245.

[129] A. Penzkofer, W. Leupacher, *J. Luminesc.* (1987) **37**: 61-72.

[130] W.H. Melhuish, *J.Phys. Chem.* (1961) **65**: 229–235.

[131] Technical data sheet of Kodak.

[132] D.E. Spence, P.N. Kean, W. Sibbett, *Opt. Lett*. (1991) **16**:42-44.

[133] A. Dubietis, G. Jonusauskas, A. Piskarskas, *Opt. Commun.* (1992) **88**: 437-440.

References

[134] P. Weidner, A. Penzkofer, *Opt. Quant. Electron.* (1993) **25**: 1–25.

[135] G. Weber, in: E.C. Slater (Ed.), *Flavins and Flavoproteins*, Vol. **8**, B. B. A. Library, Elsevier, Amsterdam, (1966), p. 15-21.

[136] W. Holzer, A. Penzkofer, M. Fuhrmann, P. Hegemann, *Photochem. Photobiol.* (2002) **75**: 479-487.

[137] W. Holzer, A. Penzkofer, P. Hegemann, *J. Luminesc.* (2005) **112**: 444-448.

[138] W. Holzer, A. Penzkofer, P. Hegemann, *Chem. Phys.* (2005) **308**: 79-91.

[139] G. N. Lewis, M. Randall, The activity coefficient of strong electrolytes, *J. Am. Chem. Soc.*, (1921) **43**: 1112-1154.

[140] C.A. Parker, *Photoluminescence of Solutions*, Elsevier, Amsterdam, The Netherlands, (1968).

[141] M. Orrit, *Science* (2003) **302**: 239-240.

[142] TH. Förster, *Fluorescence Organischer Verbindungen*, Vandenhoeck and Ruprecht, Göttingen, (1951).

[143] G.R. Fleming, *Chemical Applications of Ultrafast Spectroscopy*, Oxford University Press, New York, (1986).

[144] F. Ammer, A. Penzkofer, P. Weidner, *Chem. Phys.* (1995) **192**: 325-331.

[145] W, J. Shirdel, P. Zirak, A. Penzkofer, P. Hegemann, R. Deutzmann, E. Hochmuth, *Chem. Phys.* (2005) **308**: 69-78.

[146] A. Penzkofer, W. Leupacher, *J. Lumin.* (1987) **37**: 61-72.

[147] J.T.M. Kennis, S. Crosson, M. Gauden, I.H.M. Stokkum, K. Moffat, R. Grondelle, *Biochem.* (2003) **42**:3385-3392.

[148] F. Müller, *Chemistry and Biochemistry of Flavoenzymes, Volume I*, (1990), CRC Press.

[149] B.A. Palfey, V. Massey, Flavin-dependent enzymes, in: M. Sinnott (Ed.), Comprehensive Biological Catalysis. A Mechanistic Reference, Vol. III: Radical Reactions and Oxidation/Reduction, Academic Press, San Diego, USA, 1997 pp. 83-154.

[150] J.L. Johnson, S. Hamm-Alvarez, G. Payne, G. B. Sancar, K. V. Rajagopalan, A. Sancar, *Proc. Natl. Acad. Sci. U.S.A.* (1988) **85**: 2046-2050.

[151] S.D.M. Islam, T. Susdorf, A. Penzkofer, P. Hegemann, *Chem. Phys.* (2003) **295**: 137-149.

[152] P. Drössler, W. Holzer, A. Penzkofer, P. Hegemann, *Chem. Phys.* (2002) **282**: 429-439.

[153] J.R. Barrio, G.L. Tolman, N.J. Leonard, R.D. Spencer, G. Weber, *Proc. Natl. Acad. Sci. U.S.A.* (1973) **70**: 941-943.

[154] R.D. Spencer, G. Weber, *Pergamon Press, Oxford*, (1972) p. 393-399.

[155] P.A.W. Berg, J. Widengren, M.A. Hink, R. Rigler, A.J Visser, *Photochem. Photophys. Aspects, Spectrochim. Acta A* (2001) **57**: 2135-2144.

References

[156] A.J. Visser, *Photochem. Photobiol.* (1984) **40**: 703-706.

[157] P. Wahl, J.C. Auchet, A.J. Visser, F. Müller, *FEBS Lett* (1974) **44**: 67-70.

[158] P.A. Berg, K.A. Feenstra, A.E. Mark, H.J. Berendsen, A.J. Visser, *J. Phys. Chem. B* (2002) **106**: 8858-8869.

[159] D. Zhong, A.H. Zewail, *Proc. Natl. Acad. Sci. U.S.A.* (2001) **98**: 11867-11872.

[160] N. Mataga, H. Chosrowjan, Y. Shibata, F. Tanaka, Y. Nishina, K. Shiga, *J. Phys. Chem. B* (2000) **104**: 10667-10677.

[161] Y.-T Kao, C. Saxena, L. Wang, A. Sancar, D. Zhong, *Proc. Natl. Acad. Sci. U.S.A.* (2005) **102**: 16128-16132.

[162] P.-S. Song, R.D. Fugate, W.R. Briggs, *In Flavins and Flavoproteins*: Baltimore, MD, (1980).

[163] P.A. Berg, A.J. Visser, Tracking molecular dynamics of flavoproteins with time-resolved fluorescence spectroscopy, in: B. Valeur, J.-C. Brochon (Eds.), New trends in Fluorescence Spectroscopy: Applications to Chemical and Life Sciences, Springer-Verlag, New York, 2001, p. 457-485.

[164] T.E. Creighton, *Biochem J.* (1990) **270**: 1-16.

[165] J. E. Baggott, *Biochem.* (2000) **39**: 14647-14653.

[166] S. Weiss, *Nature Structural Biology* (2000) **7**: 724-729.

[167] G. Luo, P. Karnchanaphanurach, T.-M. Louie, I. Rech, S. Cova, L. Xun, X.S. Xie, *Scinece* (2003) **302**: 262-266.

[168] S. Weiss, *Scinece* (1999) **283**: 1676-1683.

[169] M. Hercher, *Appl. Opt* (1967) **6**: 947-953.

[170] S.J. Strickler, R.A. Berg, *J. Chem. Phys.* (1962) **37**: 814-822.

[171] J.B. Birks, D.J. Dyson, *Proc. Roy. Soc. London, Ser. A* (1993) **275**: 135-148.

[172] A.V. Deshpande, A. Beidoun, A. Penzkofer, G. Wagenblast, *Chem.Phys.* (1990) **142**: 123-131.

[173] S.-T. Kim, P.F. Heelis, T. Okamura, Y. Hirata, N. Mataga, A. Sancar, *Biochem.* (1991) **30**: 11262-11270.

[174] T. Klar, R. Pokorny, A. Batschauer, L.O. Essen, to be published.

.

8.Appendix

Amino Acids

Each amino acid contains an "amine" group (**NH₃**) and a "carboxy" group (**COOH**).

Amino Acids Abbreviated Words

A	Ala	Alanine	CH_3-$CH(NH_2)$-COOH
A	Asx	Asp+Asn	
C	Cys	Cysteine	HS-CH_2-$CH(NH_2)$-COOH
D	Asp	Aspartic acid	HOOC-CH_2-$CH(NH_2)$-COOH
E	Glu	Glutamic acid	HOOC-$(CH_2)_2$-$CH(NH_2)$-COOH
F	Phe	Phenylalanine	Ph-CH_2-$CH(NH_2)$-COOH
G	Gly	Glycine	NH_2-CH_2-COOH
H	His	Histidine	NH-CH=N-CH=C-CH_2-$CH(NH_2)$-COOH |_____|
I	Ile	Isoleucine	CH_3-CH_2-$CH(CH_3)$-$CH(NH_2)$-COOH
K	Lys	Lysine	H_2N-$(CH_2)_4$-$CH(NH_2)$-COOH
L	Leu	Leucine	$(CH_3)_2$-CH-CH_2-$CH(NH_2)$-COOH
M	Met	Methionine	CH_3-S-$(CH_2)_2$-$CH(NH_2)$-COOH
N	Asn	Asparagine	H_2N-CO-CH_2-$CH(NH_2)$-COOH
P	Pro	Proline	NH-$(CH_2)_3$-CH-COOH |_____|
Q	Gln	Glutamine	H_2N-CO-$(CH_2)_2$-$CH(NH_2)$-COOH
R	Arg	Arginine	HN=$C(NH_2)$-NH-$(CH_2)_3$-$CH(NH_2)$-COOH
S	Ser	Serine	HO-CH_2-$CH(NH_2)$-COOH
T	Thr	Threonine	CH_3-CH(OH)-$CH(NH_2)$-COOH
V	Val	Valine	$(CH_3)_2$-CH-$CH(NH_2)$-COOH
W	Trp	Tryptophan	Ph-NH-CH=C-CH_2-$CH(NH_2)$-COOH |_____|
X	-	Unknown or unstandard amino acid	
Y	Tyr	Tyrosine	HO-p-Ph-CH_2-$CH(NH_2)$-COOH
Z	Glx	Gln+Glu	

131

9. Acknowledgements

Many thanks for Professor Dr. Bernhard Dick and Professor Dr. Alfons Penzkofer. Professor Bernhard Dick gave me good chances to study in Regensburg and thereby here in Germany, the mirror of scientific mind in the world, I could absorb a developed scientific mind what real scholar should think and do. Professor Alfons Penzkofer was kind enough to lead me. He had the goodness to teach scientific knowledge for me even in his busy schedule and to show me how scientist should think. I, novice scientist, could be converted to better scientist. So in my life I will be very much obliged to them for their kindness in showing me around. I also appreciate Prof. Dr. Peter Hegemann's discussion for LOV1/2 domain. Prof. Dick, Prof. Penzkofer, and Prof. Hegemann considered me, thereby I could study continuously in Regensburg, I will repay professors' favor with being a great scientist.

Prof. Dr. Alfred Batschauer, Prof. Dr. Lars-Oliver Essen, and Dr. Richard Pokorný in Marburg gave us good professional advices so cryptochrome 3 working was carried out successfully. To work with them was in itself a privilege.

I am thankful to Prof. Dr. Aziz Sancar and Prof. Dr. Dongping Zhong for their encourgement during my study. Sincerely, I appreciate them for the beginning of my journey on Cryptochrome/Photolyase in my life as they did and do.

It is nice of these people for kind assistance in my study: Dr. Uwe Kensy (Chemistry), Dr. Alexander Dobryakov (Berlin), Dr. Tilman Kottke (Jülich), and Dr. Thomas Schödl (Biology). Specially, Christian Vogl helped me to clear some doubts in biology.

I thanks to my friends; Always kindly guide me German culture, Thomas Susdorf and Walter Finkenzeller, I hope them to find good job. I thank my friend Amit Tyagi, who always glad me and I wish his bright future. Peyman Zirak sincerely helped my experiment and took good care of me in case of need, specially I thanks for him. Javid Shirdel is very nice friend to me and because of him I have it good. Ashu Bansel also helped my work so I thanks for him and I expect his good achievements. Mrs. Merkel, Mrs. König, and Mrs. Schäfer in physics, Mrs. Müller, Dr. Silvia, and Dr. Jeong in Chemistry at university of Regensburg, and Dr. Chung Young-Ho and Dr. Choi Kwang-Yong in USA.

From Korea many people cheered me with impressive e-mail, phone or sometimes visited here, I really thanks for them; Prof. Tschang-Uh Nahm, Prof. Young-Pak Lee, and Prof. Sang-Min Lee; my good friends: Park Sang-Ug, Shin Tae-Woo, Ban Gyu-Hyun, Yang U-Jin, Shin Je-Kwan, Choi Dong-Ug, Lee Jeong-Ho; Hanyang University: Mun Gyung-Ju, Yun Han-Jun, Yu Kwon-Kug, Kim Young-Deong; my Relatives: Song Yong-Seon, Ahn So-Young, Song Sang-Min; other friends: Yang Seoung-Sug, Lee Jeong-Ha, Kim Ne-A, Dr. Kim Young-Hae, You Yong-Cheol and Lee Ja-Young.

Since I have not yet visited home in Korea, so my mother, father and sister Ji-Eun always bears feeling irresistible yearning for me but they everyday prayed for me. Specially I thanks for my family. I dedicate this dissertation to my Grandmother.

I give thanks to Buddha for the instruction of cultivation - the sprit of tolerance in my life. I want to give this honor to Buddha.

At the end I appreciate Deutsche Forschungsgemeinschaft for financial support in the Graduate College, "Sensory Photoreceptors in Natural and Artificial System" and the DFG-Forschergruppe 526 "Blue Light Photoreceptors".

May. 2006, Regensburg, Germany